

ABSTRACT

Title of Dissertation: RIBOSOME IN THE BALANCE: STRUCTURAL
EQUILIBRIUM ENSURES TRANSLATIONAL
FIDELITY AND PROPER GENE EXPRESSION

Sharmishtha Musalgaonkar, Doctor of Philosophy, 2014

Dissertation Directed by: Professor Jonathan D. Dinman
Department of Cell Biology and Molecular Genetics

At equilibrium, empty ribosomes freely transit between the rotated and un-rotated states. In translation elongation, the binding of two translation elongation factors to the same general region of the ribosome stabilizes them in one of the two extremes of intersubunit rotation; rotated or unrotated. These stabilized states are resolved by expenditure energy in the form of GTP hydrolysis. Here, mutants of the early assembling integral ribosomal protein uL2 (universal L2) are used to test the generality of this hypothesis. A prior study employing mutants of a late assembling peripheral ribosomal protein suggested that ribosome rotational status determines its affinity for elongation factors, and hence translational fidelity and gene expression. rRNA structure probing analyses reveal that mutations in the uL2 B7b bridge region shift the equilibrium towards the rotated state, propagating rRNA structural changes to all of the functional centers of

ribosome. Shift in structural equilibrium affects the biochemical properties of ribosomes: rotated ribosomes favor binding of the eEF2 translocase and disfavor that of the elongation ternary complex. This manifests as specific translational fidelity defects, impacting the expression of genes involved in telomere maintenance. A model is presented here describing how cyclic intersubunit rotation ensures the unidirectionality of translational elongation, and how perturbation of rotational equilibrium affects specific aspects of translational fidelity and cellular gene expression.

RIBOSOME IN THE BALANCE: STRUCTURAL
EQUILIBRIUM ENSURES TRANSLATIONAL FIDELITY AND
PROPER GENE EXPRESSION

By

Sharmishtha Musalgaonkar

Dissertation submitted to the Faculty of the Graduate School of the
University of Maryland, College Park, in partial fulfillment
of the requirements for the degree of
Doctor of Philosophy
2014

Advisory Committee:

Professor Jonathan D. Dinman, Chair

Professor James N. Culver

Associate Professor Stephen M. Mount

Adjunct Professor Zvi Kelman

Associate Professor Jason D. Kahn, Dean's Representative

© Copyright by
Sharmishtha Musalgaonkar
2014

Dedications

I wish to dedicate this work to my parents and my sisters for being the greatest source of inspiration and strength for me and to my husband for his support and love through all the phases difficult or fun.

Acknowledgements

I would like to thank my advisor Dr. Dinman for years of mentorship, friendship, and relentless support, to my committee members for their counselling and sharing their insights which helped me improve my research and all the members of Dinman lab past and present for their support and assistance in conducting research. I want to extend special thanks to Dr. Rasa Rakauskaite and Dr. Ashton T. Belew for many insightful discussions and their help and guidance through my very first laboratory experiences and always thereafter.

This work was supported in part by a grant to JDD by the Public Health Service NIH R01-GM058859. I would also like to acknowledge and thank the hard working faculty and staff members of the Department of Cell Biology and Molecular Genetics for their guidance and assistance with academic as well as administrative matters.

Table of Contents

ABSTRACT.....	ii
Dedications.....	ii
Acknowledgements	iii
Table of Contents	iv
List of Figures.....	vii
List of Abbreviations	ix
Chapter 1: Ribosomes and Translation	1
Introduction.....	1
Ribosome Structure	2
Ribosome biogenesis and assembly	11
Transcription of Pre-rRNAs	12
Processing, folding and modification of Pre-rRNA	13
Nuclear export of Pre-40S and Pre-60S particles	15
Cytoplasmic maturation of Pre-40S and 60S subunits	17
Surveillance and Turnover of misassembled ribosomes	18
Translation	19
Initiation.....	19
Viral Hijack of translation initiation.....	22
Elongation.....	26
Aminoacylation and accommodation of tRNAs.....	26
Peptidyltransfer Reaction	31
Translocation	33
Termination and Ribosome Recycling	37
Antibiotics: Inhibitors of Ribosome Functions	40
Translational Recoding	45
Programmed -1 Ribosomal Frameshifting.....	45
Programmed +1 ribosomal frameshifting.....	50
Missense and nonsense suppression.	51

Diseases of ribosomal malfunction: Ribosomopathies	51
Diseases of SSU biogenesis.....	52
Diseases of LSU biogenesis.....	53
Diseases of snoRNP malfunction	53
Diseases of ribosomal proteins	54
Cancer onset in ribosomopathies	55
Scope of the current study.....	57
Ribosomal Protein uL2	58
Chapter 2: Coordination of Ribosomal Rotation through Bridge B7b	61
Introduction.....	61
Results	63
Genetic characterization of uL2 mutants in the vicinity of B7b Bridge.....	63
uL2 mutants in the B7b intersubunit bridge region disrupt the rotational equilibrium of ribosomes.....	71
Some mutants of uL2 in the B7b region cause defects in ribosome biogenesis pathway and subunit joining defects in elongation pathway.	78
Disruption of ribosome rotational equilibrium by uL2 mutants affects binding of translation elongation factors.	80
Mutants of <i>rpl2A</i> encoding uL2-248-254Δ and uL2-K177A do not affect the rates of puromycyl-peptidyltransferase reaction, a proxy for peptidyltransfer reaction.	83
The uL2-K177A and uL2-Y133A mutants promote significant changes in translational fidelity.....	85
The uL2-K177A mutant affects gene expression and telomere maintenance through changes in programmed ribosomal frameshifting.....	85
Discussion	87
Chapter 3: Materials and Methods	92
Strains, Plasmids and media in generation of <i>rpl2A</i> mutants.....	92
Growth and Drug Sensitivity assays	92
Translation fidelity assays.....	93
Polysome analyses	94
Ribosome purification	94
Aminoacylation of tRNA ^{Phe}	95

Assays of Ribosome and tRNA interactions	96
Peptidyltransferase assay	97
Ribosome protein interactions	98
rRNA Structure probing analysis	99
mRNA Abundance and Telomere length assay.	99
Chapter 4: Conclusions and Future Direction	101
Summary.....	101
Medical relevance and Future Direction	104
Appendix 1: Yeast strain list.....	109
Appendix 2: List of synthetic oligonucleotides	110
Appendix 3: Genetic analyses of uL2 basic extension loop mutants	112
Appendix4: Biochemical and functional analyses of uL2-basic extension mutants	113
Appendix 5: Contributions to other Projects	115
References	118

List of Figures

Figure 1 Free hand drawings of the three-dimensional consensus model of the ribosome in 1980s.....	4
Figure 2 Architecture of the 80S ribosome. Location of ribosomal Proteins	6
Figure 3 Yeast 80S ribosome structure.....	8
Figure 4 Intersubunit bridges of ribosomal subunits.	9
Figure 5 tRNA and elongation factor binding sites on ribosomes.	10
Figure 6 Yeast chromatin spreads of eukaryotic nucleolar contents analyzed by electron microscopy.....	11
Figure 7. Yeast pre-rRNA processing pathway.....	15
Figure 8 Preribosomal maturation pathway to form 40S and 60S ribosomal subunits. ...	16
Figure 9 Late Steps of maturation of Pre-60S subunits in cytoplasm.....	18
Figure 10 Canonical eukaryotic translation initiation pathway.	21
Figure 11 Alternate ways of recruitment of 40S ribosomal subunit to viral mRNAs.	24
Figure 12 The eukaryotic translation elongation pathway.....	25
Figure 13 The domain structure of LeuRSEC.	28
Figure 14 Schematic of EF-Tu-dependent aa-tRNA binding to the A site.....	30
Figure 15 Schematic of peptide bond formation on the ribosome.....	32
Figure 16 Mechanism of Peptidyl transfer.....	33
Figure 17 Mechanism of Translocation.	35
Figure 18 Comparison of tRNA and eRF1 crystallographic structures.....	36
Figure 19 Mechanism of peptidyl-tRNA hydrolysis and Release factor mediated peptide release.	38
Figure 20 Sites of antibiotic action during protein synthesis.....	44
Figure 21 A typical -1 Programmed ribosomal frameshift signal.	46
Figure 22 The mechanism of -1PRF.....	47
Figure 23 -1 Programmed ribosomal frameshift in viruses.	49
Figure 24 Deregulation of translation control contributes to each step of cellular transformation and cancer progression.	56

Figure 25 A. Structural features of yeast ribosomal protein uL2. B. Ribosomal Proteins with basic extensions approach the peptidyltransferase center very closely.	60
Figure 26 Location of L2 within the yeast ribosome ribosome:	64
Figure 27 List of mutants of L2 ORF generated in this study and their location on uL2. 65	
Figure 28 Multiple sequence alignment of uL2 amino acid from different species.	67
Figure 29 rpL2A bridge mutants promote various phenotypic defects.	68
Figure 30 Drug sensitivity assays.	69
Figure 31 uL2 mutants promote defects in translational fidelity.	70
Figure 32 uL2 B7b bridge mutants alter the rotational equilibrium of the ribosome.	72
Figure 33 Structural probing analysis of 18S rRNA of Wild-type and uL2-K177A.	73
Figure 34 Structural probing analysis of 25S rRNA of Wild-type and uL2-K177A.	74
Figure 35 Magnified view of the Structure probing in SSU.	75
Figure 36 Magnified view of the Structure probing in SSU.	76
Figure 37 Three dimensional representation of 1M7 reactivity difference.	77
Figure 38. Comparison of SHAPE reactivity of individual ribosomal bases to non-rotated and rotatated control ribosomes.	78
Figure 39 Polysome profiles of cells expressing WT and mutant uL2.	79
Figure 40 uL2 B7b bridge mutants of alter the binding of translation elongation factors.81	
Figure 41 Biochemichal analyses of <i>rpl2A</i> mutants.	82
Figure 42 Single turnover peptidylpuromycin reactions.	83
Figure 43 Translation fidelity assays for selected uL2 mutants.	84
Figure 44 uL2-K177A mutant ribosomes promote defects in cellular gene expression and telomere maintenance through altered frameshifting.	86
Figure 45 Model describing the effects of disturbed ribosomal rotational equilibrium on tRNA selection and translational fidelity.	91
Figure 46 Model describing the disease progression and cancer onset in ribosomopathies	106
Figure 47 rpL2A basic extension loop mutants promote various phenotypic defects....	112
Figure 48 Mutations of uL2 basic extension domain affect peptidyl-tRNA binding in the P-site	113
Figure 49 Polysome profiles of cells expressing WT and mutant uL2.	114

List of Abbreviations

1M7	1-methyl-7-nitroisatoic anhydride
aa-tRNA	Aminoacyl tRNA
AF	Assembly factor
ARS	Aminoacyl-tRNA synthetase
ATP	Adenosine triphosphate
CP	Central protuberance
Cryo-EM	Cryogenic electron microscopy
DBA	Diamond-Blackfan anemia
DC	Decoding center
EF	Elongation factor
eEF	Eukaryotic elongation factor
eIF	Eukaryotic initiation factor
eRF	Eukaryotic release factor
GAC	GTPase-associated center
GDP	Guanosine diphosphate
GEF	Guanine exchange factor
GGQ	Glycine-glycine-glutamine motif
GTP	Guanosine triphosphate
HIV-1	Human immunodeficiency virus type 1
IF	Initiation factor

IRES	Internal ribosomal entry site
LSU	Large ribosomal subunit
M ⁷ G	7-methylguanosine
mRNA	Messenger RNA
NGD	No-go decay
NMD	Nonsense mediated decay
ORF	Open reading frame
PABP	Poly-A binding protein
Pol	Polymerase
Poly A	Poly-adenosine
PRF	Programmed ribosomal frameshifting
PTC	Peptidyltransferase center or premature termination codon
RF	Release factor
RP	Ribosomal protein
RRF	Ribosomal recycling factor
rRNA	Ribosomal RNA
SARS	Severe acute respiratory syndrome
SBDS	Shwachman-Bodian Diamond syndrome
SHAPE	Selective 2'-hydroxyl acylation analyzed by primer extension
snoRNAs	Small nucleolar RNAs
SSU	Small ribosomal subunit
tRNA	Transfer RNA

Chapter 1: Ribosomes and Translation

Introduction

Protein synthesis is a complex but indispensable biological process and the ribosome plays a central role in it. Ribosomes are large ribonucleoprotein particles, conglomerates of RNA and proteins that evolved in the pre-biotic times. Mechanically they function like a nano-scale machine in a highly orchestrated manner in order to convert the genetic information from RNA to protein with tremendous speed and accuracy. To accomplish their tasks the ribosomes have to function in an active collaboration with the tRNAs and a zoo of translation factors throughout all the steps. Translation is an endergonic process fuelled by several ATP/GTP hydrolysis reactions. Recent high resolution crystal structures and Cryo-electron microscopic reconstructions have revolutionized our understanding of both the ribosome structure and the mechanism of translation in bacterial and eukaryotic systems.

Despite the early focus on proteins, the mechanism of protein synthesis largely remained unclear until the end of 1940s. Some early speculations of ribosome's existence were made following the development of UV absorption methods for measuring nucleic acids and UV microscopy. The granular nature of cytoplasm was explained by high speed centrifugation leading to sedimentation of what was called "small particles" from chick embryo cells by Albert Claude ^{1,2}. They were later termed "microsomes", smaller than mitochondria and their chemical composition was explained. Between 1950 and 1960, the microsomes were linked to in vitro protein synthesis by Paul Zamecnik. Later he also

discovered aminoacylated tRNA in cell free systems and the microsomes got a new self-explanatory name “ribonucleoparticle”. Sodium deoxycholate treatment displayed a protein: RNA ratio of 1:1. George Palade, who won a Nobel Prize for his discovery, used a combination of advanced specimen preparation techniques and electron microscopy and was able to visualize microsomes, the electron dense particles in the cytoplasm and on endoplasmic reticulum³. These macromolecules were further calibrated using velocity sedimentation and electrophoretic mobility⁴. These electron microscopic images of the “microsomes” were the first visual insights into the ribosome structure and they helped in constructing the first three dimensional models of ribosomal subunits that were later established. During 1950s RNA-containing particles attracted more and more attention. Around 1955, RNA was agreed to be providing template upon which amino acids were assembled into protein threads. In 1958, Howard Dintiz coined the term ‘ribosomes’ for the first time. From 1960s onwards was marked the “golden age of translation” research. Research on mRNA, components of the ribosome and investigation into stages in translation emerged. Biochemistry of protein synthesis became the focus of molecular biology and in vitro systems remained central to the field but the procedures changed. With the advent of atomic resolution crystal structures of ribosomes, the translational research took off like never before.

Ribosome Structure

Ribosomes are universally composed of two subunits: a large subunit (50S in bacteria, and 60S in eukaryotes) and a small subunit (30S in bacteria, and 40S in eukaryotes). The general outline of the 70S ribosomes was characterized by several

electron microscopic techniques in 1980s. From these investigations, the structure of 30S subunit is explained as consisting of a head, connected by a neck to a body with a shoulder and a so-called platform. The 50S subunit was described as having a more compact structure. It has a rounded base with three almost cylindrical extensions (figure 1). The three protuberances as seen from the interphase between the two subunits are called the L1-stalk, the central protuberance and the L7/L12 stalk. Introduction of single particle cryo-electron microscopy (cryo-EM) images marked a leap in achieving high resolutions ribosome structures. With improved resolution, details like the beak and toe or spur on the 30S and a tunnel through the 50S were added to the already existing structural features^{5,6}.

Structural studies of bacterial 70S ribosomes namely, the *Thermus Thermophilus* SU^{7,8}, *Haloarcula marismortui* and *Deinococcus radiodurans* LSU^{9,10}, and *E.coli* and *T.thermophilus* 70S ribosomes. Crystal structure of the ribosome at 5.5 Å resolution^{11–13} have pioneered in the field of high resolution X-ray crystallography studies of translational apparatus. They have revealed the complex architecture resulting from the network of interactions connecting the ribosomal(r)-proteins with each other and ribosomal RNA (rRNA).

In contrast to their bacterial counterparts, eukaryotic ribosomes are much larger and more complex. They contain additional rRNA called expansion segments, additional r-proteins and r-protein extensions (figures 3A and 3B).

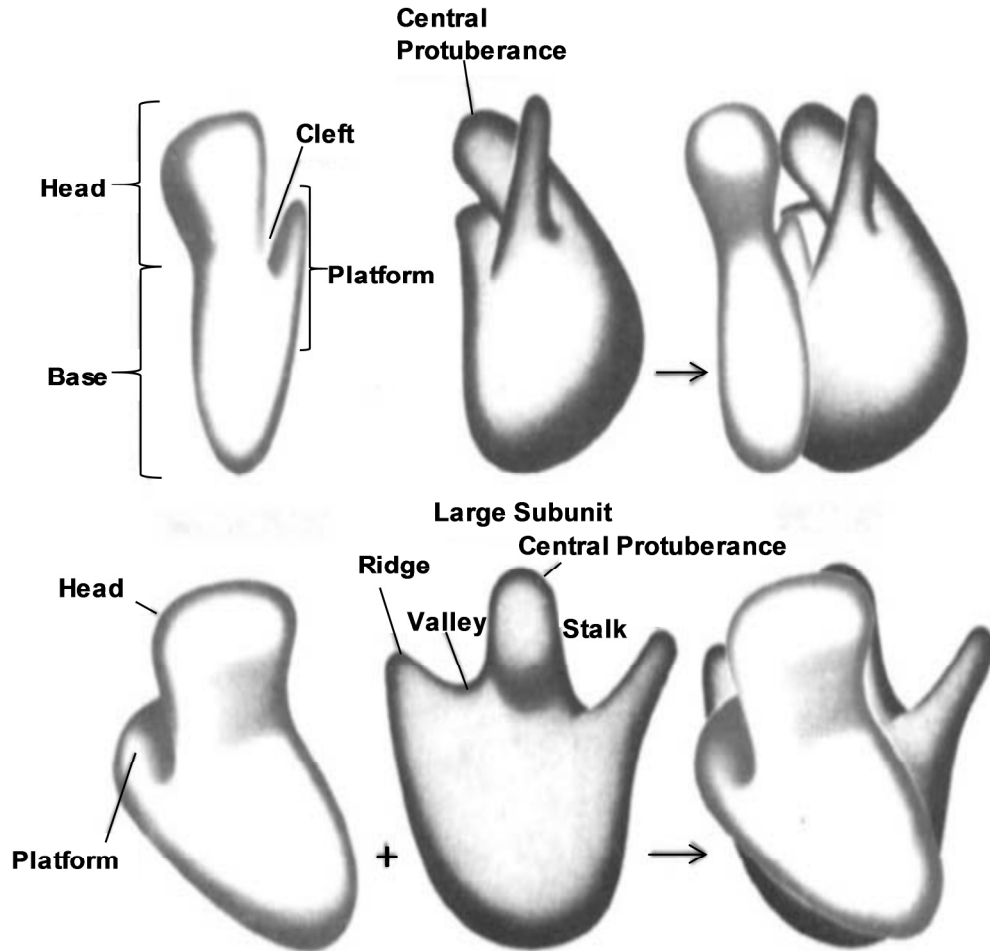


Figure 1 Free hand drawings of the three-dimensional consensus model of the ribosome in 1980s.

The ribosome consists of two asymmetrically shaped subunits. The shape of small subunit includes a head, a base and a platform. The large subunit has a central protuberance, flanked by stalks (L1 and L7/L12) on both sides. Figure adopted from Lake (1985)¹⁴

Eukaryotic ribosomes contain >5,500 nucleotides of rRNA (18S, 25S, 5S and 5.8S) and 80 proteins (79 in yeast). Initially, the structure of eukaryotic ribosome was also explained using cryo-EM maps fitted with structures of bacterial and archaeal subunits^{8,9}; which led to the placement of 46 eukaryotic proteins with bacterial/archaeal homologs as well as many expansion segments (ES)^{15,16}. Subsequent cryo-EM reconstructions led to identification of the location of other bacterial or archaeal r-

proteins homologs, eukaryote-specific r-proteins and additional ESs^{17–20}. However, the full assignment of r-proteins in yeast and fungal ribosomes, became possible only with the high resolution crystal structures of SSU and LSU of *Tetrahymena thermophila*^{21,22} and *Saccharomyces cerevisiae* 80S ribosomes²³.

The overall structures of the two subunits are preserved in eukaryotes. Addition of extra rRNA and r-proteins however, results in a more complex 3.6KDa ribonucleoprotein particle. The major difference between the bacterial and eukaryotic rRNA lies in the presence of five ESs (ES3^S, ES6^S, ES7^S, ES9^S and ES12^S) and five variable regions (VRs) (h1, h16, h17, h33, h41) on the SSU, as well as 16 ESs (ES3^L, ES4^L, ES7^L, ES9^L, ES10^L, ES12^L, ES15^L, ES19^L, ES20^L, ES24^L, ES26^L, ES27^L, ES31^L, ES39^L and ES41^L) and two VRs (H18-18 and H38). Most ES^Ls are present on the back and sides of the particle in LSU, particularly behind the P-stalk (ES7^L and ES39^L), behind the L1-stalk (formed by the clustering of ES19^L ES20^L ES26^L ES31^L) and the flexible ES27^L; leaving the subunit interphase, the core and the exit tunnel unaffected^{18,19,21,23}. On the SSU, majority of the additional rRNA comprises of ES3^S and ES6^S, which cluster together to form an additional feature on the SSU called the “left foot”^{19,22,23}.

35 of the 79 yeast ribosomal proteins have bacterial or archaeal homologs, whereas 32 only have archaeal homologs and thus 12 r-proteins of yeast are eukaryote specific. Cytoplasmic ribosomes of *Tetrahymena* and higher eukaryotes contain an additional r-protein, L28e. Together with the ES, the additional r-protein mass also predominantly locates to the solvent surfaces of the ribosome.

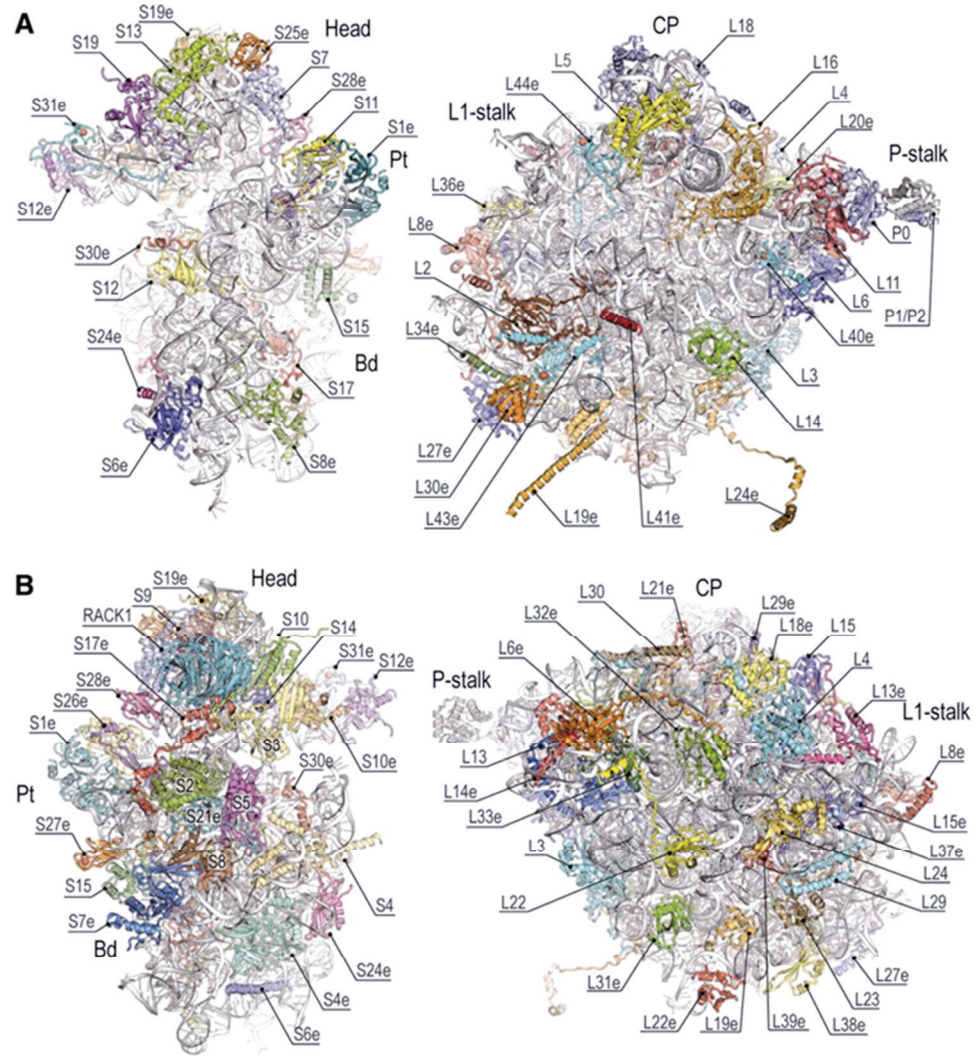


Figure 2 Architecture of the 80S ribosome. Location of ribosomal Proteins

(A) Interface or “front” view of the 60S subunit (left) and 40S subunit (right). Landmarks include head, body (Bd), and platform (Pt) of 40S as well as central protuberance (CP), L1 stalk, and P stalk of 60S. (B) Solvent-side or “back” view of the 60S and 40S subunits. Figure from Ben-Shem et al.²³

Most of the conserved r-proteins have extensions which can establish long-distance interactions up to 100 Å from the globular core of the protein (S5, L4, L7 and L30). Most of the additional protein mass is also located in a ring around the back and the sides of the LSU. Several eukaryote specific r-proteins and r-protein extensions of

conserved proteins interact with expansion segments to make the extra LSU mass. In the SSU, most of the eukaryote specific r-proteins and expansion segments are concentrated to the back of the SSU particle, forming a web of interactions with each other as well as other r-proteins and rRNA. The beak of the SSU acquired three r-proteins, S10e, S12e, and S31e. R proteins also interact with the expansion segments through S4e, S5e, S7e and S8e. The long carboxy-terminal of S6e is thought to be involved in recruitment of specific regulatory factors²². Differences are observed in the mRNA exit site. rRNA features in bacterial ribosomes are also replaced by r-proteins in eukaryotic ribosomes. Distinct elements found within the 5' untranslated mRNA region and divergence from the bacteria in initiation phase of translation can be explained by the change in ribosomal architecture.

During translation, ribosomes undergo a number of conformational rearrangements. These changes involve intersubunit rotation and swiveling of SSU. The interactions between two ribosomal subunits are called intersubunit bridges that change with each conformational rearrangement, and are therefore dynamic in composition. The bridges in eukaryotic ribosomes have been mapped using cryo-EM and X-ray crystallographic methods^{19,20,23}. Unlike bacterial ribosome that preferentially adopts unrotated state; the eukaryotic ribosome seems to prefer the rotated state^{23,25–27}. The surface interactions at the intersubunit region between the two subunits are nearly twice in number as compared to the bacterial 70S. These additional bridges appear at the periphery of the subunit interface and composed mainly of protein-protein and protein-RNA contacts.

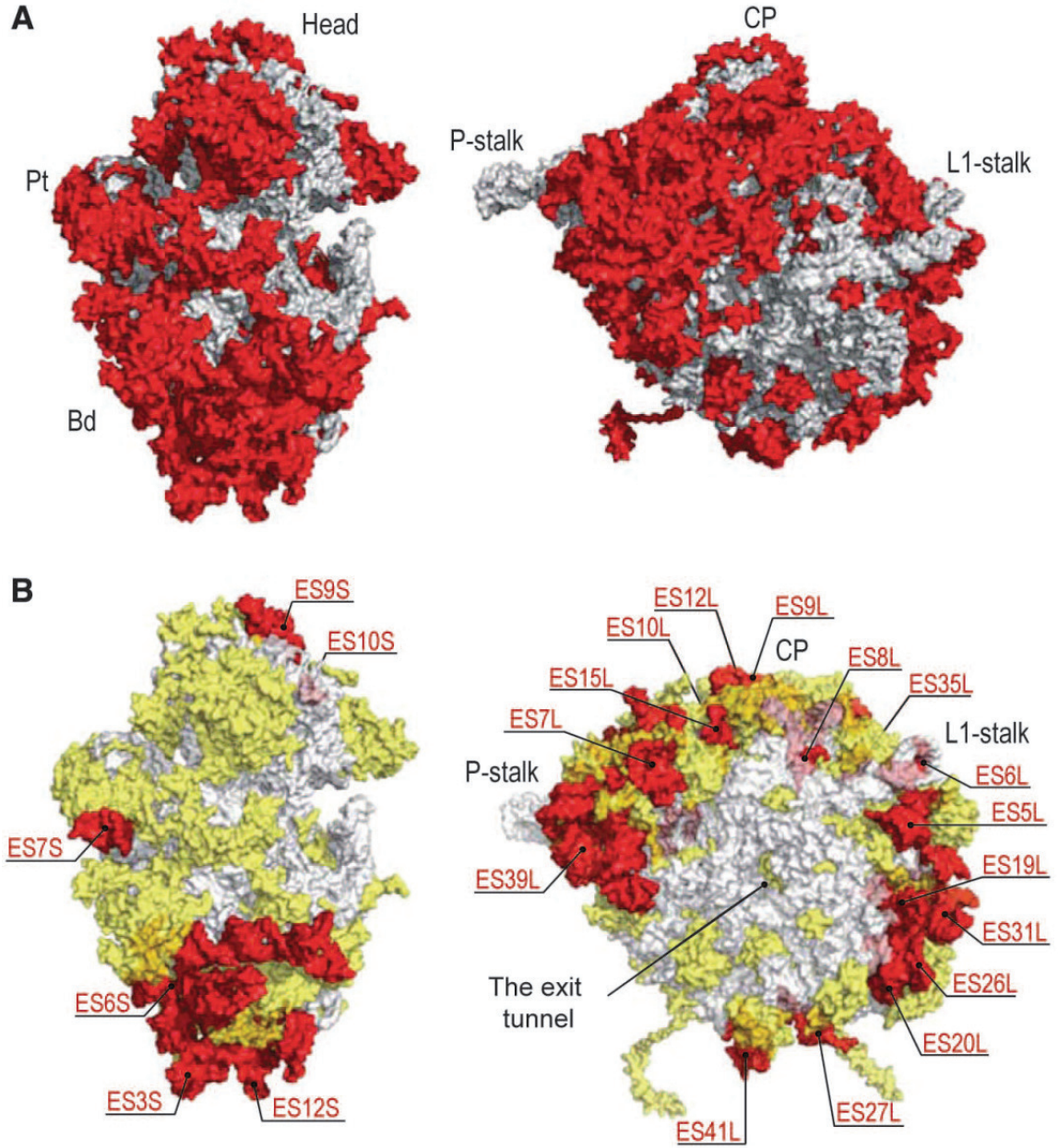


Figure 3 Yeast 80S ribosome structure.

(A) Solvent side of both subunits: Abundance of eukaryote-specific elements in red. (B) Views of the 40S and 60S from back through the peptide exit tunnel. Eukaryote-specific protein moieties are in yellow, rRNA expansion segments in red and the conserved core in gray. Figure from Ben-Shem et al (2011)²³.

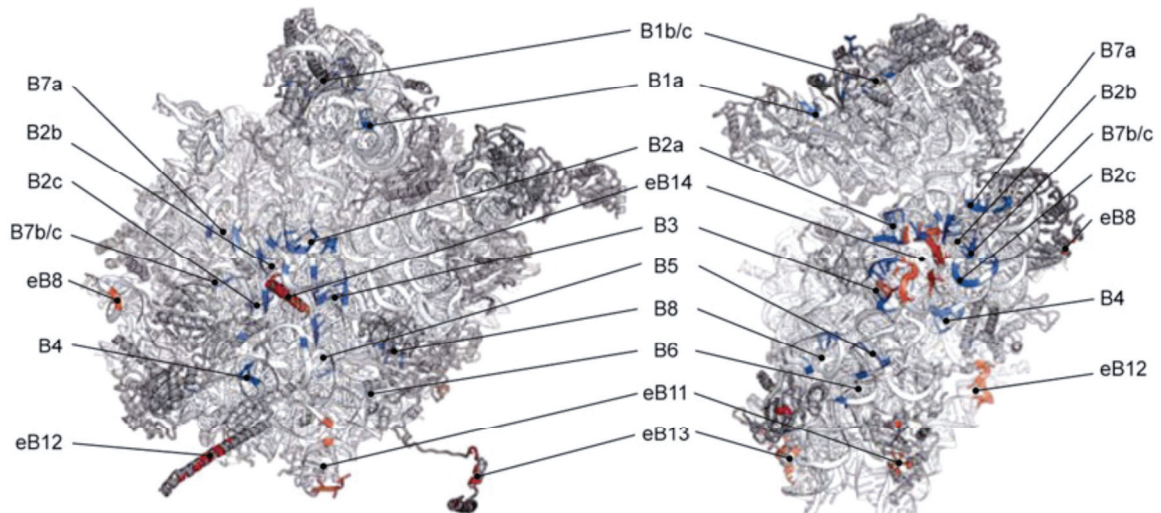


Figure 4 Intersubunit bridges of ribosomal subunits.

Subunit Interface showing residues forming eukaryote-specific bridges in red and conserved ones in blue.

The binding sites for aminoacyl tRNA (A site), peptidyl-tRNA (P-site) and deacylated tRNA (exit or E-site) are predominantly composed of rRNA, which is conserved in eukaryotic ribosomes, suggesting that the mechanism of tRNA selection is also conserved^{28,29}. Many r-proteins also encroach into the tRNA binding sites and appear to play important roles in a slight variation in steps like tRNA accommodation, decoding and translocation in eukaryotes^{23,30}. At the peptidyltransferase center (PTC) in the LSU, the CCA ends of tRNAs are stabilized through interactions with highly conserved (in sequence and structure) A- and P-loops of the 25S rRNA, suggesting that the mechanism of peptidyltransfer is also conserved. However, variable specificity for antibiotic binding between eukaryotic and bacterial ribosomes has indicated subtle differences in their PTCs. These differences are likely to be arising due to the r-proteins. The interactions of E-site tRNA CCA-ends with the ribosomes are also altered because of replacements of L28p with L44e in yeast and archaea.

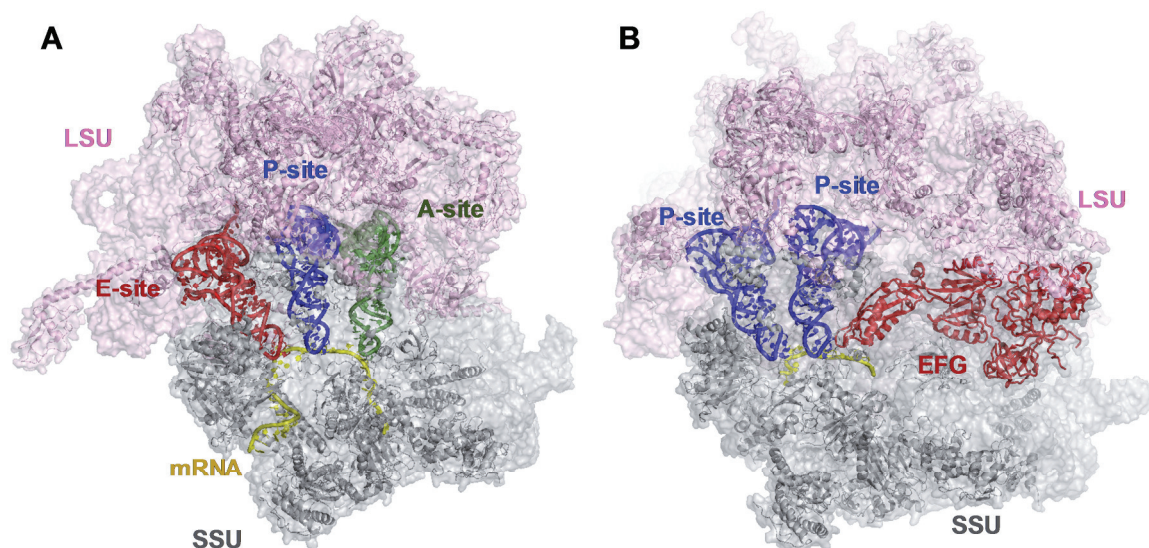


Figure 5 tRNA and elongation factor binding sites on ribosomes.

A. Ribosomes with three tRNAs bound to A-site, P-site and E-sites in green, blue and red. mRNA in yellow. **B.** Ribosome with tRNAs bound in P and E-sites and EF-G in factor binding site. Figures prepared in pymol from atomic resolution crystal structures of *T.thermophilus* ribosomes^{11,31}.

As the nascent peptide chain (NC) is being synthesized, it passes through the tunnel in the LSU and emerges on the solvent side of it. The dimensions of exit tunnel are universally conserved (80Å long and 10-20Å wide), as shown by the cryo-EM reconstructions and X-ray crystallography structures^{10,21,23,32-34}. It is predominantly composed of core rRNA with an overall electronegative charge. Extensions of r-proteins L4 and L22 contribute towards formation of a constriction in the tunnel where it narrows. In eukaryotes and archaea, L39e has replaced bacterial-specific extensions of L23 near the exit of the tunnel^{10,32}. In contrast to its previously suspected role of being a passive conduit for the NC, growing evidence indicates that the exit tunnel plays more active roles in regulating the rates of translation and early protein folding³⁵. Folding of NCs in

the exit tunnel can also have effects on downstream events such as recruitment of the chaperones.

Ribosome biogenesis and assembly

In order to maintain a turnover of about 2000 ribosomes per minute³⁶, rapidly growing yeast cells have to devote a significant fraction of their resources for ribosome synthesis and the membrane trafficking involved. All three RNA polymerases participate; RNA polymerase (Rpol) I and III transcribe the rRNAs and about 60% of the transcripts produced by RNA polymerase II encode r-proteins or ribosomal assembly factors. Majority of the molecular transport going across the nuclear membrane also comprises of the r-proteins and the assembly factors entering the nucleus and the pre-ribosomes exiting the nucleus. More than half of the introns removed by the splicing machinery in yeast occur in the r-protein coding mRNAs³⁷.

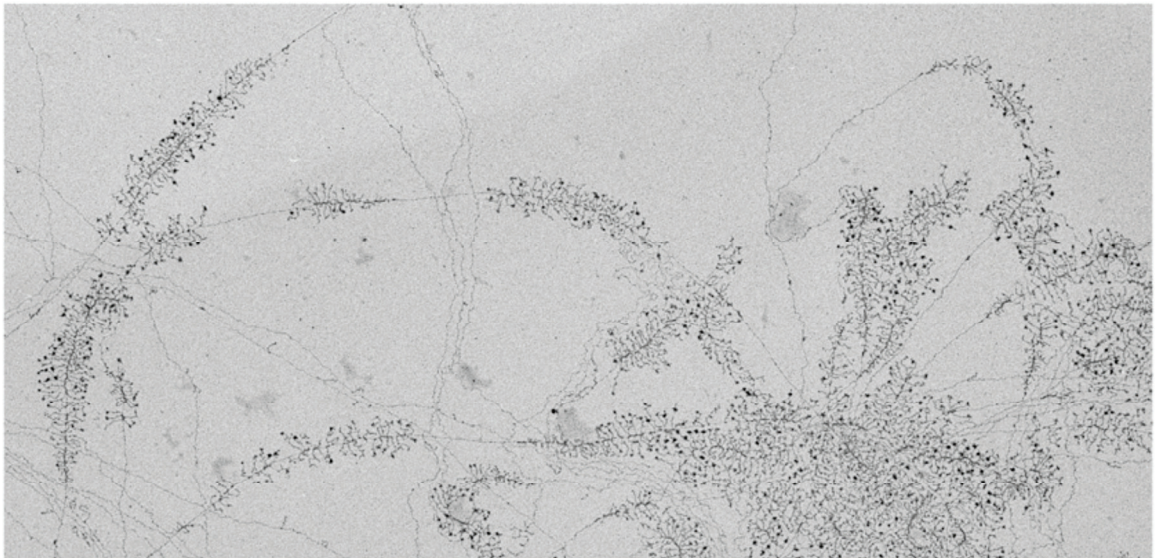


Figure 6 Yeast chromatin spreads of eukaryotic nucleolar contents analyzed by electron microscopy.

Transcription of rDNA repeats can be visualized here as “Christmas trees”; the rDNA depicts the tree trunk, extending rRNA depict branches and then nascent RNPs are the knobs at the branches depicting the ornaments. Figure from Woolford and Baserga (2013)^{37,38}

Transcription of Pre-rRNAs

Ribosome biogenesis takes place in the non-membrane bound compartment of the cell nucleus called the nucleolus. The nucleolus is formed around the ~150 tandem rDNA repeats found on chromosome XII and is defined by the extent of ongoing transcription by Rpol I for ribosome biogenesis³⁹. Rpol I maintains an elongation rate of 40-60 nt/sec⁴⁰ and accounts for 60% of total cellular transcription in yeast. The holoenzyme has 14 subunits most of which are either shared or homologous to the subunits of RNA polymerase II or III. Its recruitment to the rDNA is regulated by general transcription factors like UAS-upstream activity factor (UAF), TATA-binding protein (TBP), core factor (CF) and Rm3. The rRNA synthesis step is regulated by transcription initiation and the ratio of active to inactive rDNA repeats^{41,42}. During growth of *S.cerevisiae*, the number of active rDNA genes decreases from growth to stationary phase.

Transcription of 35S primary transcript by Rpol I generates an initial 6.6 kb pre-rRNA, which includes RNA sequences destined for 18S, 5.8S and 25S and also the additional 5'externally transcribed spacer (5'ETS), internally transcribed spacers 1 and 2 (ITS1 and ITS2), and a 3' externally transcribed spacer (3'ETS). The 5S rRNA is transcribed by Rpol III in the opposite direction as shown in figure 7.

Processing, folding and modification of Pre-rRNA

The four spacers contained in the pre-rRNA transcript are removed by endonucleolytic and exonucleolytic processing. RNase III endonuclease Rnt generates 3'-end of the primary PreRNA 35S to begin the processing. Cleavage of either of the 5'ETS or ITS1 at one of the sites amongst A₀, A₁ and A₂ can occur first generating 33S, 32S and 20S+27S_A respectively. Cleavage at site A₂ in ITS1 splits the pathway for pre-rRNA processing and subunit maturation. Optionally, there can be a separating cleavage in the site A₃, 23S and 27S_{A2} pre-rRNAs. The 20S pre-rRNA is packaged in 43S particles and 27S pre-rRNA is assembled into 66S pre-RNPs. The 43S pre-RNPs are exported from the nucleolus through nucleoplasm to the cytoplasm where the 20S pre-RNA undergoes final endonucleolytic cleavage at site D to remove the remaining ITS1 segment.

However, the maturation 66S pre-ribosomal particle is more complex and takes longer. 27S_{A2} pre-RNA processing continues in the nucleolus in two alternative ways; about 85-90% of 27S_{A2} Pre-rRNA is shortened to 27S_{A3} form by endonucleolytic cleavage and finally the remaining ITS1 spacer is removed by 5'-3' exonuclease to form 27S_{B_S}, while the other 10-15% of 27S_{A2} pre-RNA undergoes direct endonucleolytic cleavage at the B1_L site to generate 27S_{B_L} pre-rRNA. 27S_{B_S} and 27S_{B_L} undergo similar identical endonucleolytic cleavage at the site C₂ in ITS2 to generate 25.5S and 7S_S or 7S_L pre-RNAs. The 5' end of the 25.5S-preRNA is trimmed by Rat1 endonuclease to generate mature 25S. The 3' ends of 7S pre-rRNA are processed in several steps to produce 5.8S_S and 5.8S_L that differ by 6 nucleotides, both functional.

The steps involved in rRNA processing in ribosome assembly are outlined in figure 7. However, there is not necessarily an obligatory order for the entire processing pathway. The apparent order of the processing reactions can be dictated by the availability and identification of sites. The pre-rRNA processing occurs co-transcriptionally, which indicates that the transcriptional precedence of sequences can decide the order of steps in processing. Pre-rRNAs undergo heavy modification, largely in the form of 2'-*O*-ribose methylation or pseudouridylation. These modifications can take place co-transcriptionally with the help of snoRNPs. snoRNPs are composed of snoRNAs and several protein components, amongst them are enzymes that catalyze nucleotide modification.

Ribosomal proteins play important role in subunit assembly. R-proteins and assembly factors bind to the 35S pre-rRNA from the very start. Binding of r-proteins is thought to stabilize the correctly folded rRNA. Binding of r-proteins alters rRNA structure locally and distally to create binding sites for subsequently joining r-proteins, or to trigger conformational switch required for spacer removal³⁷. The pre-rRNA spacer sequences can form alternative conformers by base-pairing with the sequences destined to be retained in mature ribosomal subunits. In addition to r-proteins ~200 assembly factors participate in ribosome biogenesis. Among these proteins are the endo- and exonucleases required for pre-rRNA processing, enzymes that modify rRNA or r-proteins, RNA helicases/ATPases, AAA ATPases, GTPases, kinases and phosphatases, RNA-binding proteins, putative scaffolding proteins etc.

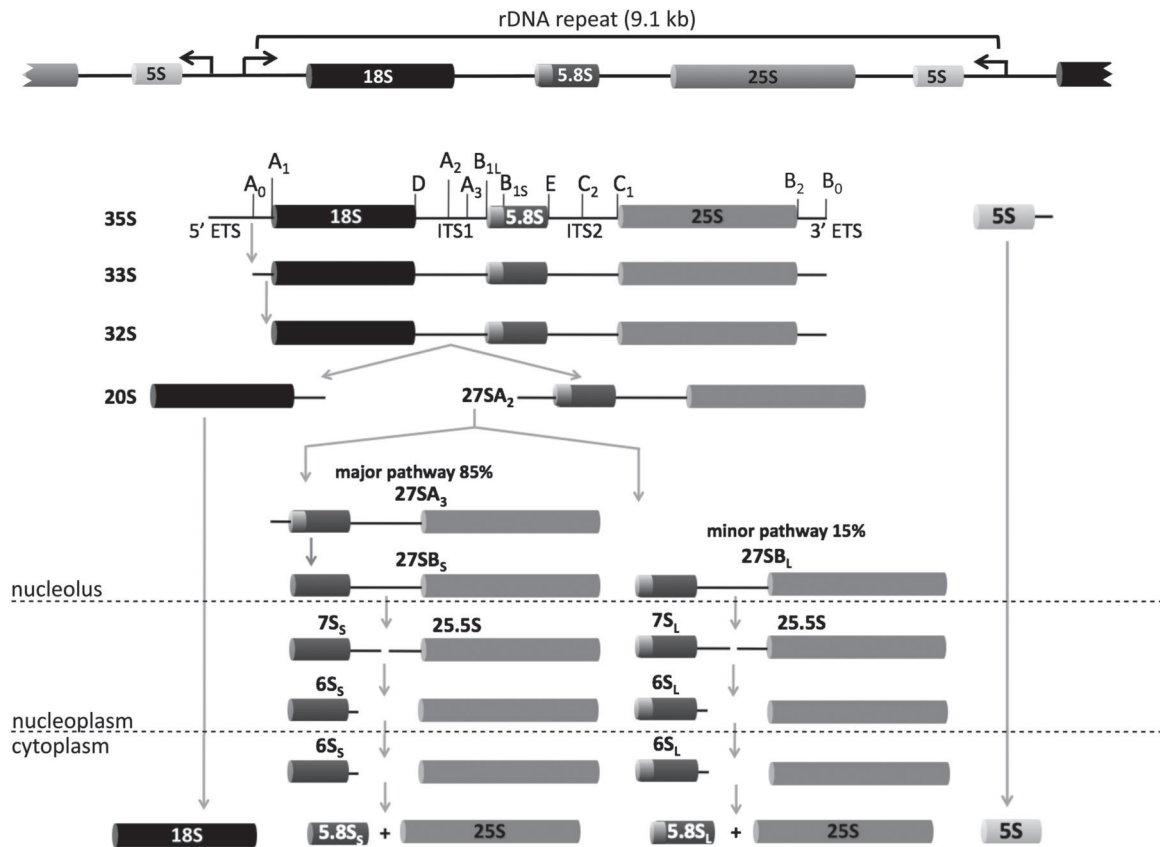


Figure 7. Yeast pre-rRNA processing pathway.

The 35S pre-rRNA synthesized by RNA Polymerase I contains sequences for 18S, 5.8S and 25S rRNA, flanked and separated by internal and external transcribed sequences. Spacer sequences are removed from the pre-rRNA by endo- and exonucleolytic processing. The 5S rRNA is transcribed by RNA polymerase III and incorporated into the 66S pre-RNP.

Nuclear export of Pre-40S and Pre-60S particles

In rapidly growing yeast cells preribosomal particles are transported through each nuclear pore at a rate of one per 2-3 seconds³⁶. The yeast cells need to overcome challenges like navigating the preribosomes with hydrophilic surfaces through the nucleoporins containing hydrophobic mesh of FG repeats and avoiding the export of incompletely or improperly assembled preribosomes. Components of the general nuclear

export machinery, that include the nuclear export receptor Crm1, Ran GTPases and several nucleoporins are necessary for export of nascent ribosomal subunits in yeast^{43–45}. Depletion of many r-proteins also affects the nuclear export of pre-ribosomal particles either directly by hampering the recruitment of export adaptors or indirectly by blocking assembly or failure to recycle export factors back to the nucleus. During late steps in nuclear assembly, mechanisms of “structural proofreading” are used by cells to ensure quality control and segregate only correctly assembled preribosomal subunits for export.

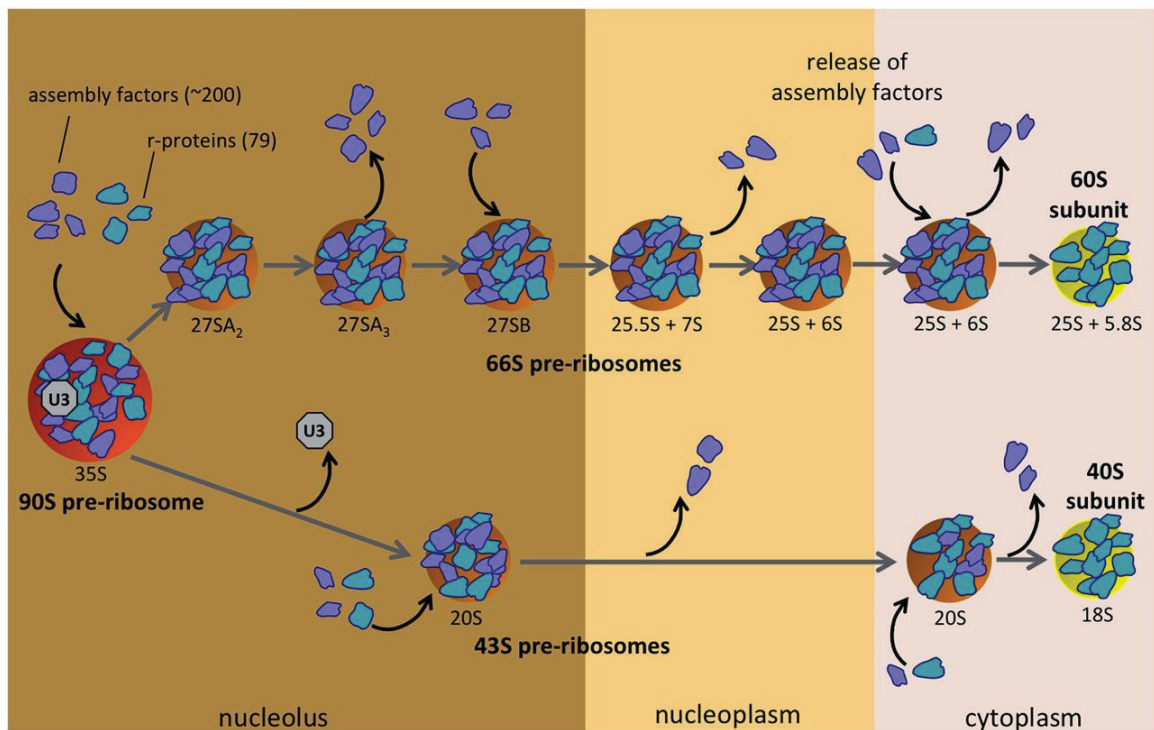


Figure 8 Preribosomal maturation pathway to form 40S and 60S ribosomal subunits.

Sequential assembly intermediates are shown, distinguished by pre-rRNA processing intermediates. Most r-proteins and assembly protein associate with the pre-RNPs in the early stages of assembly. Some bind in the middle stages and others in the late assembly. Woolford J L , and Baserga S J Genetics 2013³⁷.

Cytoplasmic maturation of Pre-40S and 60S subunits

Newly admitted nascent 40S and 60S subunits complete their maturation to functional subunits in several steps in order to overcome challenges of last stage of assembly like: 1. Assembly of last r-proteins, and release and recycling of several assembly factors. 2. Preventing premature association of newly exported, but yet inactive subunits with the translation machinery. 3. Inspection of the functional domains for their correct assembly

R-proteins assembled into the pre-60S subunit before maturation includes L10, L24, L29, L40, L42, P0, P1, and P2. NTPases like Drg1, Efl1, and Lsg1 are present on cytoplasmic pre-60S subunits. These factors need to be released and recycled back into the nucleus for early assembly of new ribosomes. Pre-40S subunit exported to the cytoplasm lacks r-proteins S10 and S26 and retains seven assembly factors which are well-positioned to shield pre-40S subunit from premature association with the translation initiation machinery. Pre-60S subunits are prevented from participating prematurely in translation by blocking their association with 40S subunits. This is achieved by the binding of Nmd3 and Tif6 in the subunit interphase region of Pre-60S⁴⁶⁻⁵⁰.

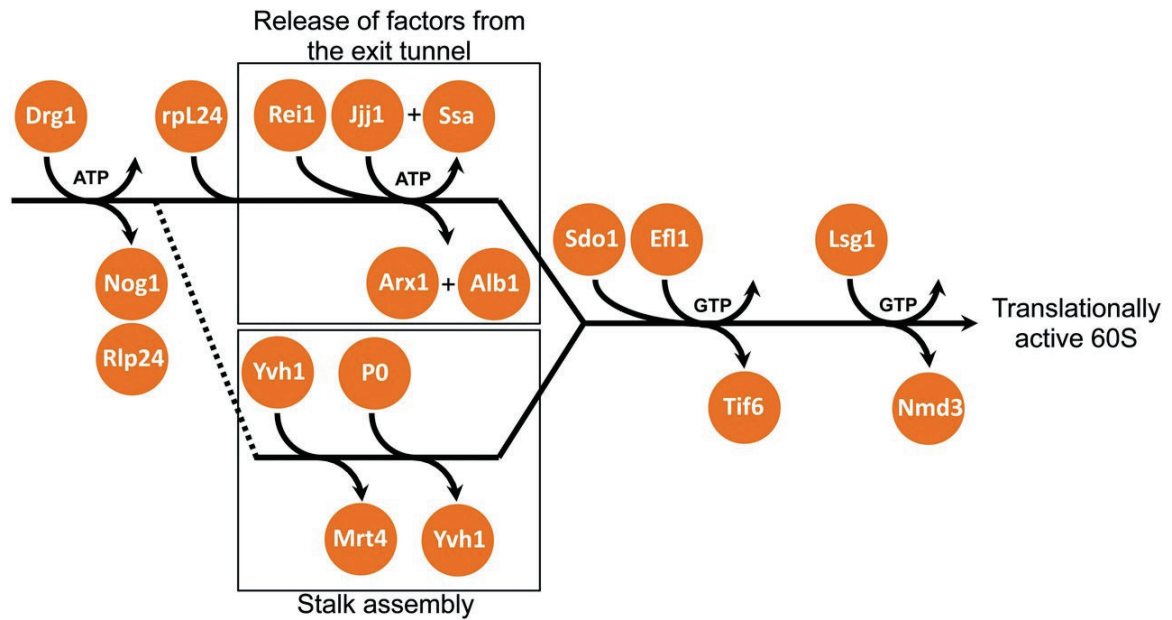


Figure 9 Late Steps of maturation of Pre-60S subunits in cytoplasm.

A bulk of nuclear assembly factors is released from 66S preribosomes in the cytoplasm by ATPase Drg1, GTPases Efl1 and Lsg1, and factors like Sdo1. Few last r-proteins like L24 and P0 are assembled and replace their nuclear homologues.

Surveillance and Turnover of misassembled ribosomes

In order to prevent the accumulation of malfunctioning ribosomal particles resulting from misassembled pre-ribosomes, mechanisms of destruction of such faulty subunits is of crucial importance to the cell. Exonucleases in the exosome complexes are functional in turnover of the aberrant pre-rRNA processing intermediates^{51,52}. It is not clear how improperly assembled preribosomes are recognized. However several mechanisms like turnover machinery present in the preribosomes, a hypothesized kinetic proofreading mechanism or a role of the 19 DEAD-box ATPases have been proposed to be functional in the surveillance of ribosome biogenesis.

Translation

Once properly assembled and after passing through a strict quality control, the two ribosomal subunits can begin synthesizing proteins by adding amino acids to the growing peptide chain at the rate of 60s^{-1} and accuracy of 1 error per 10^4 incorporations⁵³. Ribosomes accomplish the task of protein synthesis by decoding the mRNA one codon at a time with the help of matching charged tRNAs and other associated translation factors. Ribosomes go through three distinct phases of translation called initiation, elongation and termination. After completing the initiation step, as the ribosomes move on to decode the rest of the mRNA in elongation, new ribosomes can start initiation and begin protein synthesis. Thus, at any given time there can be several ribosomes synthesizing proteins on the same mRNA forming polysomes. Translation terminates when ribosomes encounter stop codon and release the polypeptide chain. Peptide release is followed by a much less understood ribosome recycling step which results in separated ribosomal subunits ready for a new round of translation. Structural differences between bacterial and eukaryotic ribosomes have led to differences in mechanism of translation as well. While the elongation step is mostly conserved, significant differences lie between bacterial and eukaryotic translation initial and termination steps.

Initiation

Initiation of translation is the rate limiting step in protein synthesis. It requires a steady supply of ribosomal subunits, initiator tRNA, mRNA and a long range of initiation factor proteins, and thus it is an important target for regulation. Figure 10 presents the

basic outline of eukaryotic cap-dependent initiation pathway. Translation initiation begins with identification of initiation codon by the translation machinery.

The first step is formation of ternary complex (TC) composed of initiator methionyl-tRNA (Met-tRNA_i) and the GTP-bound form of eukaryotic initiation factor 2 (eIF2); which then binds to the small (40S) subunit to form the 43S pre-initiation complex (PIC). In yeast, eIFs 1, 1A, 5 and eIF3 form a multifactor complex with TC, resulting in a network of physical interactions linking them all together and promoting TC binding to the 40S⁵⁴.

Equipped with the MFC, 43S PIC is now ready to bind to the mRNA near the 5'-7 methylguanosine cap in a process facilitated by the eIF3, the poly(A) –binding-protein (PABP), eIFs 4B, 4H and 4F. The eIF4F complex comprises of, cap-binding protein eIF4E, RNA helicase eIF4A, and scaffold protein eIF4G that harbors binding domains for PABP, eIF4E, eIF4A, eIF3 and RNA. This enables eIF4G to coordinate interactions with mRNA via the cap, poly(A) tail, and sequences in the mRNA body to assemble a stable, circular messenger ribonuclearprotein (mRNP), referred to as the “closed loop” structure. The helicase activity of eIF4A is thought to generate a single stranded landing platform on the mRNA where the 43S PIC loads with the help of stimulating interactions between eIF4G and eIF3^{55,56}.

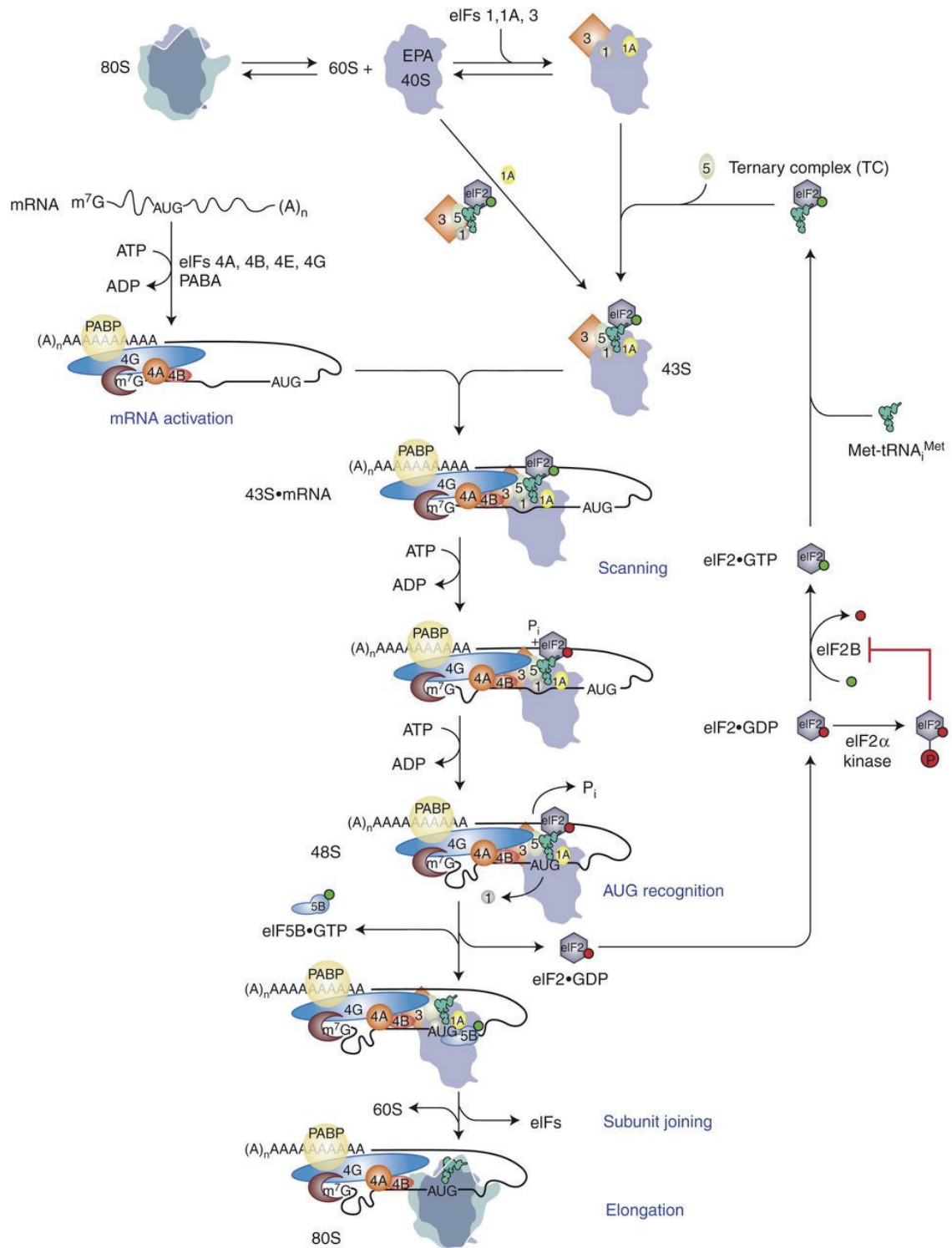


Figure 10 Canonical eukaryotic translation initiation pathway.
Hinnebusch and Lorsch (2012)⁵⁷

After binding near the cap, the 43S PIC scans the mRNA leader sequence for an AUG start codon in a suitable context^{56,58}. Start codon recognition occurs by base-pairing between the AUG codon and Met-tRNA_i anticodon in the P site of the 40S subunit causing arrest of scanning PIC and triggering conversion of eIF2 in the TC to its GDP bound state via gated P_i release. Following GTP hydrolysis, the eIF2·GDP is released from the PIC and must be recycled to eIF2·GTP for renewed TC assembly through a reaction catalyzed by the hetero-pentameric guanine exchange factor (GEF) eIF2B. After the start codon has been recognized, the remaining factors must dissociate from the complex and the 60S subunit must join the 40S subunit to form the final 80S initiation complex (IC) with Met-tRNA_i and start codon in the P-site ready to begin the elongation phase of protein synthesis^{55,56}. Subunit joining is facilitated by a second GTPase initiation factor eIF5B⁵⁹. Interactions of the initiation factors with each other, with the ribosome, mRNA and tRNA have been characterized in detail using mutational analysis, high resolution X-ray crystallography, cryo-EM, hydroxyl radical mapping and toe printing experiments⁶⁰⁻⁶⁵. Additional structural studies are still required to fully elucidate the roles of different initiation factors in conformational transitions associated with scanning, start codon recognition and subunit joining.

Viral Hijack of translation initiation

Viruses are obligate intracellular parasites, and their replication requires exploiting the host cellular functions. Lacking their own translational apparatus, they must recruit host cellular ribosomes in order to translate viral mRNAs and produce

proteins required for their replication. Viruses employ variety of strategies to exploit the translation machinery to their advantage and impairing the translation of host mRNAs.

One of the strategies is to impair the host translation initiation called “host shut-off”, while the viral protein synthesis proceeds via an alternate initiation mechanism relying on cis-acting RNA elements. Some viruses do this directly. Poliovirus (an enterovirus), feline calcivirus and retroviruses encode proteases that can cleave eIF4G, rendering it non-functional and impairing the host translation initiation^{66–68}. Enterovirus 7 infection induces miRNA expression which reduces eIF4E abundance, while Vesicular stomatitis virus, influenza virus and adenovirus reduce the phosphorylation levels of eIF4E, hampering host translation⁶⁹. Some viruses impacts indirectly like Encephalomyocarditis virus infection causes inactivation of 4E-BP, a protein that indirectly affects translation initiation⁷⁰. In influenza virus, hantavirus and yeast L-A virus infections, a unique phenomenon called “cap-snatching” occurs, where m⁷GTP caps on the viral RNAs are derived from host mRNAs, inducing viral but inhibiting cellular translation^{71–73}.

Cap-independent translation is implemented in some viral mRNAs to circumvent host defense. For e.g. in Calcivirus has the VPg, a virus-encoded protein is covalently attached to the 5' end of their RNA genome instead of m⁷GTP. The VPg can interact with the initiation factors allowing translation of viral RNAs.



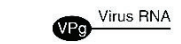
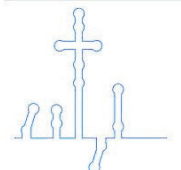
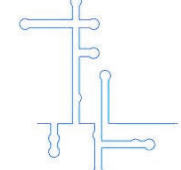
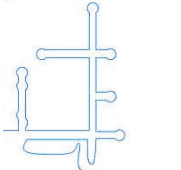

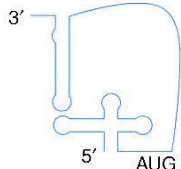
RNA structure		Primary eIF target(s) for 40S recruitment/virus
 m ⁷ Gppp Virus mRNA	5' cap	eIF4F/herpesvirus, poxvirus, ASFV
 m ⁷ Gppp Cell virus mRNA	Cap-stealing	eIF4G/influenza eIF3?/hantavirus
 VPg Virus RNA	Cap-substitute	eIF4E/TEV eIF3/calicivirus eEF1A/TuMV
	Type I IRES	eIF4G (C-term)/poliovirus eIF4G, 4E/HAV
	Type II IRES	eIF4G/EMCV
	Type III IRES	eIF3/HCV
	Type IV IRES	None/CrPV
	3' CITE	eIF4E/PEMV eIF4G/BYDV eIF4F/STNV, MNeSV

Figure 11 Alternate ways of recruitment of 40S ribosomal subunit to viral mRNAs. Borrowed from Walsh D et al. Cold Spring Harb Perspect Biol (2013)⁷⁴⁷⁴.

Several viruses contain internal ribosomal entry sites (IRESs) within their 5' untranslated regions that directs initiation through interactions with eIFs or r-proteins⁷⁵. IRES dependent translation initiation may require no initiation factors at all. Various classes of IRESs have been described as shown in figure 11. The complicated structures of IRESs mimic the Pre-initiation complex and trick the 40S to be recruited. This

overcomes the rate limiting step of initiation and thus the cap-independent translation of IRES containing messages can proceed. Recently IRESs have been discovered in important cellular mRNAs coding proteins like Bip, p53, c-myc, VEGF, ornithine decarboxylase etc. In the events of stress or starvation when the cap-dependent cellular translation is shut down, IRES mediated translation goes on and at times even favored.

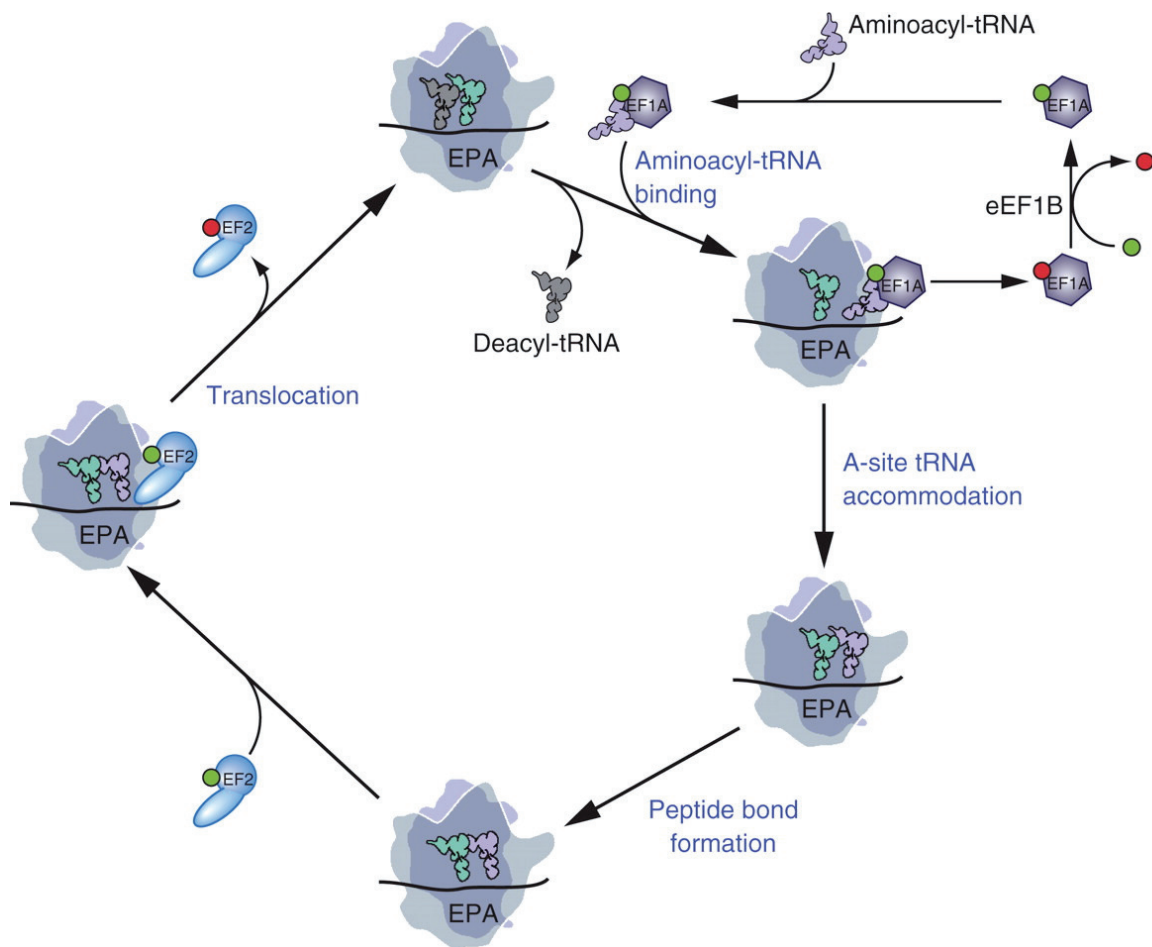


Figure 12 The eukaryotic translation elongation pathway.
Dever T E , and Green R Cold Spring Harb Perspect Biol (2012)⁷⁶

Elongation

Once the ribosome is stably localized on the mRNA at the end of initiation phase, elongation cycle starts proceeding very fast adding one amino acid at a time to the growing peptide chain. The mechanism of elongation is well conserved between eukaryotes and bacteria⁷⁷. Elongation cycle is the fastest phase of translation and most thoroughly studied as well. Summarized below is the current understanding of the key steps in translation elongation cycle.

Aminoacylation and accommodation of tRNAs

Aminoacyl-tRNA binding as a ternary complex with eukaryotic elongation factor1 (eEF1) and GTP to the A-site of the 80S initiation complex is the first step of translation elongation. However, even before it binds to the A-site, the tRNA molecule has to be charged with its cognate amino-acid in a two-step reaction catalyzed by a class of enzymes called aminoacyl-tRNA synthetases (ARS). First, the enzyme activates the cognate amino acid by condensing it with ATP to form a transient molecule, aminoacyl adenylate (AA-AMP) that remains bound to the enzyme's active site ready for the second reaction catalyzed by ARS resulting in formation of an ester linkage between the carboxyl group of amino acid and a hydroxyl group of the terminal 3' adenosine of the tRNA. Cells require at least 20 synthetases, one for each of its amino acids. The aminoacyl tRNA synthetases are the actual translators of genetic code. Their faithful recognition of cognate tRNA depends upon specific interactions between the proteins and identity elements present in tRNA sequences and structures, which are located not only the anticodon bases of the tRNA but also the tRNA acceptor stem⁷⁸⁻⁸⁰. With minor

exceptions, all aminoacyl tRNA synthetases with the same amino acid specificity are orthologs and most individual synthetases have been conserved throughout speciation events and predate the separation of three kingdoms of life. In addition to their aminoacylation activity, several subclasses of ARSs (e.g. Valyl-, leucyl-, and isoleucyl tRNA synthetases) possess an editing activity to prevent misacylation (resulting from activation of stereochemically similar amino acids⁸¹ of their cognate tRNA. This editing domain that catalyzes the hydrolysis of noncognate aminoacyl adenylates or misacylated tRNAs, is inserted into the catalytic domain for aminoacylation, creating a separate active site^{82,83}.

For high efficiency of translation, the ARSs stay in close proximity to the ribosome. Recent evidence has shown that mSerRS and ArgRS interact directly with archaeal ribosomes suggesting a mechanism of tRNA recycling in which ARSs associate with the L7/L12 stalk (P0/P1 stalk in eukaryotes) region to recapture the tRNA released from the preceding ribosome in polysomes⁸⁴. A similar mechanism is suggested by a study on ribosome associated protein Scp160p which might increase the efficiency of tRNA recharging, or prevent diffusion of discharged tRNAs⁸⁵. Specificity of aminoacylation by ARSs, plus their editing capacity and their maintenance in the specific codon niche near the translating ribosomes adds to the efficiency and accuracy of translation. ARSs serve as a potential target for translation control. In bacteria, ARSs serve as antibiotic targets for inhibiting prokaryote specific translation⁸⁶.

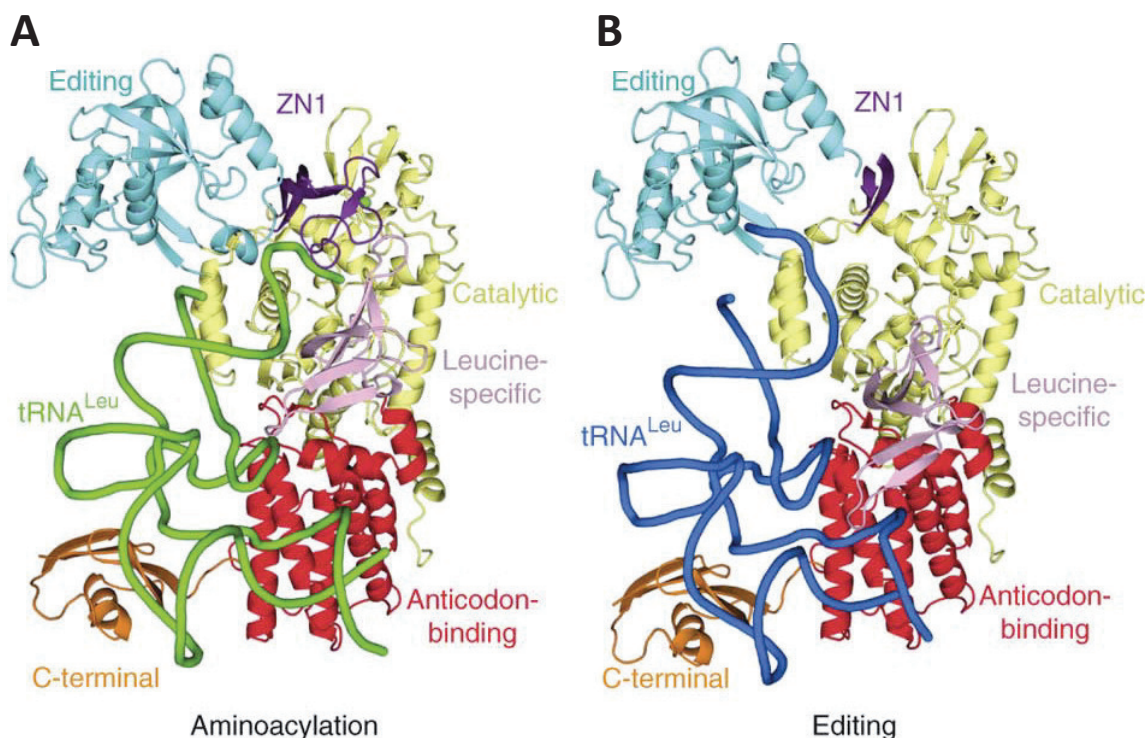


Figure 13 The domain structure of LeuRSEC.

Residue numbers indicate domain boundaries. The color code used throughout this paper for the various domains is as follows: yellow, catalytic domain; purple, ZN1 domain (zinc ion in green); cyan, editing domain; pink, **leucine**-specific domain; red, anticodon-binding domain; orange, C-terminal domain. (b) Aminoacylation conformation with the tRNA in green. (c) Editing conformation with the tRNA in blue. In this state, the ZN1 domain is partially disordered⁸⁷.

A correctly charged tRNA forms ternary complex with eukaryotic Elongation Factor 1 (eEF1) and GTP, in order to get delivered to the A-site of the ribosome for translation to proceed. Details of tRNA accommodation are pictorially explained in figure 14. The eukaryotic Elongation Factor 1 (eEF1) comprises eEF1A, which delivers aa-tRNA to the ribosomes and eEF1B, which acts as a Guanine exchange factor (GEF) composed of two subunits eEF1B α and eEF1 γ . eEF1A is a member of GTPase superfamily and binds and hydrolyses GTP. It binds tRNA in a GTP-dependent manner

and then directs tRNA to the A-site of the ribosome. Codon recognition by the tRNA completes the accommodation triggering GTP hydrolysis by eEF1A, releasing the factor in complex with GDP as a result of conformational change. The spontaneous rate of GDP dissociation from these factors is slow and the GEF is required to recycle the inactive GDP-bound factor to its active GTP bound state. eEF1B α subunit of eEF1B inserts an essential lysine residue into the Mg⁺ and γ -phosphate binding site to destabilize Mg⁺ binding leading to GDP release^{77,88}.

Ternary complex binding to the ribosome is a two-step process. Initial binding or sampling of the ternary complex is the first step in tRNA accommodation, and it results in transient interactions of the ternary complex with elements composing the A-site and placement of the anticodon in the decoding center of the small subunit. Base pairing between the mRNA codon and tRNA anticodon forms the final basis of cognate (or sometimes near-cognate) tRNA selection, rejecting non-cognate ternary complexes quickly and efficiently. Codon-anticodon interaction leads to the formation of a small helix leading to changes in its local environment, such as flipping of 18S rRNA bases A1755, A1756, and G577 from syn to anti-conformation⁸⁹. Accompanying conformational changes lead to the activation of eEF2 GTPase center. Recent high resolution structures of bacterial ribosomes bound to EF-Tu and aminoacyl-tRNA have shown that tRNA anticodon stem suffers structural distortion between the acceptor and the D-stems, allowing it to interact with the decoding site on the small subunit and EF-Tu. It is believed that the codon-anticodon base-pairing occurring only in case of cognate tRNA binding, accompanied by stabilizing interactions between small subunit A-site and

tRNA can energetically allow such a distortion in tRNA, thus promoting high fidelity decoding^{29,90}.

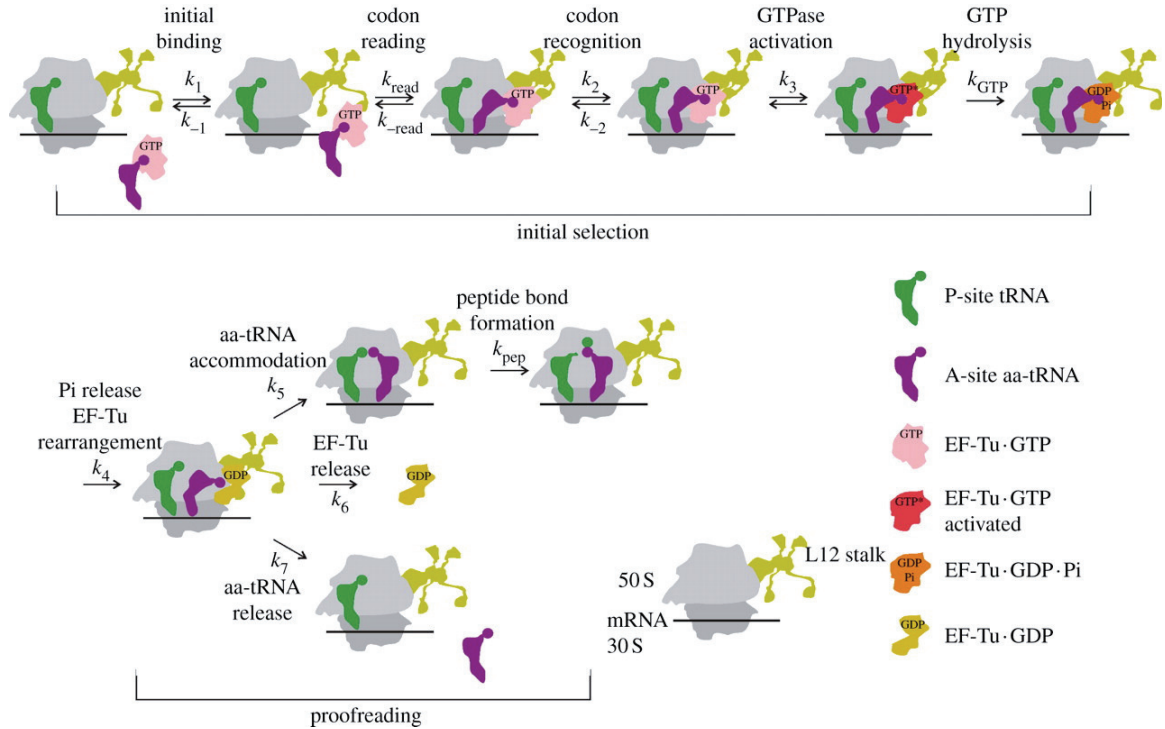


Figure 14 Schematic of EF-Tu-dependent aa-tRNA binding to the A site.

Two step recognition of cognate tRNA by the ribosome. Various steps in tRNA accommodation, represented by forward and reverse rate constants were measured by rapid kinetics or single molecule FRET by Geggier et al. and Blanchard et al.^{91,92} Figure from Wohlgemuth et al.⁹³

The next step in tRNA accommodation, “kinetic proofreading”, which happens after irreversible GTP hydrolysis reaction, ensures the high fidelity of translation⁹⁴. The initial selection of tRNA offers comparatively little discrimination between the cognate and near cognate tRNAs; it is the proofreading step comprising of conformational changes following the codon-anticodon base-pairing, causing an induced fit of cognate tRNA in the ribosomal A-site that accelerates the tRNA accommodation leading to quick peptidyl-

tRNA reaction. Near cognate tRNAs fail to cause such an induced fit and can be rejected even after GTP hydrolysis⁹⁴. It has been shown that in addition to lower dissociation rates cognate tRNAs also have higher forward rates for GTPase activation and tRNA accommodation compared to near-cognate tRNA⁹⁵. The two kinetic steps in tRNA accommodation work in concert contributing towards cognate tRNA selection and translational fidelity.

Peptidyltransfer Reaction

As soon as the aa-tRNA is fully accommodated into the A-site, amino-acyl end of the tRNA enters the peptidyltransferase center, peptide bond formation occurs rapidly and spontaneously⁹⁶. Nucleic acids were not believed to be capable of catalytic activity until the discovery of catalytic RNA^{97,98}. Despite evidence hinting towards it, rRNA was not thought to catalyze peptidyltransferase reaction; instead ribosomal proteins were implicated in catalyzing the reaction. Later, biochemical evidence for the role of 23S rRNA in peptidyltransfer started to accumulate⁹⁹. 50S subunits from *Thermus aquaticus* retained most of their peptidyltransferase activity even after losing 80% of its constituent protein¹⁰⁰. Some of the proteins, like L2 and L3 required for reconstituting the peptidyltransferase activity in-vitro were earlier thought to have the enzyme activity; but later it was shown that these proteins are responsible for maintaining the structural integrity of ribosomal rRNA essential for trapping the tRNA reducing the entropy penalty for peptidyltransferase reaction. The peptidyltransferase center on the large subunit is built up of highly conserved rRNA elements; thus the reaction mechanism is also very likely to be conserved. High resolution X-ray crystal structures demonstrated that the A-

site and P-site substrates align stably and precisely in the active site because of their conserved CCA ends and α -amino groups interacting with the residues of 23S rRNA in the active site. The chemistry of peptide bond formation is explained in figure 15. Peptide bond is formed by nucleophilic attack on the ester carbonyl group of peptidyl-tRNA in the P-site by the α -amino group of aa-tRNA bound to the A-site of PTC.

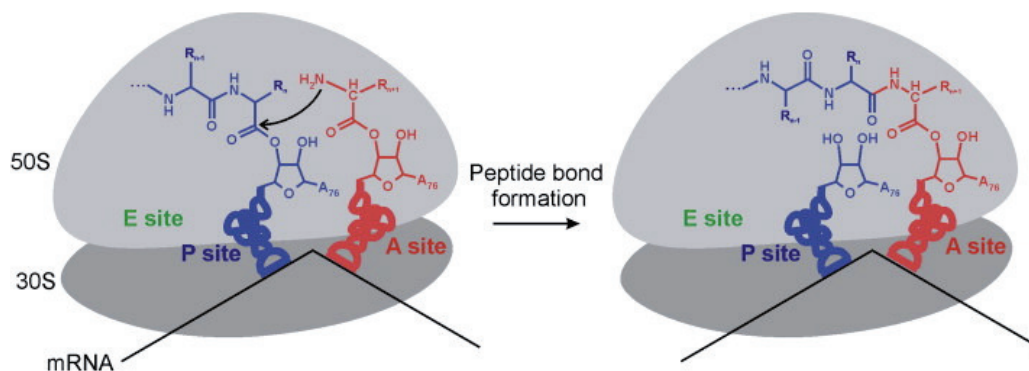


Figure 15 Schematic of peptide bond formation on the ribosome.

The α -amino group of the amino-acyl tRNA in the A-site (red) attacks the carbonyl carbon of peptidyl tRNA in the P-site (blue) resulting into formation of one amino acid longer peptidyl tRNA in the a-site and deacylated tRNA in the P-site¹⁰¹.

The ribosome accelerates this rate by more than 10^6 –fold with respect to the unassisted reaction. Catalysis seems to involve a six-member transition state and the proton shuffling takes place via the 2'-OH of A76 of peptidyl-tRNA^{102,103} (figure 16). Recent studies have shown that the 2'-OH group of the A76 in the peptidyl-tRNA is pivotal in orienting substrates in the active site required for optimal catalysis¹⁰⁴. A favorable entropy change drives the reaction; whereas the usual driving force, change in enthalpy remains small and unfavorable¹⁰⁵. The ribosome provides an electrostatic micro-environment that shields the environment from bulk water, helps in proton shuttle and reduces the free energy of forming a highly polar transition state.

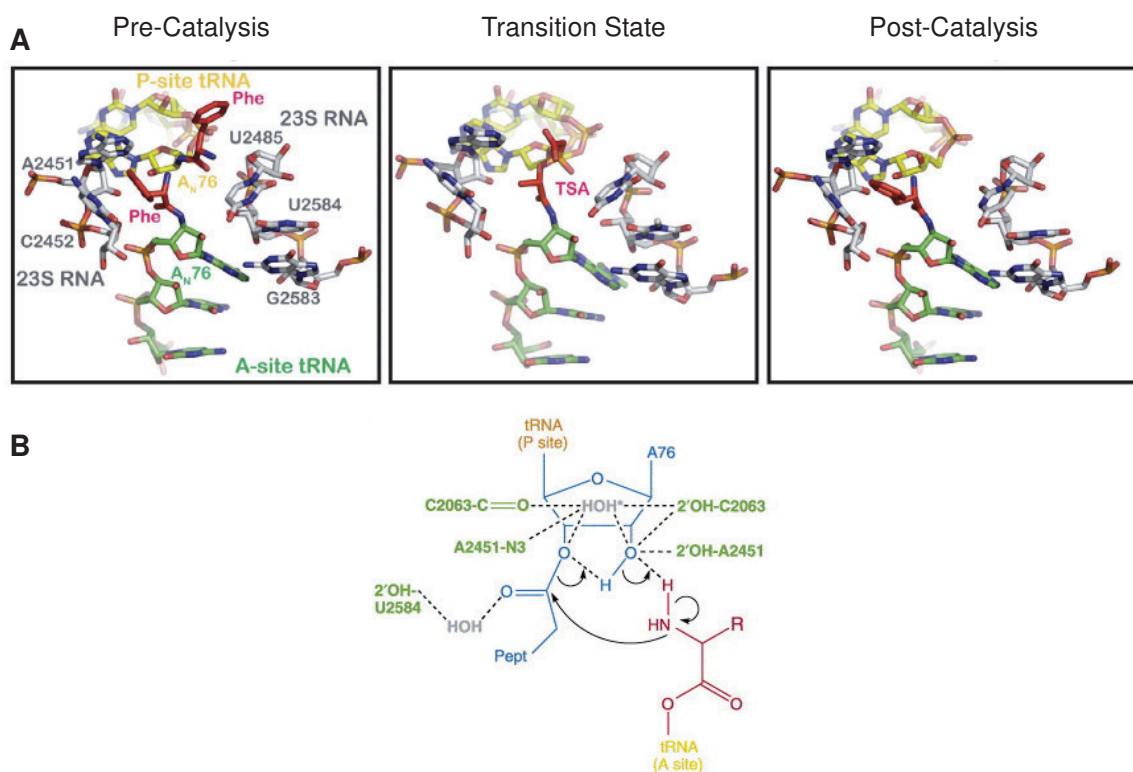


Figure 16 Mechanism of Peptidyl transfer.

(A) The environment of active site during peptidyl transfer: structure of PTC shows the proximity of the 2'-OH group of A76 to the nucleophile and leaving group to the 2'-OH group of A2451. (B) A six membered transition state formed during the peptidyltransferase reaction shows the concerted proton shuttle mechanism^{104,105}

Translocation

With the completion of peptidyltransfer reactions, the peptide chain is transferred to A-site tRNA and covalently bound to it. Interactions of the growing peptide with the peptide exit tunnel anchor the acceptor end of the peptide carrying tRNA to the P-site of the large subunit¹⁰⁶. Thus, as a result of peptidyltransfer reaction, peptide chain grows by one residue and spontaneously forces the acceptor end of the A-site tRNA to the P-site of large subunit and similarly the acceptor stem of the newly de-acylated tRNA is forced to move into the large subunit E-site while the anticodon end is still bound to the P-site in

small subunit. As a result the tRNAs assume hybrid P/E and A/P states leading to inter-subunit ribosomal rotation as shown in the figure 17^{16,107,108}. Due to the formation of hybrid states, the tRNA molecules move with respect to the ribosomes only one end at a time while the other end acts as an anchor stably attached to one of the subunits. The classical and hybrid states of tRNAs in unrotated and rotated states of ribosomes respectively seem to maintain dynamic equilibrium¹⁰⁸⁻¹¹⁰. The event of eEF2 binding in complex with GTP, catches the ribosomes in hybrid state; binds to the ribosomes and shifts the equilibrium towards the rotated state by stabilizing or locking them in rotated state. The ribosomal ability to rotate and interactions of P-site tRNA with the E-site in large subunit are necessary requirements for eEF2 binding^{111,112}. The next step is translocation of the other end; i.e. the anticodon stem loop of tRNA along with the base paired mRNA codon, leading to classical state tRNAs (P/P and E) and unrotated ribosome followed by a quick exit by the deacylated tRNA. The rotated/hybrid state of ribosomes is an early substrate for translocation. After EF2 binding, the GTPase center is activated causing the GTP hydrolysis and phosphate release. As a result, large scale conformational changes are induced in eEF2^{113,114} causing its release from the ribosome, coupled to phosphate release, which helps in preventing the backward movement of tRNAs³¹. Thus, eEF2 has several functions in translocation; stabilizing the formation of hybrid state; inducing the unlocked conformation of ribosomes and preventing the backward movement of tRNA. As the eEF2 is released the subunits are locked in unrotated/classical post-translocation state ready for a new ternary complex to bind and translation to proceed further.

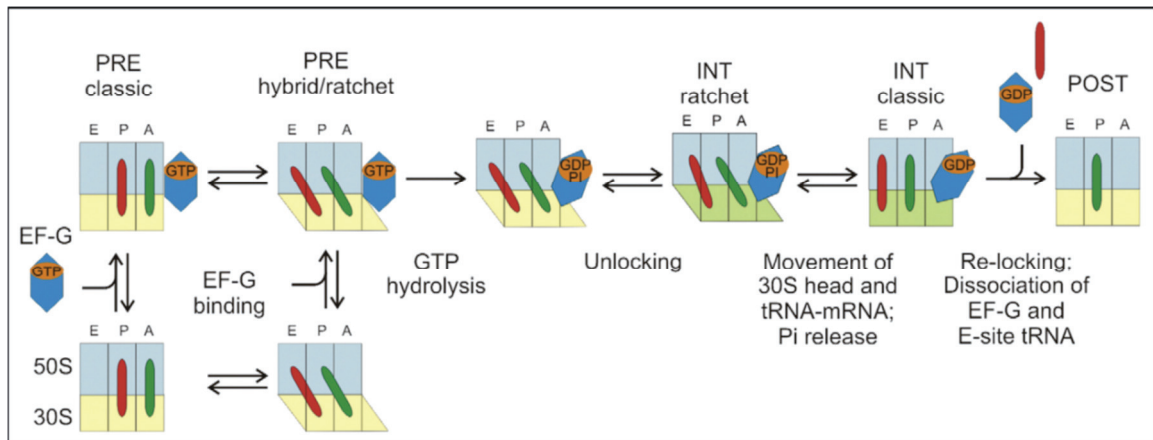


Figure 17 Mechanism of Translocation.

The pre-translocation state tRNAs can be in classical (A/A and P/P) state or hybrid (A/P and P/E) states. The formation of hybrid state correlates with intersubunit rotation. EF-G•GTP binding stabilizes the rotated states. Rapid GTP hydrolysis drives conformational change in EF-G and ribosome rearrangements leading to mRNA-tRNA translocation on SSU, and drives the pre-translocation hybrid state to post-translocation classical state⁷⁷.

eEF2 in eukaryotes and EF-G in bacteria promote translocation by binding to the ribosome and inserting domain IV of the factor into the decoding center of small subunit. A conserved histidine residue (His 699 in yeast eEF2) is modified to diphthamide. This modification is universally conserved amongst all eukaryotes but non-essential for cell viability¹¹⁵. However, it has been shown that knock-out mice lacking the ability to do the diphthamide modification were either embryonically lethal or showed severe developmental defects^{116–118}, suggesting a critical role for diphthamide at a specific time during development in multicellular organisms.

In addition to the highly conserved eEF1 and eEF2, translation elongation in yeast requires a fungal specific factor eEF3 that is not essential in bacterial or other eukaryotic translation. It is an ATPase that contains two ATP-binding cassettes. eEF3 binds to the

ribosomes in complex with ATP and ATP hydrolysis is required for its dissociation from the ribosome. eEF3 spans across on top of the two subunits and makes contact with the central protuberance in the large subunit and the head of the small subunit. A chromodomain of eEF3 binds near the E-site of the ribosome and is suspected to facilitate the release of deacylated tRNA from the E-site^{119,120}. Further genetic, biochemical and structural analyses are needed to determine the function and unique requirement of eEF3 by fungi.

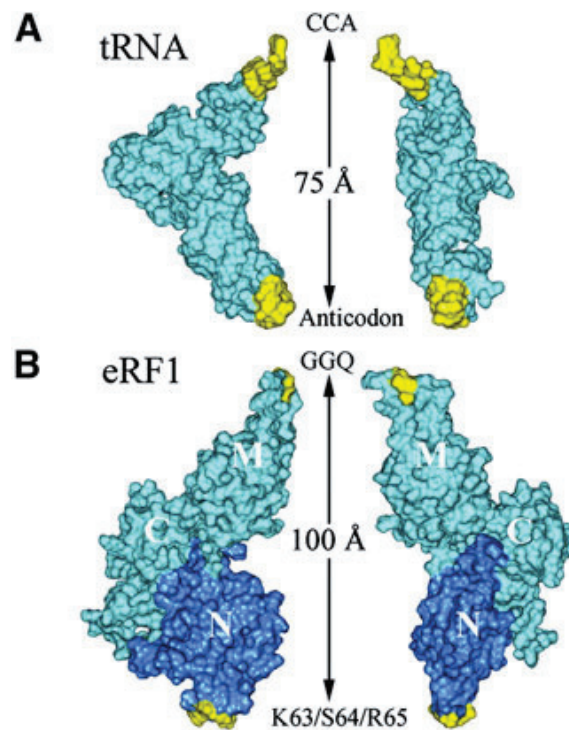


Figure 18 Comparison of tRNA and eRF1 crystallographic structures.

The similarity in structures of (A)tRNA and (B) eRF1 is shown by side view (left) and front view (right).

Termination and Ribosome Recycling

When a ribosome reaches the end of coding sequence of mRNA and a STOP codon (UAA, UGA or UAG) enter the decoding center, termination of translation occurs and peptide chain is released from the tethering tRNA. There is no tRNA that can make base pairs with these codons. Thus translation factors that are structural and mimics of tRNA bind to the ribosome in the event of termination. Figure 18 demonstrates the structural similarities between eRF1 and tRNA.

In eukaryotes, termination is catalyzed by two protein factors called release factors 1 and 2 (eRF1, and eRF3) that work collaboratively in the process. The class I factor eRF1 is responsible for high-fidelity STOP codon recognition and peptidyl tRNA hydrolysis. The class II factor eRF3, is a translational GTPase and closely related to EF-Tu and EF-G. eRF1 associates with eRF3•GTP to form a ternary complex just like the one in elongation cycle. Overall structure of eRF1 resembles that of a tRNA. It has three domains¹²¹. The N-terminal domain is responsible for codon recognition through a highly conserved NKS motif that is proposed to decode stop codons through codon: anticodon like interactions. The middle (M) domain of eRF1 is functionally analogous to the acceptor stem of tRNA, and extends itself into the PTC and contains a universally conserved Gly-Gly-Gln (GGQ) motif; mimicking the CCA end of a tRNA, essential for catalyzing peptidyl-tRNA hydrolysis (shown in bacteria) because of its probable involvement in positioning of hydrolytic water or stabilizing the transition state in the highly conserved RNA rich PTC of the ribosome in a way similar to that observed in peptide bond formation^{122–124}. The carboxyl terminus of eRF1 is involved in facilitating

interactions with eRF3. eRF3 has a variable amino terminal and a more conserved carboxyl terminal that directly interacts with the M and C domains of eRF1^{125–127}. High binding of eRF1 to eRF3 promotes its recruitment to the ribosome in complex¹²⁸ because eRF1 acts as an inhibitor of GTP dissociation from eRF3, which is unusual and entirely different from prokaryotes. GTP hydrolysis by eRF3 is a prerequisite for peptide release. GTP hydrolysis induces a rearrangement in the eRF1 binding state such that the correct placement of GGQ motif could trigger GTP hydrolysis. This is different in prokaryotes where the peptide release precedes and is required for GTP hydrolysis. The reaction mechanism for peptidyl tRNA hydrolysis is shown in figure 19.

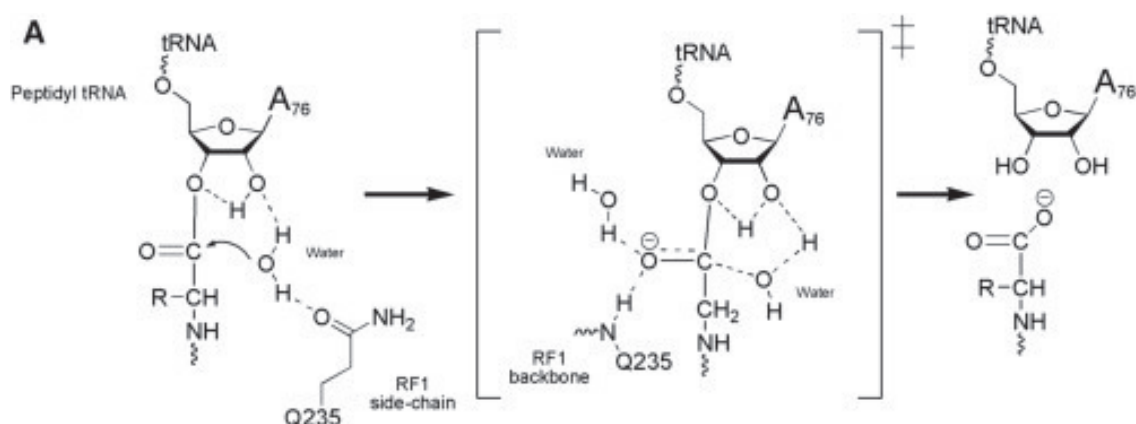


Figure 19 Mechanism of peptidyl-tRNA hydrolysis and Release factor mediated peptide release.

Post-termination ribosomes need to be recycled to free subunits to start over again in translation. In bacteria, recycling is well defined and involves specialized ribosome recycling factor (RRF). After the RF3 stimulated dissociation of RF1/2 from the bacterial ribosomes, RRF in association with EFG•GTP interacts with rotated state ribosomes holding mRNA and deacylated tRNA in the hybrid P/E state and destabilizes the

intersubunit interactions^{129,130}. GTP hydrolysis promotes subunit dissociation; IF3 binds to the small subunit and stabilizes the dissociation event and promotes the release of deacylated tRNA and mRNA^{131–133}. In eukaryotes there is no homolog of RRF and the mechanism of recycling is unclear yet appears distinct bacteria. Current evidence suggests that the post-termination complex consists of unrotated mRNA bound ribosomes with eRF1 and deacylated tRNA in A and P sites respectively¹³⁴. Recently, several studies have identified a conserved cytosolic ATPase, ABCE1 as a likely candidate for promoting ribosome recycling. ABCE1 is an ABC family protein conserved in eukaryotes and archaea. Mechanistic insights into ribosome recycling surprisingly came from the studies of proteins involved no-go decay (NGD) pathway, an mRNA decay pathway of messages with stalled ribosomes. Dom34 and Hbs1 are functional paralogs of eRF1 and eRF3 in NGD¹³⁵. They bind to the A-site of the ribosomal complex and promote subunit dissociation in a codon independent manner, and without causing peptide release due to the lack of the two necessary motifs, NIKS for codon recognition and GGQ for peptide release^{136–139}. Dom34 dependent subunit dissociation activity is substantially promoted (~20 fold) by the presence of Rli1 (yeast homolog of ABCE1)¹⁴⁰. Similar enhancements of ribosomal recycling are seen in in-vitro reconstituted mammalian systems. . Rli has also been shown to directly promote the rate of peptide release by eRF1•eRF3^{140,141}. Thus the protein Rli1/ABCE1 is proposed to be playing a role similar to bacterial RRF such that by promoting the release activity, it can be staging the sequential events of termination and recycling. Deacylated tRNA and mRNA are likely to be dissociated from the small subunits following recycling, with their departure enhanced

by Ligatin or CT-1/DENR interactions. Release of tRNA and mRNA from recycled 40S subunits can also be stimulated by eIF1, eIF1A and eIF3.

Antibiotics: Inhibitors of Ribosome Functions

Protein synthesis is indispensable to cell cycle progression and thus translation serves as a fundamental cellular mechanism available for external intervention using much smaller molecules called antibiotics. Structural differences between bacterial and eukaryotic ribosomes and mechanistic differences between their translational processes have aided in discovery and development of clinical antibiotics specifically targeting bacterial translation. Being several orders of magnitude larger in size than the antibiotic molecules, the ribosomes and accompanying translational apparatus harbor multitude of drug targets. About 50% of all antibiotics are translation inhibitors. Antibiotics have been identified for inhibiting almost every step in translation, although with varying levels of specificity^{142,143}.

Recent high resolution ribosomal structures have demonstrated the precise binding sites for several antibiotics^{144–151}. These structural studies have shown that antibiotics predominantly target the functional centers of the ribosomes, namely the tRNA-mRNA pathway on the small subunit, the PTC, the adjacent exit tunnel on the LSU and translation factor binding sites. Generally ribosome-targeting antibiotics tend to interact with rRNA with the exception of compounds like thiopeptides, streptomycin and spectinomycin, where r-proteins L11, S12 and S5 contribute to their respective binding sites. Antibiotics like edeine and sparsomycin, which bind to the highly conserved, functionally important centers of ribosome, can act as universal inhibitors of translation.

However, many ribosome targeting drugs are prokaryote specific translation inhibitors. The target specificity appears to be conferred by biochemical differences between the regions surrounding the drug binding site or mutations or alterations in nucleotides or ribosomal proteins that do not directly interact with the drug directly but rather affect the nucleotides in the drug binding site indirectly. Most ribosome-targeting antibiotics are bacteriostatic except aminoglycosides that are bactericidal¹⁵² and induce cell death by causing increased rates of amino acid misincorporations in proteins causing misfolding of membrane proteins which eventually leads to oxidative stress and cell death^{153,154}.

Translation initiation inhibitors: Kasugamycin (Ksg) binds to the bacterial SSU, 30S within the path of the mRNA in two sites, first site overlapping the position of the first nucleotide (+1) of the P-site codon and last nucleotide of the E-site codon (at the top of h44 on 30S) and the second binding site in the E-site (30S). Ksg inhibits binding of initiator fMet-tRNA^{Met} to the 30S P-site indirectly by perturbing the path of mRNA¹⁵⁵. Edeine (Ede) also prevents binding of the initiator tRNA (tRNA_i) to the 30S. It binds to the solvent side of the 30S platform between h23, h44, and h45 and causes unusual base-pairing between bases at the tips of h23 and h24. As a result, Ede perturbs the path of mRNA, preventing the correct positioning of mRNA at the P-site and thus inhibiting the initiator tRNA binding¹⁵⁶. Pactamycin (Pct) inhibits translation initiation as well as elongation in both bacteria and eukaryotes. It allows the binding of tRNA_i, but forms non-functional 70S. Pct binds to a site located between h23 and h24 on 30S and mimics the mRNA, blocking its path. As a result it inhibits the first translocation reaction. The orthosomycins such as evernimicin and avilamycin inhibit IF2-dependent subunit

joining¹⁵⁷. GE81112 represents a family of tetrapeptides isolated from the fermentation of *Streptomyces sp.* species. It binds to the 30S and inhibits initiator tRNA binding¹⁵⁸.

Inhibitors of the elongation cycle: Some antibiotics have more than one mode of inhibition in translation. For e.g. streptomycin and aminoglycosides inhibit translation by influencing translational fidelity as well as inhibiting translocation. Tetracyclins prevent the initial binding ternary complex (aa-tRNA•EF-Tu•GTP) to the ribosome. Kirromycins trap the aa-tRNA•EF-Tu on the ribosome. Pulvomycin prevent ternary complex formation. Sterptomycina and aminoglycosides like paromomycin induce translation fidelity defects. Puromycin (Puro) belongs to a class of drugs that bind to the A-site of PTC. It mimics the 3' end of aa-tRNA with an exception that the amino acid residue is linked to the ribose via an amide link instead of ester. After binding to the PTC, Puro undergoes peptidyl transfer accepting and covalently linking to the NC. Subsequently, the peptidyl-Puro is released from the ribosomes because of low affinity. Puromycin inhibits translation across all kingdoms, thus it is not used clinically but it has been an important tool for studying peptidyl transfer reaction. Hygromycin A binds to the A-site of the PTC and inhibits the peptidyl transfer reaction. Chloroamphenicol binds the PTC and displays substrate-specific inhibition. Oxazolidinones like linezolid inhibit the A-site tRNA accommodation. Anisomycins bind in the A-site of PTC on the LSU. Basticidin mimics the CC of the CCA end of a P-tRNA. Sparsomycin prevents A-site tRNA accommodation and enhances P-site tRNA binding. Pleuromutilions such as tiamulin bind the PTC in a position overlapping both A- and P-site tRNA. Macrolide antibiotics like erythromycin

inhibit protein synthesis by blocking the progression of nascent polypeptide chain. These antibiotics bind in the exit tunnel of the 50S LSU.

Translocation inhibitors: The thiopeptide antibiotic thiostrepton perturbs protein synthesis by disrupting the accommodation of translation factors. Fusidic acid inhibits the dissociation of GDP bound EFG from the ribosome after GTP hydrolysis. Alpha-sarcin cleaves the SRL to prevent the GTPase activation of translation factors. Spectinomycin stabilizes an intermediate during translocation thus preventing it from finishing. Viomycin blocks translocation by stabilizing the hybrid state formation.

Bacterial cells have displayed an ever-increasing emergence of antibiotic resistance by adopting mechanisms like altered membrane permeability of the drug, mutation or modification of the drug target, overexpression and protection of the target or drug modification and degradation etc. (discussed in Wilson (2013))¹⁴³. It is thus important to develop novel strategically designed drugs against the bacterial translation machinery.

Antibiotics have also been useful in understanding the ribosome structure, both in bacteria and in eukaryotes. Compounds like viomycin, fusidic acid, cycloheximide and kirromycin have aided in arresting transient intermediate complexes in the translation and made them available for high resolution crystallographic analyses^{31,159,160}.

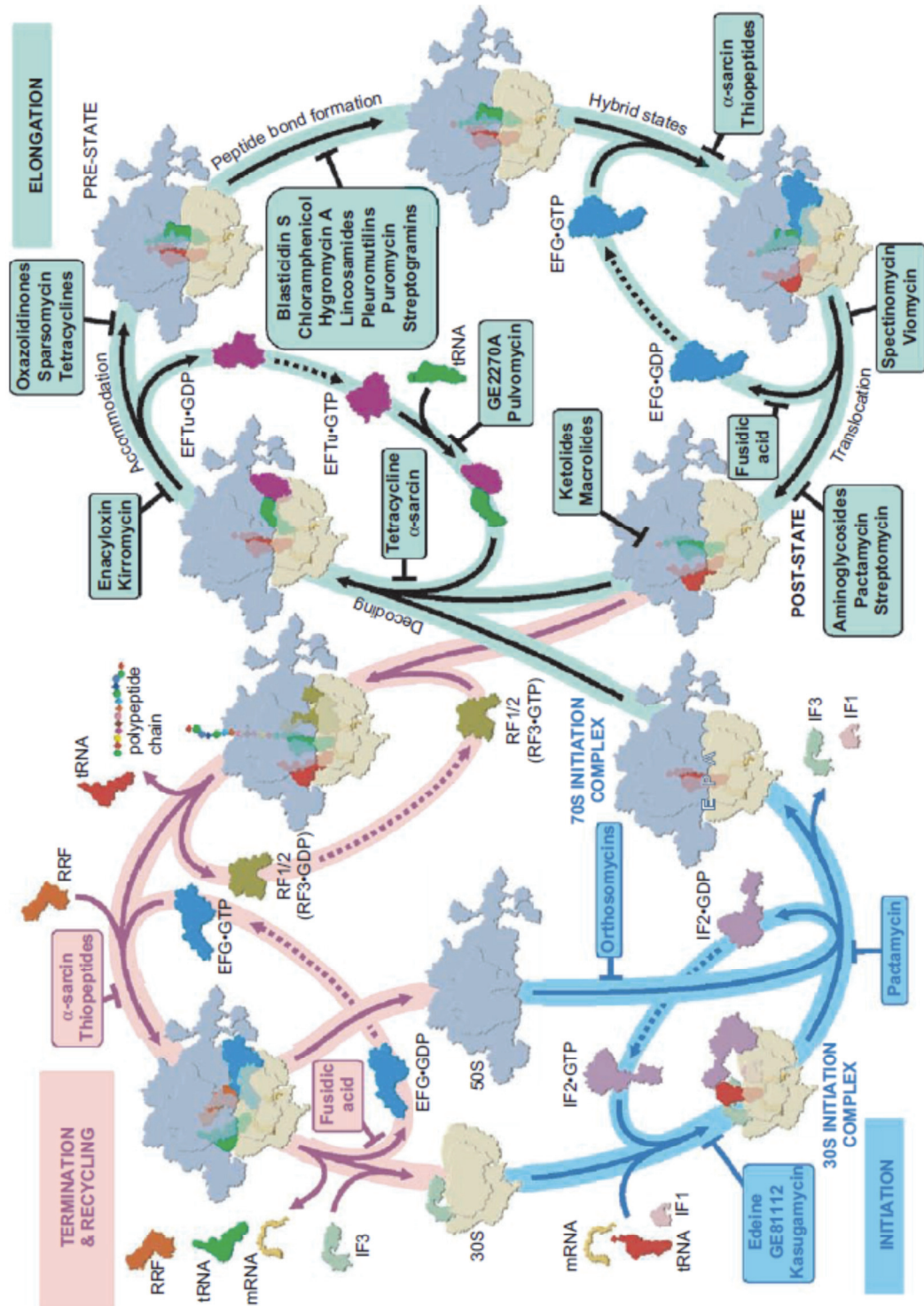


Figure 20 Sites of antibiotic action during protein synthesis.

Schematic diagram shows sites of action of different antibiotics during different stages of protein synthesis¹⁴².

Translational Recoding

The bulk of translation takes place with high speed and accuracy during the elongation phase of translation. During canonical translation, the mRNA codons are read one triplet at a time aided by formation of codon-anticodon base pairs. This results in yielding a single polypeptide whose extension terminates as the ribosomes reach the stop codon. However, like any rules, the process of translation also has exceptions. A variety of non-canonical pathways exist that induce reading of alternate code by the ribosomes and synthesis of new proteins. Such non-canonical translational events are collectively referred to as “translational recoding”. Intrinsically the spontaneous rates of recoding are low¹⁶¹, but cis-acting mRNA elements act as inducers of recoding events. Some exceptions to the canonical translation include mRNA decoding in alternate frame (frameshifting), redirection ribosomes to initiate translation at an alternate start codon, and suppression of a stop codon. Most of these pathways were originally identified in viruses and essential for viral replication. Translation recoding pathways also have been shown to exist in bacterial cells. Recently, there is a growing amount of evidence indicating that robust translation recoding exists in eukaryotic cells and it functions in fine-tuning gene expression^{162,163}.

Programmed -1 Ribosomal Frameshifting

The first evidence and hence most of the understanding about -1 programmed ribosomal frameshifting (-1 PRF) comes primarily from viruses. Viruses exploit this phenomenon to condense their genomes in order to be able to accommodate them economically and safely in their limited nucleocapsid space. -1 PRF allows the viruses to

code multiple proteins from a single unaltered mRNA. Most of the well-defined -1 PRF phenomena are directed by mRNA sequence motif composed of three important elements: a slippery site composed of seven nucleotides where the frameshift actually takes place, a short spacer sequence of usually less than 12 nucleotides, and a downstream stimulatory structure which is usually an mRNA pseudoknot¹⁶⁴. Figure 21 shows a typical -1PRF signal.

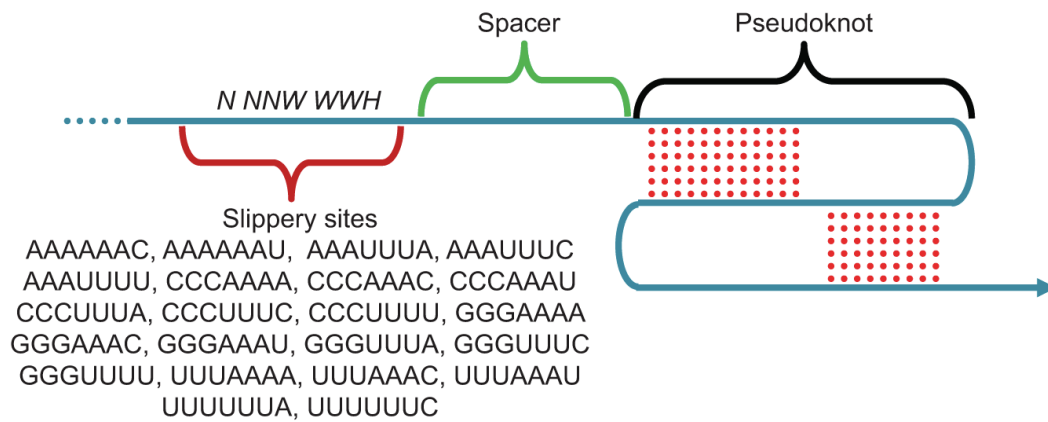


Figure 21 A typical -1 Programmed ribosomal frameshift signal.

It contains a heptameric slippery site, a short spacer and a mRNA secondary structure (H-type pseudoknot here). 22 functional slippery site sequences are given. Figure from Dinman (2013)¹⁶⁵.

The slippery heptameric motif has a sequence *N NNW NNH*, where the incoming reading frame is denoted by the spaces¹⁶⁶. According to a general notion, the complex downstream secondary structure causes the elongating ribosomes to pause. The slippery site allows the non-wobble bases of both A-site and P-site tRNA anti-codons to re-pair with the codons in -1 frame. While mRNA secondary structure studies have shown that pseudoknots are the most common -1PRF inducing structures, other mRNA structures are also capable of causing frameshifting events^{167–169}. The primary function of a secondary

structure is to provide an energy barrier to the translating ribosomes and cause a resulting change in frame; once the energy barrier is overcome, the ribosomes can continue translating in the chosen reading frame. The thermodynamic stability of the of the stimulatory RNA structure is however only one of the many determining parameters for frameshift efficiency¹⁷⁰.

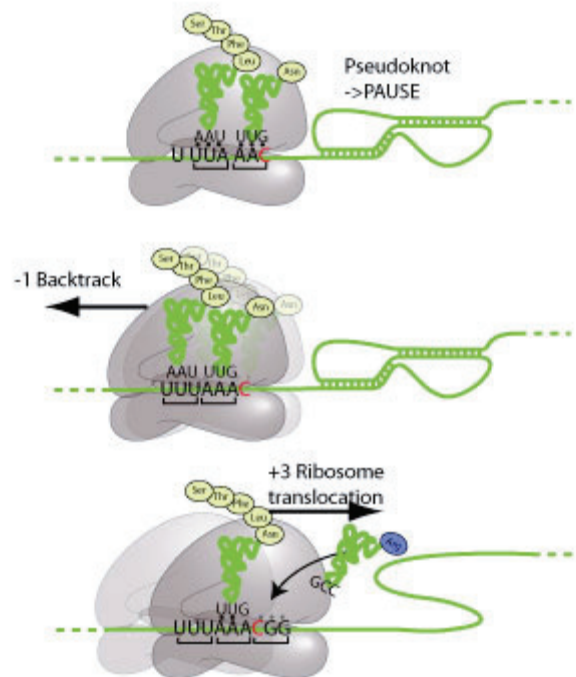


Figure 22 The mechanism of -1PRF.

An mRNA pseudoknot forces elongating ribosome to pause over the slippery sight which induces frameshift by 1 base in 5'direction and repairing of A- and P-site tRNA. As the pseudoknot is resolved, elongation resumes in new (-1) frame. Figure from viralzone.expasy.org

Several pathways and mechanistic models have been proposed in order to describe the order of events and the time of slippage of tRNAs in -1 PRF^{164,166,171}. There is strong evidence supporting many of these models, suggesting that -1PRF can be

explained by more than one mechanism. It is suggested that -1PRF should be viewed as a problem of kinetic partitioning which occurs along the steps of elongation pathway. It is through kinetic partitioning indeed, recently shown that -1PRF occurs due to and during impeded translocation¹⁷². Recently, the general mechanistic framework of -1PRF, highlighting multiple kinetic branch points during elongation was explained by single molecule fluorescence tracking¹⁷³.

Many RNA viruses utilize -1PRF to regulate the expression of multiple genes encoded by their monocistronic RNA. The mRNA of these viruses contains two or more overlapping open reading frames (ORFs), in which the 5'ORF codes the viral nucleocapsid protein gene (Gag) while the second ORF in -1 frame with respect to the first and codes for an enzymatic protein (Pro or Pol). The Pol gene is only translated in fusion with the Gag protein in an event of -1PRF which occurs at a specific frequency of for every virus. The maintenance of specific frequency is important for achieving a specific ratio of Gag to Gag-pol. In *S.cerevisiae* L-A virus, the Gag-Pol fusion protein nucleates the Gag polymerization to form a viral particle. An increased ratio of frameshifting leads to high levels of fusion protein which act as too many nucleating points leading to formation of incomplete viral particles. Decrease in frameshifting, on the other hand may not promote efficient dimerization¹⁷⁴. -1 PRF functions in similar way in Totiviruses, most Retroviruses like HIV-1, and Murine Leukemia Virus¹⁷⁵⁻¹⁷⁸.

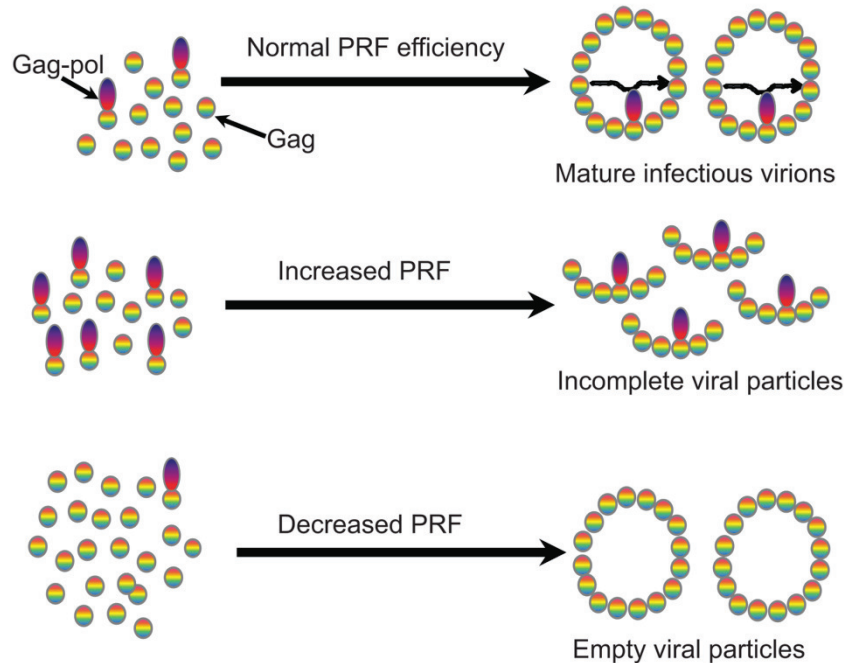


Figure 23 -1 Programmed ribosomal frameshift in viruses.

Optimum extent of frameshifting is crucial for viral replication. Both increased and decreased levels of frameshifting results in defects in viral assembly¹⁶⁵.

In coronaviruses also, -1PRF produces a C-terminally extended fusion peptide that is subsequently proteolytically processed. However, genes involved in -1PRF are involved in replicase or transcriptase function¹⁷⁹. Optimum levels of -1PRF being so crucial in viral propagation, it becomes a target for antiviral therapeutics. -1PRF can be intervened by mutagenizing the -1PRF signal, the host translation apparatus or by using small molecule inhibitors of frameshifting.

Several functional -1PRF signals have been identified in eukaryotic mRNAs. Genomic -1PRFs function in a context different from the viral mRNAs. More than 95% of the -1PRFs that occur in cellular mRNAs, lead the elongating ribosomes to a premature termination codon. Ribosome stalling at premature termination codons invokes

mRNA decay pathways leading to an inverse relation between -1PRF and mRNA abundance. In *Sachharomyces cerevisiae* -1PRF functions as an mRNA destabilizing factor via both non sense mediated decay and no-go decay pathways^{180,181}. One study shows that -1PRF in the EST2 mRNA encoding the catalytic subunit of the telomerase, acts as a destabilizing agent, and can play a role in telomere length homeostasis¹⁸². Another study shows that -1PRF in a human gene coding protein CCR5, also works an mRNA destabilizing element in mammalian cells through NMD. This -1PRF signal is subject to manipulation by miRNA.

Programmed +1 ribosomal frameshifting

+1PRF is a much less common and much less understood event in translation recoding. It is also utilized by viruses and transposable elements to regulate gene expression of structural and enzymatic proteins. +1PRF is also driven by cis acting elements. The precise mechanisms of frameshift are different for +1PRF, but it is detected in human, mouse, bacterial and yeast genomes^{183–186}. A slippery site is required for +1PRF while a downstream stimulatory structure is not. While -1PRF has a more or less one coherent mechanism for -1PRF, +1PRF is more case dependent. +1PRF take place during the translation of *Ty1* retrotransposable elements. The situation of “hungry codons” or rare codons in the A-site induces the shift of frame. Due to the lack of adequate amount of cognate rare codons, a near-cognate tRNA wobble-base pairs with skipping one base on the mRNA¹⁸⁶. +1PRF in the OAZ is primarily driven by the slippage of P-site tRNA from CUU to UUA. +1PRF signals were detected in yeast EST3 mRNA etc¹⁸⁷.

Missense and nonsense suppression.

Translational fidelity of elongating ribosomes can be disturbed in a way other than change of reading frame. This includes missense suppression (accommodation of near or non-cognate tRNAs mistakenly) and non-sense suppression (incorporation of suppressing tRNAs at stop codons in place of release factors, thus reading through and continuing elongation past the stop codon). Missense suppression often occurs when the elongating ribosomes encounter a rare codon, thus in the lack of presence of rare cognate tRNA, a near-cognate or non-cognate tRNA is misincorporated. Viruses use the nonsense suppression strategy to make the gag-pol type fusion proteins, with the help of cis-acting mRNA elements in a way similar to -1PRF^{188,189}. Nonsense suppression is also utilized as a method to incorporate the rare and essential 21st amino acid selenocysteine (Sec) in cellular protein in all three kingdoms. It requires specific trans-acting elements and mRNA secondary structures in order to miscode a UGA stop codon and incorporate a Sec-tRNA instead^{190,191}. Another rare amino acid pyrrolysine described only in bacteria and archaea is encoded by the stop codon UAG¹⁹². Regulation of gene expression of Sec containing proteins has been linked to human disorders including cancer.

Diseases of ribosomal malfunction: Ribosomopathies

Since ribosomes and translation are vital for survival, until recently it was believed that defects in ribosome biogenesis factors or translation machinery would either lack successful biogenesis or protein synthesis or have a translation apparatus not fit for survival. However, in last few decades very specific diseases of ribosome biogenesis have been discovered. These diseases are collectively called “ribosomopathies”.

Although these diseases encompass deficiencies in very fundamental and ubiquitous processes, their clinical manifestations are varied and tissue specific. Most of these diseases are congenital, and they share several common features like small stature, defects in early developmental pathways, cancer predisposition and hematological disorders.

Diseases of SSU biogenesis

Mutations in the gene encoding Treacle (*TCOF1*) cause an autosomal dominant craniofacial disorder called Treacher Collins Syndrome. Treacle is a putative nucleolar phosphoprotein that plays a role in rDNA transcription and methylation of 18S rRNA¹⁹³. The disease appears to be due to haploinsufficiency of Treacle than due to dominant negative effects in heterozygous patients with *TCOF1* mutations in one allele¹⁹⁴. Male infertility is caused by mutations in the gene encoding UTP14, an essential SSU processosome protein required for 18SrRNA maturation. The disease develops due to haploinsufficiency of protein UTP14c expressed by one of the variants of *UTP14* genes *UTP14c*, an active retroposon expressed only in the testes and ovaries¹⁹⁵. Cirhin/UTP4 is a member of a sub-complex of SSU processosome required for optimal transcription of rDNA in both yeast and humans. A missense mutation in the C-terminus of Cirhin causes North American Indian childhood cirrhosis, an autosomal recessive disorder in a specific human population¹⁹⁶. Bowen-Conardi syndrome (BCS) is a lethal autosomal recessive disorder observed primarily in Hutterite population. The associated symptoms are growth retardation, psychomotor delay, microcephaly and multiple joint disorders and caused by

a missense mutation in the gene coding EMG1, a putative methyltransferase required for 40S biogenesis¹⁹⁷.

Diseases of LSU biogenesis

Alopecia, neurological defects, and endocrinopathy syndrome (ANE syndrome) is a clinically heterogeneous autosomal recessive disease caused by mutation in RBM28 protein coding gene. RBM28 is important for 60S biogenesis. Shwachman-Bodian-Diamond syndrome (SDS) is a pleiotropic autosomal recessive disorder, manifesting several hypoproliferative symptoms such as short stature, neutropenia, hematologic disorders, anemia and predisposition to leukemia. 90% cases of SDS are reported to be caused by mutations in gene coding SBDS, a protein involved in maturation and export of 60S subunit^{47,198}.

Some mutations in ribosome biogenesis factors act as modifiers of pre-existing conditions. E.g., mutations in gene encoding WDR36, a member of a sub-complex of SSU processosome causes a more severe form of disease in patients with Primary open angle glaucoma (POAG), the leading cause of blindness.

Diseases of snoRNP malfunction

RNase MRP is a ribonucleoprotein involved in ribosome biogenesis. It is an endonuclease which cleaves the pre-rRNA and separates precursors for SSU and LSU rRNA processing. Mutations in genes for the non-coding RNA component of RNase MRP are genetically linked to skeletal dysplasias which can be clinically classified from mild, moderate to severe dysplasia. The abnormalities include hypotrichosis, hypoplastic

anemia, immunodeficiency and increased predisposition to cancer. Dyskeratosis congenital (DC) is a genetic disease caused by mutations in the components of Box H/ACA snoRNPs responsible for the pseudouridylation modification of rRNA. It is characterized by genetic as well as symptomatic heterogeneity which include mucocutaneous abnormalities, predisposition to variety of cancers, bone marrow failure, immunodeficiency, growth retardation and neurological symptoms. DC is an X-linked recessive or autosomal dominant disorder caused by mutations in the dyskerin gene, encoding an essential component of Box H/ACA snoRNPs. Prader-Willi Syndrome is a complex disease caused by silencing of genes encoding components of Box C/D snoRNPs and characterized by neonatal hypotonia, short stature, hyperphagia and obesity and hypogonadism. Box C/D snoRNPs typically catalyze 2'-O-ribose methylation of rRNA¹⁹⁹.

Diseases of ribosomal proteins

Haploinsufficiency of some r-proteins leads to diseases of the bone marrow such as Diamond Blackfan anemia (DBA). DBA is an inherited bone marrow failure syndrome of children characterized by proapoptotic hematopoiesis, bone marrow failure, birth defects and predisposition to cancer. In some cases the disease also presents with craniofacial, cardiac, limb and urogenital abnormalities. All genes currently shown to be involved in DBA are r-protein genes^{200,201}. Haploinsufficiency of these proteins resulting from mutation in their genes is likely to be the basis for DBA. Different types of mutation in genes corresponding to proteins RPL19, RPL5, RPL11, RPL35A, RPL36, RPS24, RPS17, RPS7, RPS15 and RPS27. Mutations in the r-protein genes lead to

defects in ribosome biogenesis contributing to DBA. The r-proteins involved in DBA can also have other functions that could contribute to the development of the disease or the observed predisposition to cancer. Interactions of L19 with oncoproteins like PIM-1, modulation of activities of tumor suppressor p53, c-MYC, an oncoprotein and a transcription factor by RPL11, ability of RPS7, RPL5 and RPL23 to modify p53 activity indicates that mutations in r-protein genes can have a role in onset or progression of cancer in DBA patients. 5q⁻ syndrome is characterized by defect in erythroid differentiation and associated with progression to acute myeloid leukemia. *RPS14* is the haploinsufficient tumor suppressor gene associated with the syndrome²⁰².

Cancer onset in ribosomopathies

The link between ribosomes and cancer is complex and not very well understood yet. To meet the requirements of cancer cells, ribosome biogenesis and nuclear structure are altered significantly; protein synthesis and transcription rates are increased. Dysregulation of ribosome biogenesis leads to inefficient ribosome production and hypoproliferative disorders. However, most ribosomopathies show predisposition to cancer, a hyper-proliferative phenomenon. Changes in mRNA translation control distinct cellular processes including metabolism, cell migration, cell adhesion, cell growth cell cycle control and tumorigenesis. R-proteins (RPL11 known) interact with c-MYC, p53 and MDM2 in order to regulate their oncogenic or tumor suppressor activities^{203,204}. Thus haploinsufficiency of r-proteins leads to loss of regulation by them and increased occurrence of tumors.

Cancer in translation goes further from ribosome biogenesis to translation. Genes coding translation factors are aberrantly expressed during cancer progression. Translation initiation is the most regulated of the steps in translation and hence the several checkpoints coordinated by translation factors to control the levels of translation present as opportunities for oncogenic insult.

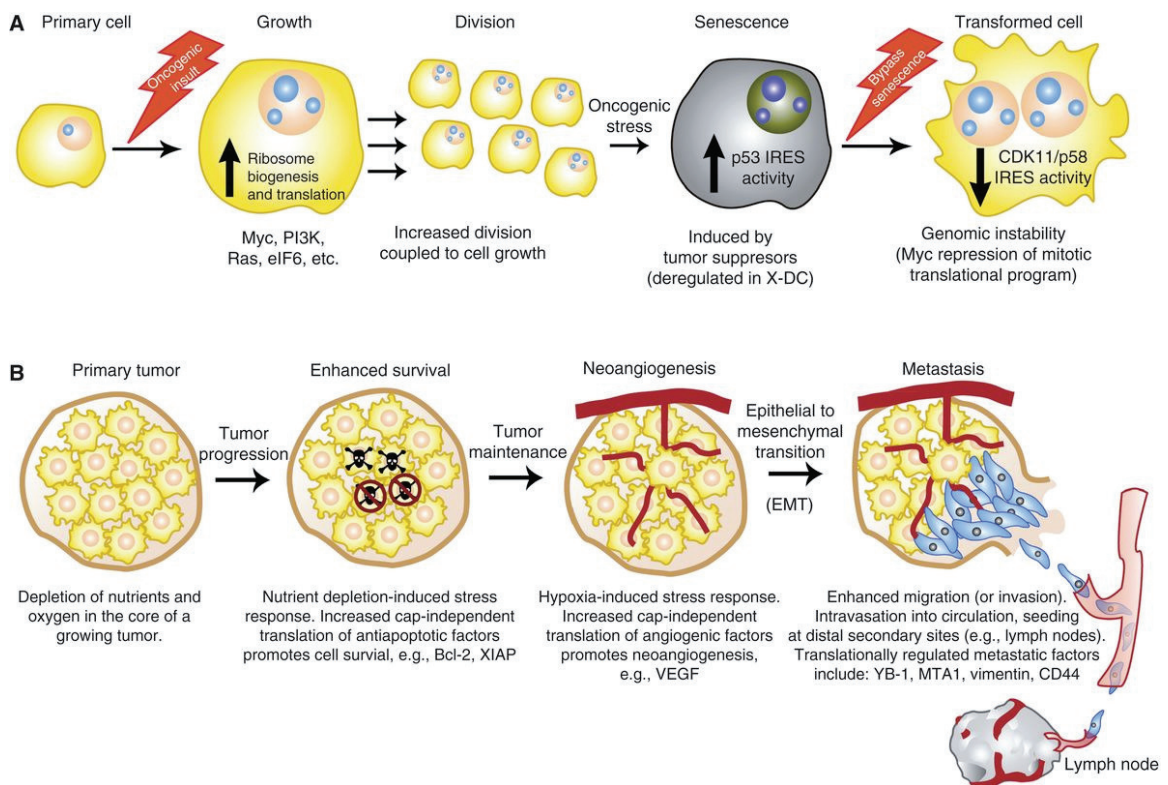


Figure 24 Deregulation of translation control contributes to each step of cellular transformation and cancer progression.
Rugggero 2013²⁰⁵.

Scope of the current study

The understanding of ribosome structure and mechanism of protein synthesis has come a long way since the earliest mid-century knowledge about the mysterious “small particles”. Atomic resolution crystal structures of ribosomes have created an explosion of knowledge about translation machinery. However, the tiny details of ribosome’s inside mechanisms are yet to be revealed. Some of the issues that need to be addressed include: a) How does the ribosome co-ordinate its rotational motion? b) How do the functional centers on a large macromolecule like ribosome communicate with each other? c) How does the ribosome maintain unidirectionality of translation d) how does it acquire a sort of “temporal specificity” for its ligands, and what changes in translation mechanism when the ribosomes go bad.

The ribosome is a macromolecular conglomerate composed of many independently synthesized rRNAs and proteins. Studies of individual ribosomal components are essential for addressing the abovementioned issues. Some of the molecular pathways followed by these components are general while others are specialized. Ribosomal proteins were considered to be belonging to such a class of proteins involved mostly in rote like functions and cellular housekeeping. However, recent evidence has suggested more unique regulatory functions for ribosomes in specific cell and tissue types²⁰⁶.

Ribosomal Protein uL2

Ribosomal protein L2 is an essential core ribosomal component that joins the ribosomal assembly process very early in the ribosome biogenesis pathway. It contacts the helices in the domains IV, V and VI and the PTC of the 23S rRNA. This region of the rRNA is transcribed last and hence uL2 is one of the last r-proteins to be incorporated in early assembly around the time when the 7S pre-rRNA is processed. uL2 (L2 in bacteria) is highly conserved in all three kingdoms and absolutely required for the peptidyltransferase activity of the ribosome.

50S subunit alone is able to catalyze peptide bond formation²⁰⁷. uL2 was identified by photocrosslinking studies employing photoreactive groups attached to the CCA-end of A-, P-, and E-site-bound tRNAs, as one of the crosslinked molecules that must be a part of or in close proximity to the catalytic center²⁰⁸. Photoaffinity labelling studies with peptidyltransferase inhibiting ribosomes have placed bacterial L2, L15, L16, L18, L22, L23 and L27 at or near the PTC²⁰⁹. Studies involving photolabile oligonucleotides complementary to the PTC rRNA have also placed bacterial L2 and L3 in the PTC vicinity²¹⁰.

Single protein omission studies showed that the proteins L2, L3, L4 and 23S rRNA are essential, while other proteins as well as 5S rRNA are dispensable for catalyzing the peptidyl transfer^{211–213}. Out of the eight to 10 proteins that were shown to be stably interacting with 23S rRNA, withstanding treatment with proteases, SDS and phenol²¹⁴, the prime candidates for peptidyl-transferase activity then were L2, L3, L4 and possibly 23S rRNA. Evolutionarily L2 was suspected to be the best candidate because it

was the most conserved protein in the large subunit²¹⁵. 50S reconstitution studies showed that a highly conserved His 229 in *E.coli* L2 was essential for peptidyltransferase activity. Mutation H229Q in L2 renders the *E.coli* ribosomes devoid of peptidyltransferase activity²¹⁶. H229 was shown to be important for translational activity of ribosomes in *in vivo* studies also²¹⁷.

Peptide bond formation was described to be catalyzed by naked mature or *in vitro* transcribed 23S rRNA^{218,219}, but this observation could not be reproduced²²⁰. Thus there remained a possibility of ribosomal proteins, particularly L2 playing a central role in peptidyl transfer. The catalytic core of serine proteases has been proposed as a molecular model for the peptidyltransferase center. The ribosomal protein L2 contains the universally conserved seryl, histidyl, and aspartyl residues characteristic of the catalytic core of serine proteases and thus remained the center of interest in ribosomal peptide bond formation²¹⁶.

Structurally, uL2 in yeast is a bilobular protein (Fig. 25A). It has a solvent accessible SH3 β -barrel globular domain that participates in the intersubunit B7b bridge formation. The other lobe is composed of highly basic extensions that bury deep into the LSU core similar to proteins uL3, uL16 and uL4, approaching the PTC very closely (Fig. 25B). The two lobes of L2 are connected by a neck region of the protein that is sheathed in rRNA helices H65, H66, H67 and H33.

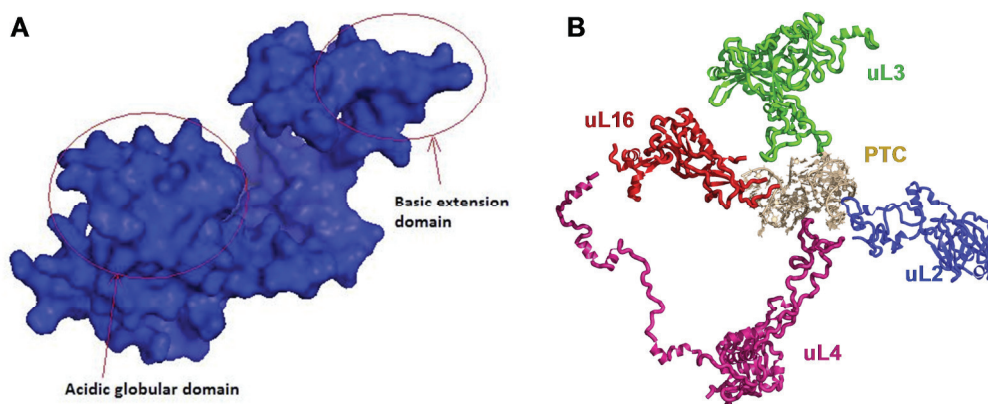


Figure 25 A. Structural features of yeast ribosomal protein uL2. B. Ribosomal Proteins with basic extensions approach the peptidyltransferase center very closely.

A. uL2 is a bilobular protein that interacts with functionally important regions of the ribosome. It harbors an acidic globular domain which interacts with small subunit to form the B7b Bridge while the basic extension interacts with Helix 93 of LSU, approaching the peptidyltransferase center very closely. The two lobes of uL2 are connected by a neck region. **B.** A view of the active PTC with most of the RNA removed. Protein uL2, uL3, uL4 and uL16 have the closest extensions to the PTC and the peptide exit tunnel. Figure prepared using 3Å crystal structure of eukaryotic ribosome²³.

In the work presented ahead, mutants of uL2 in the intersubunit bridge forming region of uL2 were generated. Through a battery of genetic, functional and biochemical analyses, these mutants are characterized as responsible for causing defects in ribosomal function, mainly translational fidelity. Structure probing analysis reveals that these mutants perturb the rotational equilibrium of the ribosomes by interfering with its intersubunit-bridge forming ability and the dynamics of their transient existence. Such a disturbance in the natural ribosomal dynamics interferes with its ability to function as a highly sophisticated nanomachine. In higher eukaryotes where protein synthesis is more complex and translation profiles vary from one tissue type to other, an understanding of the mechanism of how r-protein mutations affect ribosome function can help in understanding tissue specific disease proclivities.

Chapter 2: Coordination of Ribosomal Rotation through Bridge

B7b

Introduction

Successful conversion of genetic information from mRNA to proteins requires efficient and accurate functioning of the highly orchestrated nanomachine called the ribosome, a complex ribonucleoprotein particle universally composed of two subunits. Yeast ribosomes contain approximately 80 proteins and 4 rRNA molecules^{221,222}. Its high level of structural complexity confers the flexibility and versatility required to interact with a wide range of *trans*-acting ligands^{223,224}. These include aminoacyl-tRNA containing ternary complexes (TC), the eEF2 translocase, and a host of release and recycling factors. Unidirectionality of translation is achieved by rotational motion of the two subunits relative to each other, and is energetically supported by several GTP hydrolysis reactions^{223–227}. The two extreme stages of ribosomal rotation are called unrotated and rotated states^{228,229}. It appears that intersubunit rotation is also accompanied by intersubunit “rolling” motions in eukaryotes²⁶. During the translation elongation cycle, some intersubunit bridges function as “pivot points” upon which intersubunit rotation is balanced, while others are transient, breaking and re-forming as the subunits move between the two states. The B3 intersubunit bridge is an example of a pivot, while the B7a bridge exemplifies a rotational state dependent interaction^{130,230}. Eukaryote ribosomes contain more intersubunit bridges than eubacterial or archaeal ribosomes, most of which consist of protein-protein interactions²³. At equilibrium, empty ribosomes can

freely rotate among as many as 40 – 50 conformations^{130,231}. Previous studies have suggested that disturbing this rotational equilibrium perturbs allosteric communication pathways within the ribosome. These in turn affect the steady-state affinities for *trans*-acting factors, which manifest themselves as changes in translational fidelity²³². Programmed alterations in translational fidelity have recently been shown to be responsible for regulating the expression of specific genes in from yeast to humans^{162,163,233}, and global changes in translational fidelity, in particular in programmed -1 ribosomal frameshifting, have been linked to at least three human diseases^{234–236}.

. A correlation has been noted between defects in peripheral/late assembling ribosome proteins and a class of human diseases collectively known as ribosomopathies²³⁶. uL16 is assembled at the end of the LSU maturation process, is located on the periphery of the LSU, and directly interacts with the elongation factors³⁷. To address the question of whether the connection between rotational equilibrium and translational fidelity is specific to this class of ribosomal proteins or if it is a more generalized phenomenon, we tested it using mutants of the universally conserved core ribosomal protein uL2 (universal L2, previously known as L2)²³⁷. uL2 is incorporated into ribosomes in the early stages of biogenesis²³⁸. Structurally, uL2 contains a solvent-accessible globular domain. This is linked to a second domain that closely interfaces with the small subunit (SSU) through intersubunit bridge B7b (Fig. 26A). approaches the peptidyltransferase center through a functionally important “neck”. uL2 is an integral protein that interacts with nearly every domain of the large subunit (LSU) rRNA^{11,23}. Along with uL3, uL2 is required to maintain the peptidyltransferase center, and indeed, early ribosome reconstitution studies suggested that histidine residues in the basic

extension domain might directly participate in the peptidyltransferase reaction²³⁸. Mutants of uL2 have been characterized in both yeast and *E. coli* demonstrating conserved roles in subunit association and in ribosome structure, biochemistry, and translational fidelity^{239,240}. In the current study, mutants of uL2 located in the SSU interface region were used to test the model of the importance of maintaining intersubunit rotational equilibrium on ribosome function. Consistent with prior studies of uL16, mutations of uL2 that drive the equilibrium towards the rotated state, promote allosteric changes in functional centers of both subunits that favor binding of eEF2 and disfavor that of TC. These in turn manifest as specific alterations in translational fidelity, which are biologically manifested, in part, by decreased telomere length. A model describing how this perturbation of ribosome structural equilibrium alters specific aspects of translational fidelity is presented.

Results

Genetic characterization of uL2 mutants in the vicinity of B7b Bridge.

Ribosomal protein uL2 is roughly bilobular. One domain approaches the P-site of the peptidyltransferase center (Fig. 26B) and the other interacts with the small subunit through the B7b intersubunit bridge (Fig. 26A, Fig. 27). The results of a prior random mutagenesis study suggested that structural flexibility between the two domains may help to coordinate tRNA-ribosome interactions²³⁹. Subsequently, studies of ribosomal protein uL16 suggested that changes in the equilibrium between intersubunit rotational states underlie biochemical, translational fidelity and gene expression defects²³⁶. The current study focuses on the B7b Bridge to further test and expand upon this hypothesis.

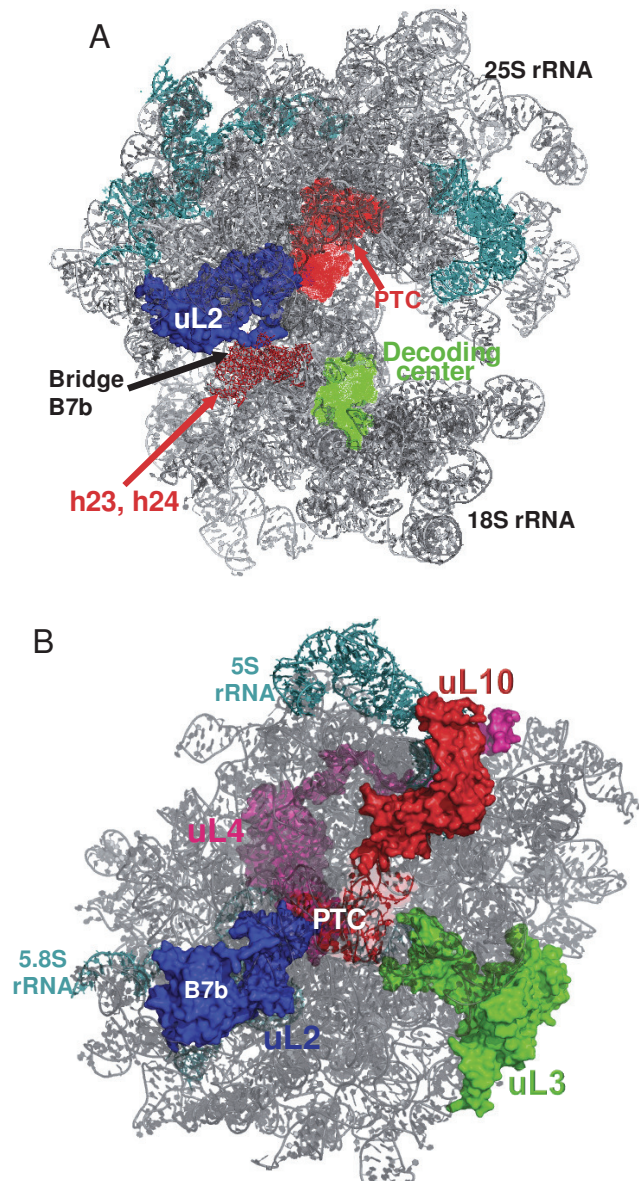


Figure 26 Location of L2 within the yeast ribosome:

A. View of the ribosome from the E-site. 18S and 25S rRNA is shown in grey, 5S and 5.8S rRNA in cyan. L2 is shown in blue, peptidyltransferase center in red and decoding center in green. L2 makes the intersubunit Bridge B7b interacting with helices h23 and h24 (shown in red) of SSU. **B.** Crown view of the large subunit shows strategic localization of ribosomal proteins near the peptidyltransferase center. Finger like basic insertion of L2 closely approaches the peptidyltransferase center (PTC) while the acidic globular domains make contact with the small subunit through the B7b Bridge.

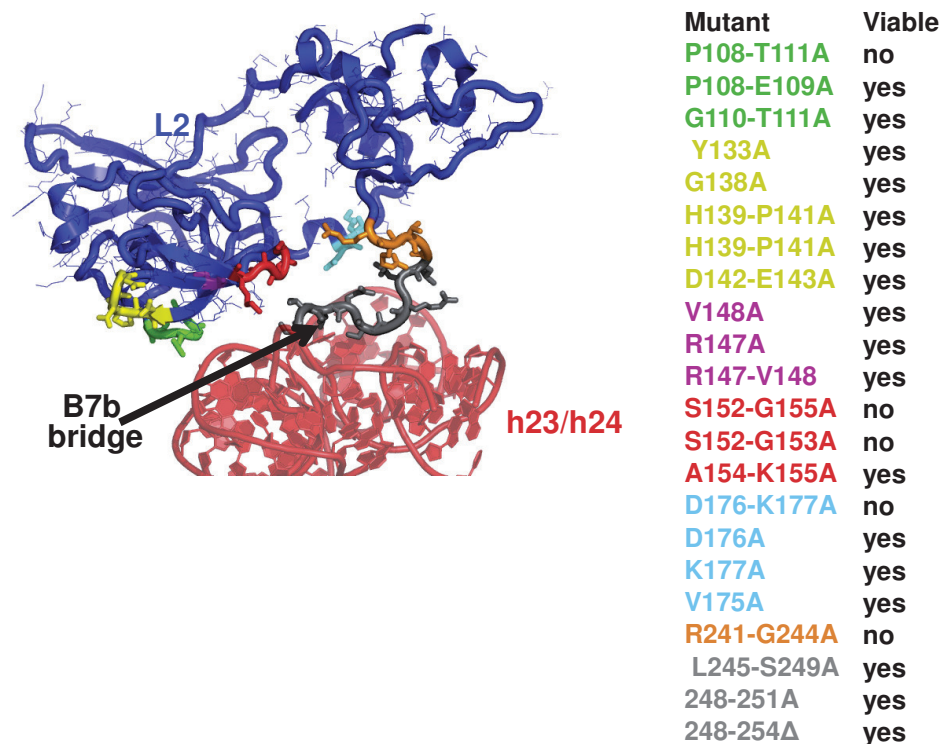


Figure 27 List of mutants of L2 ORF generated in this study and their location on uL2.

Color codes are used to highlight the general regions mutagenized in uL2. Ribosomal structures generated in PyMol using 3Å resolution yeast ribosomal structures

Using atomic resolution yeast ribosome structures as a guide²³, six different regions of uL2 were identified as potentially interacting with the SSU. These are color coded in figure 27. Initially, stretches of up to 5 amino acids in each region were mutated to alanine. With one exception, none of these were viable as the sole form of uL2 (Fig. 27). Subsequently, mutants were made containing one, two or three alanine substitutions and were scored for viability. Dilution spot assays were employed to score the growth phenotypes of the viable mutants at high and low temperatures (Fig. 29A), Yeast L-A virus.

The double stranded RNA L-A yeast killer virus maintains a toxin-encoding M1 satellite. This toxin is responsible for the killer phenotype of the K⁺ strains. Cells that can maintain this virus create a zone of growth inhibition when spotted on a lawn of killer sensitive (uninfected) strain. For maintaining a precise ratio between the structural (Gag) and enzymatic (Gag-pol) products of translation, L-A utilizes Programmed -1 frameshifting event (reviewed in Dinman, 1995). This ratio between the structural and enzymatic product is critical for the maintenance of M1 satellite (Dinman and Wickner, 1992). Unhealthy ribosomes and defective mechanism of translation can impair this critical ratio L-A translational products necessary for M1 maintenance. The maintenance and propagation of the L-A virus is also affected by defects in large subunit biogenesis. Thus the yeast killer assay provides a quick and easy method for directly screening defects in the translation machinery of yeast cells.

“Killer” assays were employed to score the ability of these mutants to maintain the yeast killer virus (Fig. 29B). Drug sensitivity was evaluated by growing cells in liquid culture containing either 25µg/ml Anisomycin or 30µg/ml Sparsomycin (Fig. 30A and B). These drugs are inhibitors of translation: anisomycin competes with the CCA-end of A-site tRNA in binding to the A-site in LSU while Sparsomycin binds to the P-site and interferes with peptidyl tRNA binding and peptidyl transferase reaction. All mutants were assayed with regard to their quantitative effects on four aspects of translational fidelity: -1 PRF, +1 PRF, UAA termination codon readthrough, and suppression of a near cognate codon (Fig. 31). From these genetic analyses, the four mutants with the most pronounced

phenotypes were selected for further characterization: H139-E143A, uL2-K177A, deletion of the C-terminal end (248 – 254Δ), and uL2-Y133A.

H.sapiens	-----MGRVIRGQRKGAG-SVFAHVHKKRKGAAARLR	30
M.musculus	-----MGRVIRGQRKGAG-SVFAHVHKKRKGAAARLR	30
D.melanogaster	-----MGRVIRAQRKGAG-SVFKAHVKKRKGAAKLR	30
S.cerevisiae	-----MGRVIRNQRKGAG-SIFTSHTLRQGAALKR	30
H.marismortui	-----MGRRIQGQRGRGTSTFRAPSHRYKADLEHR	31
E.coli	MAVVKCKPTSPGRRHVVKVNPPELHKGKFPAPLLEKNSKSGGRNNNGRITTRHIGGGHKQ	60
T.thermophilus	MAVKKFKPYTPSRRFMTVADFSEITKTEPEKSLVKPLKKTGGRNNQGRITVRFRRGGGHR	60
	: . : * . . :	
H.sapiens	AVDFAERHG----YIKGIVKDI IHDPRGAPLAKVVFRDPYRFKKRTELFIAAEGIHGTQ	86
M.musculus	AVDFAERHG----YIKGIVKDI IHDPRGAPLAKVVFRDPYRFKKRTELFIAAEGIHGTQ	86
D.melanogaster	SLDFAERSG----YIRGVKDI IHDPRGAPLAVVHFRDPYRYKIRKELFIAPEGMHGTQ	86
S.cerevisiae	TLDYAERHG----YIRGIVKQIVHDSGRGAPLAKVVFRDPYKYRLREEIFIANEGVHTGQ	86
H.marismortui	KVEDGD-----VIAGTVVDIEHDPARSAPVAAVEFEDGDR-----RLILAPEGVGVGD	79
E.coli	AYRIVDFKR-NKDGIPAVVERLEYDPNRSANIALVLYKDGER-----RYILAPKGLKAGD	114
T.thermophilus	LYRIIDFKRWKDVGPVPAKVAIEYDPNRSARIALHLYVDGEK-----RYIIAPDGLQVGQ	115
	: : . * : : * . * * : : * : : . : * . * . :	
H.sapiens	FVYCGKKAQLNIGNVLPVGTMEPTIVCCLEEKPGDRGKLARASGNYATVISHNPETKKT	146
M.musculus	FVYCGKKAQLNIGNVLPVGTMEPTIVCCLEEKPGDRGKLARASGNYATVISHNPETKKT	146
D.melanogaster	FVYCGRKATLQIGNVMPLSQMEPTIICNLEKTGDRGLARTSGNYATVIAHNQDTKKT	146
S.cerevisiae	FIYAGKKASLNVGNVPLPGSVPEPTIVSNVEKPGDRGALARASGNYVIIHNPDENKT	146
H.marismortui	ELQGVDAEIIAPGNTLPLAEIPEGVPCNVNESSPGDGGKFARASGVNAQLLTH--DRNVA	137
E.coli	QIQSGVDAAIKPGNTLPMRNI PVGSTVHNVEMKPGKGGQLARSAGTYVQIVAR--DGAYV	172
T.thermophilus	QVVAGPDAPVQVGNALPLRFIPVGTVVHAVELEPKKGAKLARAAGTSAQIQGR--EGDYV	173
	: * . * : * . : : * * : : * . . . : * * : : : : .	
H.sapiens	RVKLP SGSKKVISSANRAVGVVAGGGRIDKPI LKAGRAYHKKYAKRNCWPRVRGVAMNP	206
M.musculus	RVKLP SGSKKVISSANRAVGVVAGGGRIDKPI LKAGRAYHKKYAKRNCWPRVRGVAMNP	206
D.melanogaster	RVKLP SGAKKVPV SANRAMGVIVAGGGRIDKPI LKAGRAYHKKYAKRNCWPKTRGVAMNP	206
S.cerevisiae	RVRLP SGAKKVISSDARGVIGVIVAGGGRVDKPI LKAGRAFHKKYRLKRNSWPKTRGVAMNP	206
H.marismortui	VVKLP SGEMKRLDPQCRATIGVVGGGGRTDKPFVKAGNKHKKMARGTKWPNVRGVAMNA	197
E.coli	TLRLR SGEMRKVEADCRATIGEVGNAEHMLRLVLGKAGAAARWGRV----PTVVRGTAMNP	227
T.thermophilus	VLRLP SGELRKVHGECYATVGAVGNADHKNI VLKGAGRSRWLGRR----PHVRGAAMNP	228
	: * * * : : . : * : . . : : * * : : * . * . * . :	
H.sapiens	VEHPFGGGGNHQH-IGKPSTIRRDAPAGRKVGILIAARRTGRLRGTKTVQEKEN	257
M.musculus	VEHPFGGGGNHQH-IGKPSTIRRDAPAGRKVGILIAARRTGRLRGTKTVQEKEN	257
D.melanogaster	VEHPHGGGNHQH-IGKASTVKRGTSAGRKVGILIAARRTGIRGGKGSKDK-	256
S.cerevisiae	VDHPHGGGNHQH-IGKASTISRGA VSGQKAGLIAARRTGLLRGSQKTQD----	254
H.marismortui	VDHPFGGGGRQH-PGKPKSISR NAPPGRKVGD IASKRTG--RGNE-----	240
E.coli	VDHPHGGGEGRN-FGKHPVTPWGVQTKGKKTRSNKR-TDKFIVRRRSK----	273
T.thermophilus	VDHPHGGGEGRAPRGRPPASFWGWQTKGLKTRKRKPPSSRF I IARRKK----	276
	* : * * * : * : : : : : : : : : : : :	

Figure 28 Multiple sequence alignment of uL2 amino acid from different species. Multiple Sequence Alignment shows that uL2 is a universally highly conserved protein. The regions of the protein that were mutagenized are highlighted in appropriate colors matching to the regions shown in figure 27.

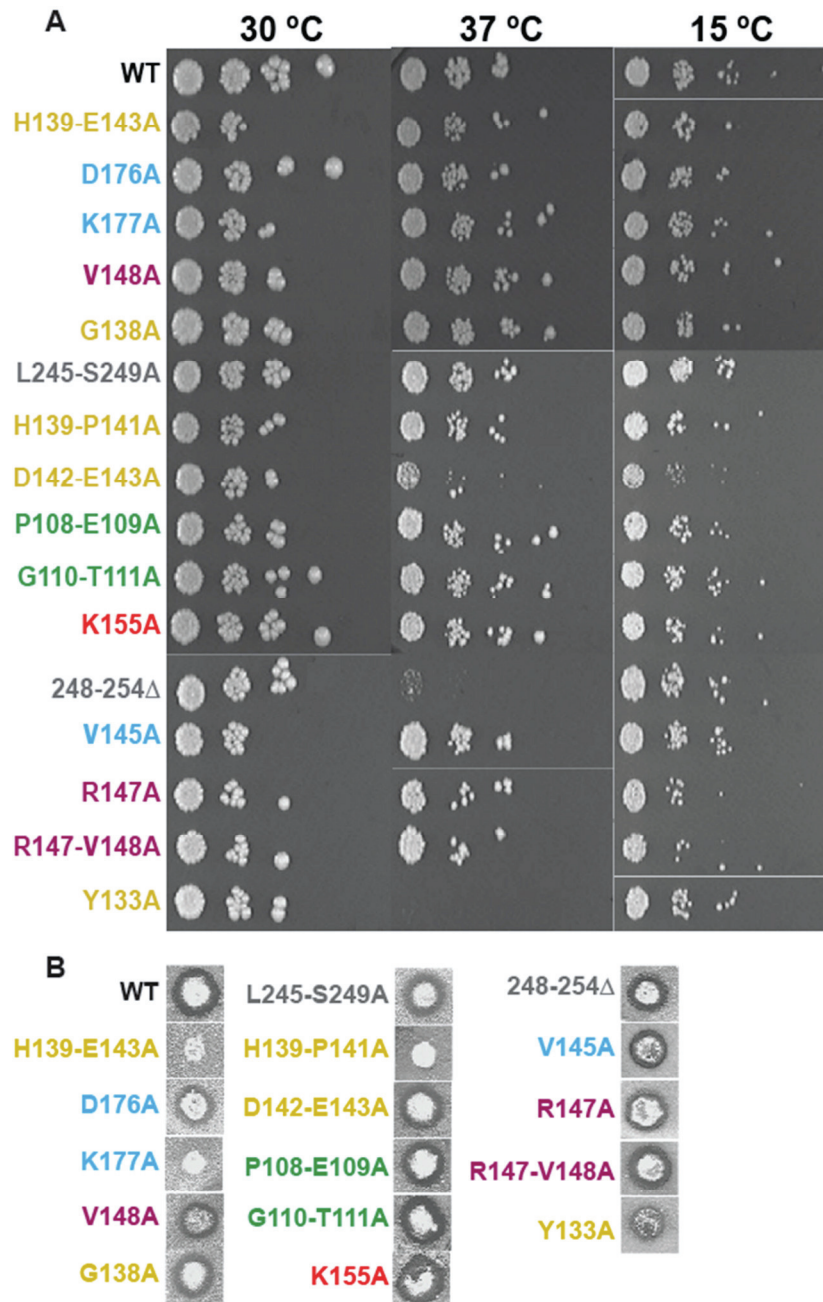


Figure 29 rpL2A bridge mutants promote various phenotypic defects.

(A) Ten-fold serial dilutions of cultures of indicated *S.cerevisiae* strains were spotted on rich medium and incubated for 48 hours at 30°C, 15°C, and 37°C to score for growth, cold and heat sensitivity respectively. (B) “Killer” virus phenotypes: The Killer+ phenotype is scored by the presence of a halo of growth inhibition around wild-type colony. Lack of the halo around colonies expressing the H139-E143A and K177A L2 mutants indicates the Killer- phenotype. Mutant Y133A displays a weak killer phenotype.

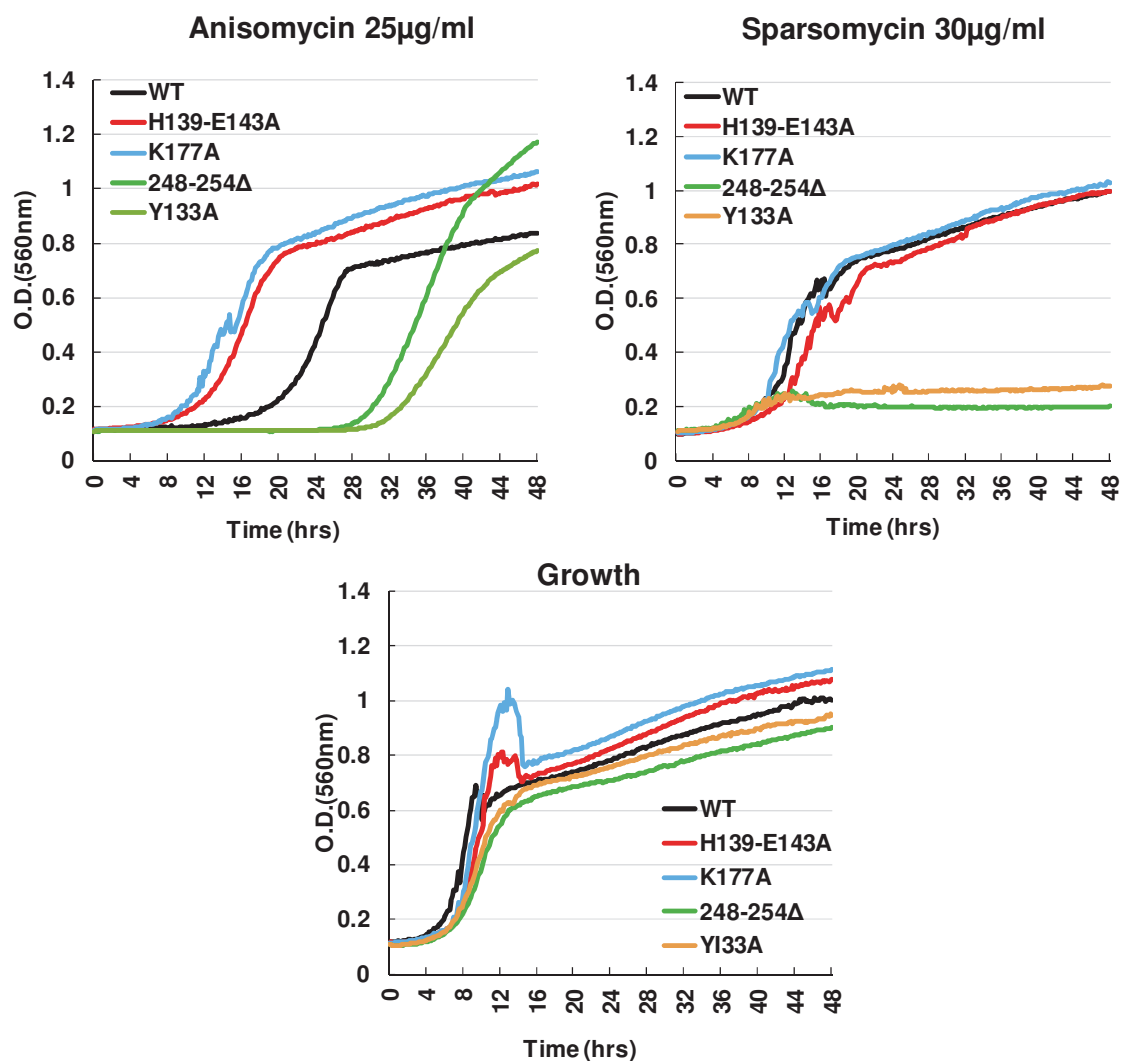


Figure 30 Drug sensitivity assays.

Growth curves were generated in quadruplicate with a Synergy HT micro-plate reader utilizing the KC4 software package (Bio-Tek Instruments, Inc., Winooski, VT). Yeast growth at 30°C was measured in 96-well plates beginning with 0.1 ml cultures of cells in YPAD medium diluted to OD₅₉₅=0.05. Cultures were subjected to constant high-intensity shaking and automatic OD₅₉₅ readings were taken of each well at 10-min intervals for 48h. Duplicate cultures were independently assayed twice and the four readings were averaged for each time point.

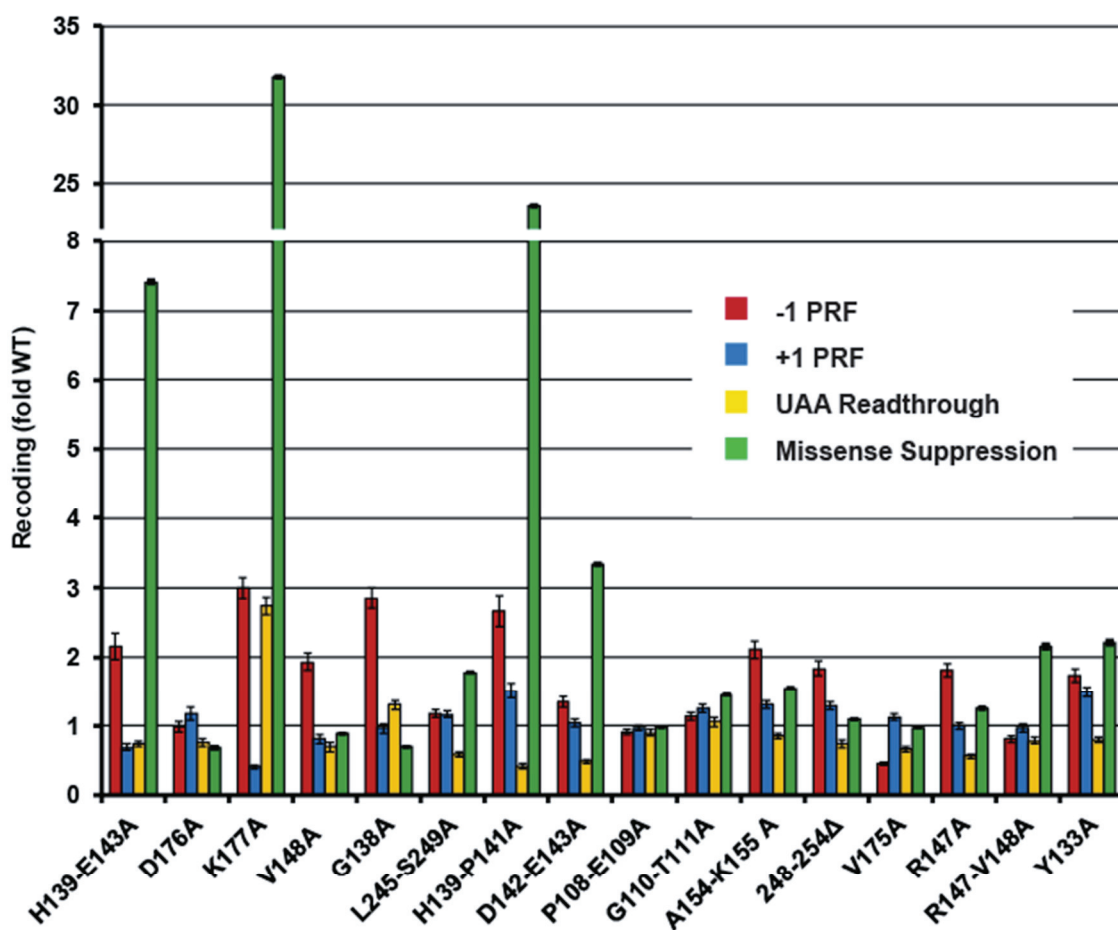


Figure 31 uL2 mutants promote defects in translational fidelity.

Isogenic yeast cells expressing either wild-type or mutant forms of uL2 were transformed with dual luciferase reporters and control plasmids and rates of translational recoding were determined. All results are graphed as fold wild type. -1 PRF was measured using the yeast L-A virus frameshift signal. +1 PRF was directed by the frameshift signal derived from the *TyI* retrotransposable element. Rates of termination codon readthrough were measured using a reporter harboring an in-frame UAA termination codon positioned between the *Renilla* and firefly luciferase reporter genes. Rates of suppression of missense suppression near- and non-cognate codons were evaluated by incorporation of an arginine (AGA) instead of a cognate serine (AGC) at the firefly luciferase catalytic codon 218. Error bars denote standard error. ***n*=4-10 biological replicates repeated in duplicate.**

uL2 mutants in the B7b intersubunit bridge region disrupt the rotational equilibrium of ribosomes

A comprehensive analysis using hSHAPE defined the chemical reactivity profiles of non-rotated and rotated yeast ribosomes²³². This study established that the reactivity of the two bases in the B7a intersubunit bridge, G913 to kethoxal and A2207 to 1M7, can be used as diagnostic markers of intersubunit rotational status. The involvement of these two bases in a base triple interaction in the unrotated state render them resistant to chemical modification, while disruption of this interaction in the rotated state allows them to react (Fig. 32A). The extent of base chemical modification was measured in bulk equilibrium using isogenic wild-type and mutant ribosomes. The reactivity of these two bases in wild-type ribosomes was used to set the baseline for rotational equilibrium at steady state. Thus, increases or decreases in base modification are indicative of shifts in equilibrium, rotated or unrotated respectively. Chemical modification analyses revealed increased extents of chemical modification for all four mutants (Fig. 32B), indicating shifts in equilibrium toward the rotated state. The most pronounced shifts were observed for the uL2-K177A and uL2-Y133A mutants. More extensive hSHAPE analyses revealed that the uL2-K177A and uL2-Y133A promoted similar changes in 1M7 base modifications in both the SSU and LSU (Fig. 33, 34, and 37). In the SSU (Fig. 33 and Fig. 37), these mutants tend to render bases in h23 more susceptible to chemical modification, i.e. more flexible. Conversely the two mutants made bases in h23a, h24 and h27 became less prone to modification, i.e. less flexible. In the LSU (Fig. 34 and Fig. 36), these two mutants had very strong effects on the chemical reactivity of bases in H93

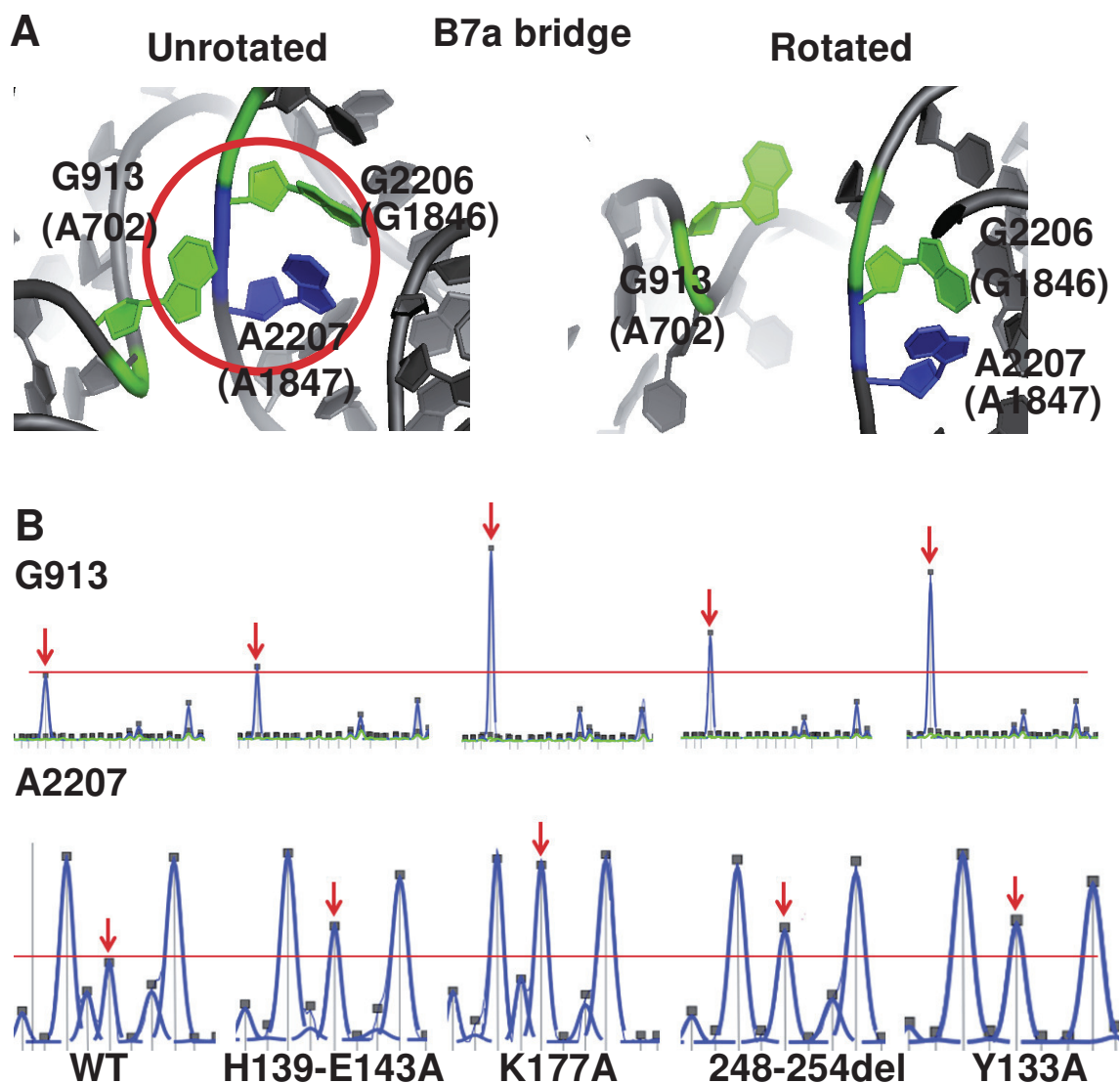


Figure 32 uL2 B7b bridge mutants alter the rotational equilibrium of the ribosome. (A) The B7a intersubunit bridge. In the non-rotated ribosome, A2207 (25S rRNA) and G913 (18S rRNA) engage in a triple base interaction along with G2206. In the rotated state, the base triple is disrupted, and the 2' OH-group on A2207 becomes accessible to modification by 1M7. Similarly, atoms on G913 become accessible to modification by kethoxal upon rotation. Images were generated in pymol using atomic resolution yeast ribosomal structures^{23,241}. *E. coli* base numbers are shown in parentheses. (B) Reactivity peaks obtained by hSHAPE after chemical probing of the landmark base G913 (arrows) at the SSU side of the B7a intersubunit bridge with kethoxal (upper panel) and probing of the landmark base A2207 (arrows) at the LSU side of the B7a intersubunit bridge with 1M7 (lower panel). Shown here are the capillary electrophoresis traces from primer extension reactions of IM7 reacted rRNA after sequence alignment and correcting for the reactivity of corresponding bases in control (DMSO) reaction.

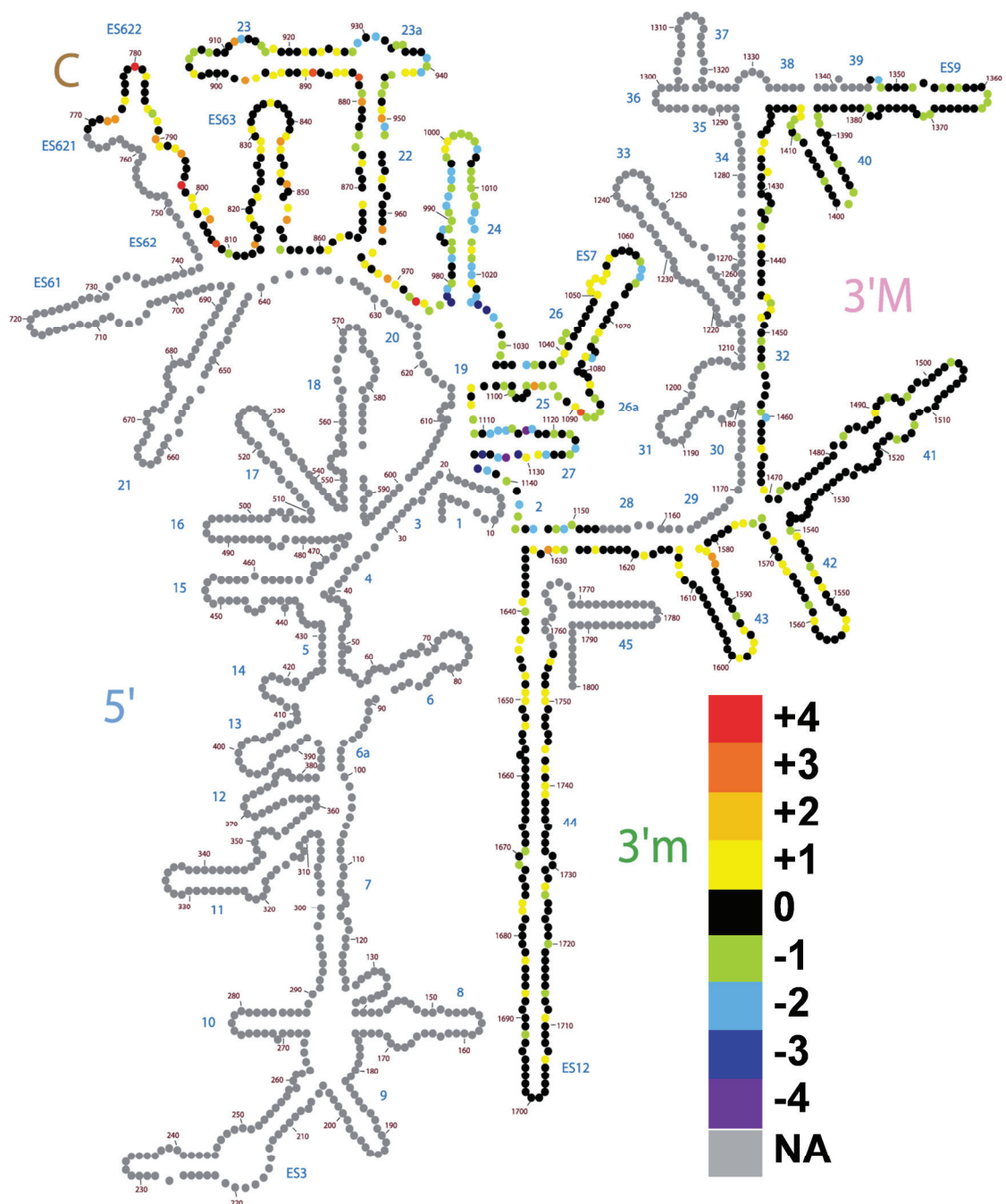


Figure 33 Structural probing analysis of 18S rRNA of Wild-type and uL2-K177A. Chemical probing analysis using 1M7 and hSHAPE was performed as described in Leshin et al.²⁴², Reactivity difference between L2-K177A and WT for the bases covered was mapped on the 2d map of 18S rRNA. The scale at right indicates the extent of differences in reactivity with each number corresponding to one standard deviation from the mean reactivity as previously described²⁴³.

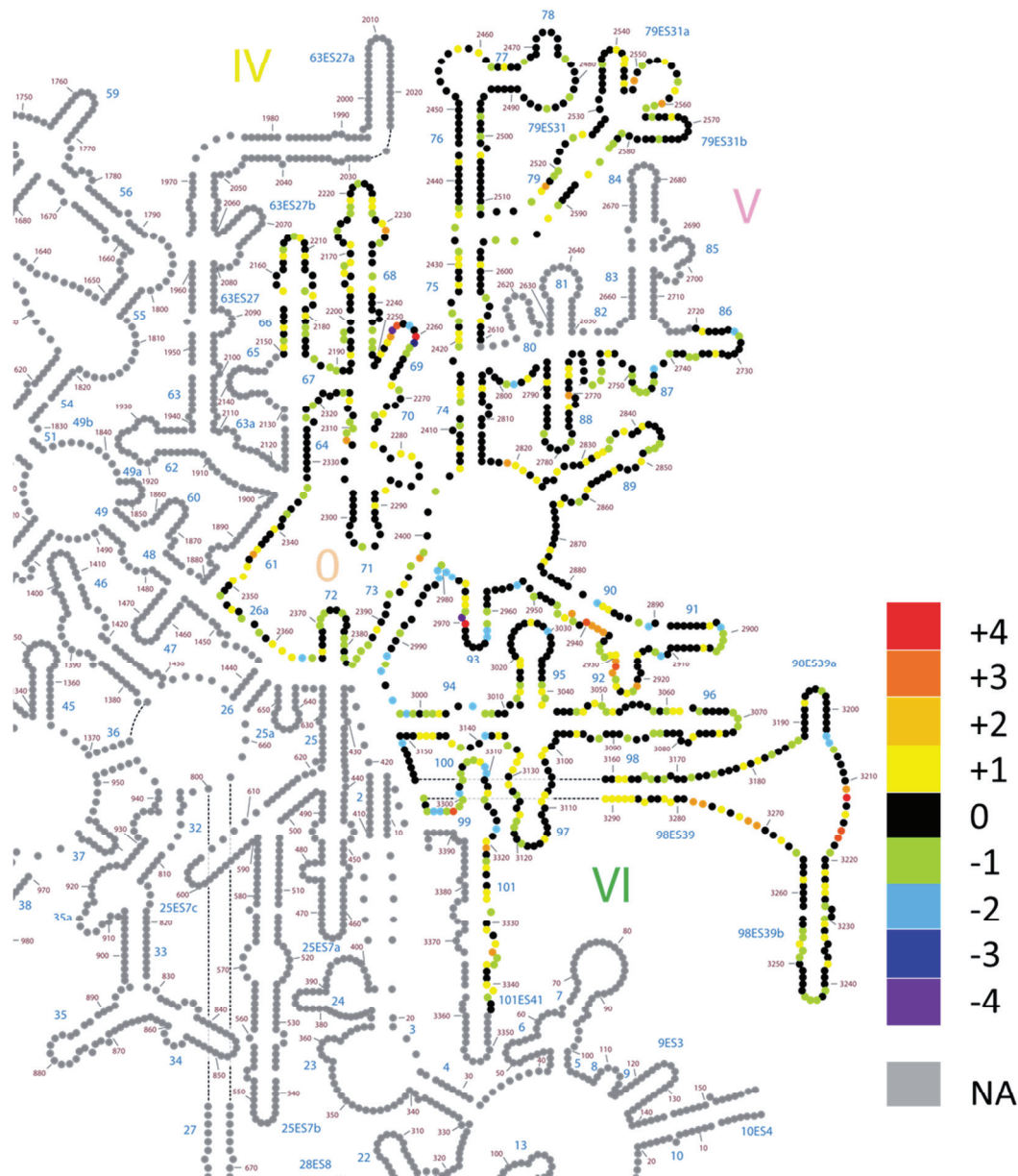


Figure 34 Structural probing analysis of 25S rRNA of Wild-type and uL2-K177A.

Chemical probing analysis using 1M7 and hSHAPE was performed as described in Leshin et al.²⁴², Reactivity difference between L2-K177A and WT for the bases covered was mapped on the 2d map of 25S rRNA. The scale at right indicates the extent of differences in reactivities with each number corresponding to one standard deviation from the mean reactivity as previously described²⁴³.

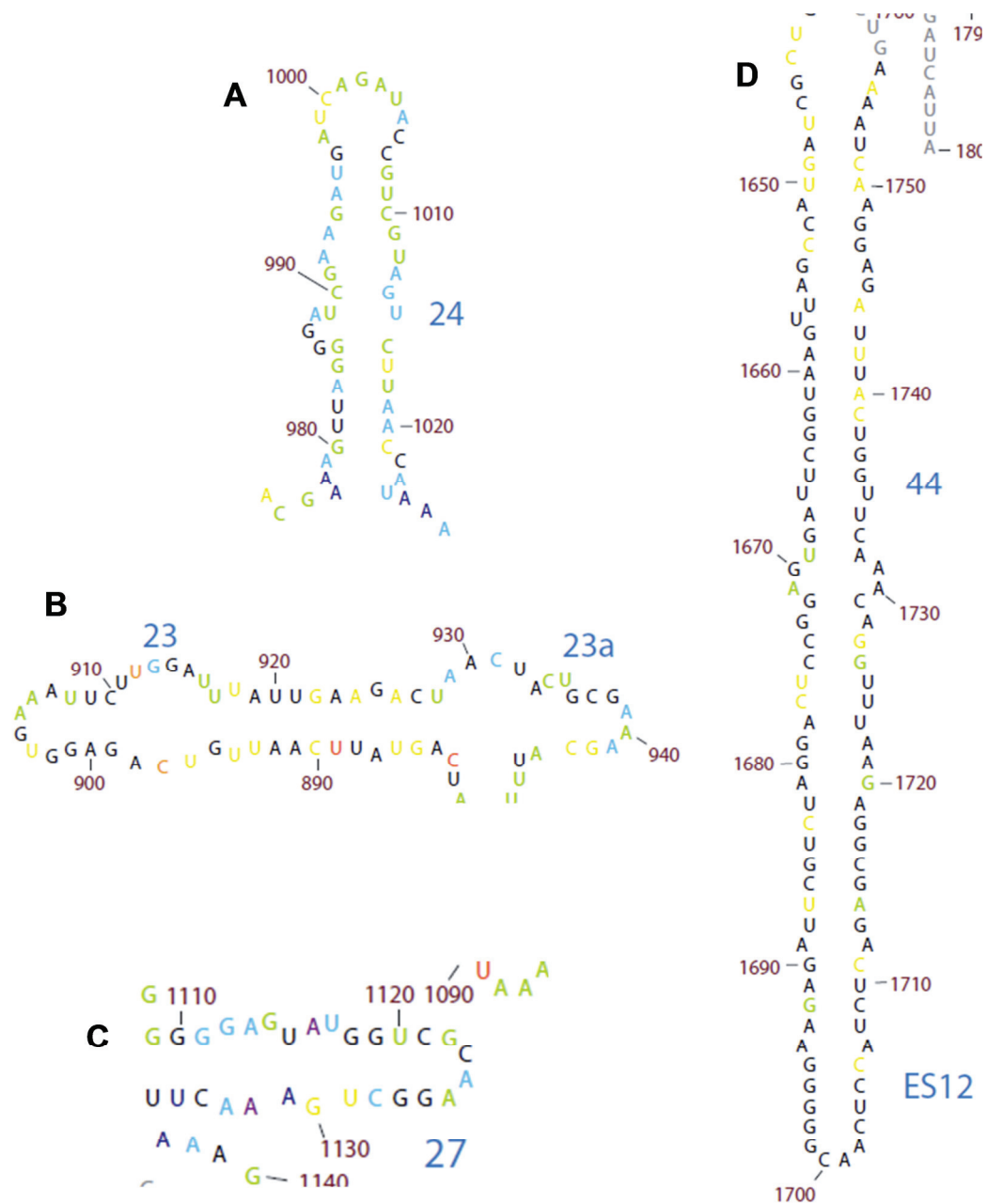


Figure 35 Magnified view of the Structure probing in SSU.

Reactivity difference between L2-K177A and WT for **A.** h24, **B.** h23 and h23a, **C.** h27, and **D.** h44

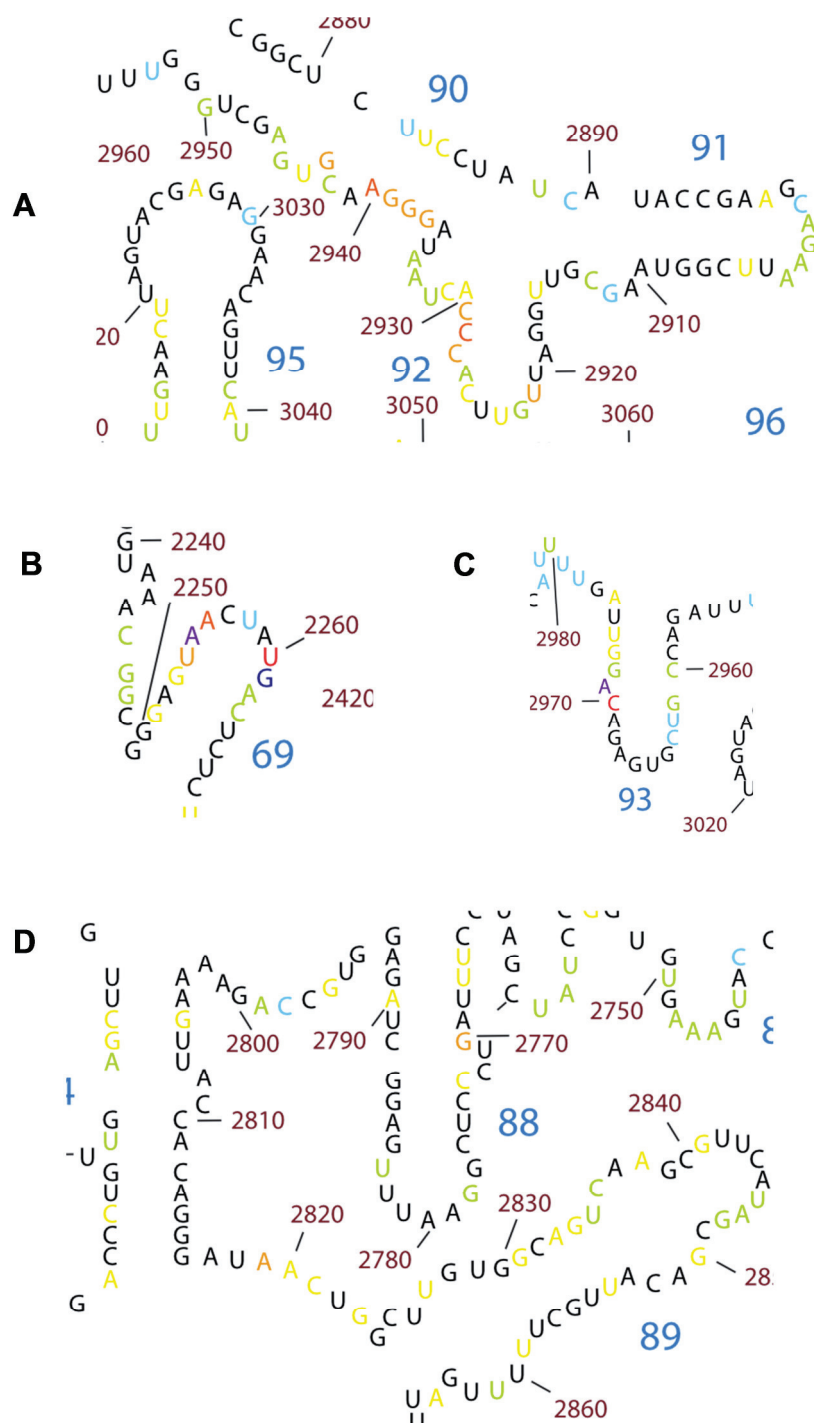


Figure 36 Magnified view of the Structure probing in SSU.

Reactivity difference between L2-K177A and WT for **A.** H90, 91, 92, and H95 **B.** H69, **C.** H93 and **D.** H88 and H89

in the peptidyltransferase center (also see Fig. 37), Helices 89 – 92 (the tRNA accommodation corridor), and H69 which interrogates the decoding center during translation elongation.

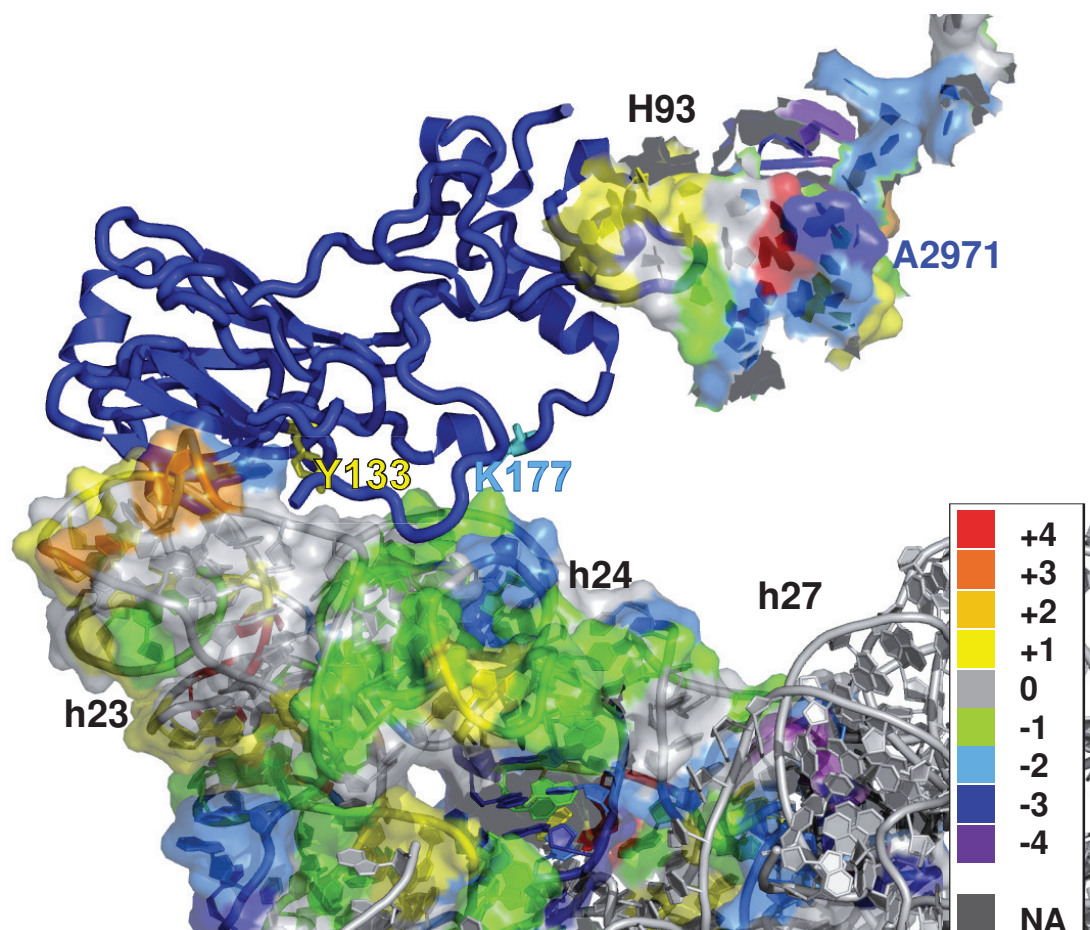


Figure 37 Three dimensional representation of 1M7 reactivity difference.

Differences in IM7 reactivity between uL2-K177A and WT 18S and 25S rRNA regions were probed by hSHAPE. The reactivity differences were assigned color codes according to the scale shown to the right. Warmer colors indicate increased reactivity and cooler colors denote decreased reactivity. Scored data were mapped on 3.0 Å resolution yeast ribosomes²³ using pymol.

Region	rRNA base	Non-rotated	WT	K177A	Rotated
B7a	A2207	2	0	2	4
B2a	U2258	2	3	4	4
	C1644 (SSU)	1	1	2	2
	G1645 (SSU)	0	1	1	1
B3	U2301	0	0	0	1
	G2302	0	0	0	0
	A1655 (SSU)	1	1	2	2
	U1656 (SSU)	2	2	2	2
AC	U2860	1	0	1	0
	U2924	4	3	3	1
	A2926	4	3	2	1
H93	A2971	4	4	1	1
SRL	U3023	1	0	0	0
	A3027	2	1	1	0

Figure 38. Comparison of SHAPE reactivity of individual ribosomal bases to non-rotated and rotated control ribosomes.

Salt washed empty uL2-WT and uL2-K177A were chemically probed with 1M7 and analyzed by hSHAPE. Reactivity values for non-rotated and rotated controls were obtained from Sulima et al²³². Non-rotated control yeast ribosomes were primed with polyU and contained Ac-Phe-tRNA^{Phe} in the P-site. Rotated control ribosomes were primed with polyU, loaded with deacylated Phe-tRNA, and incubated with eEF-2-GDPNP. Reactivity for bases involved in bridge B7a, B2a, B3, Accommodation Corridor (AC), Helix 93 (H93), AND Sarcin-Ricin loop are shown here.

Some mutants of uL2 in the B7b region cause defects in ribosome biogenesis pathway and subunit joining defects in elongation pathway.

Sucrose density gradient analyses of polysomes demonstrated that, most of the uL2 mutants generated in this study had defects mild to severe ribosome biogenesis defects. In figure 39, the first two peaks in polysome profiles correspond to the 40S and 60S subunits. In WT ribosomes the 40S:60S UV absorbance ratio is about 1.

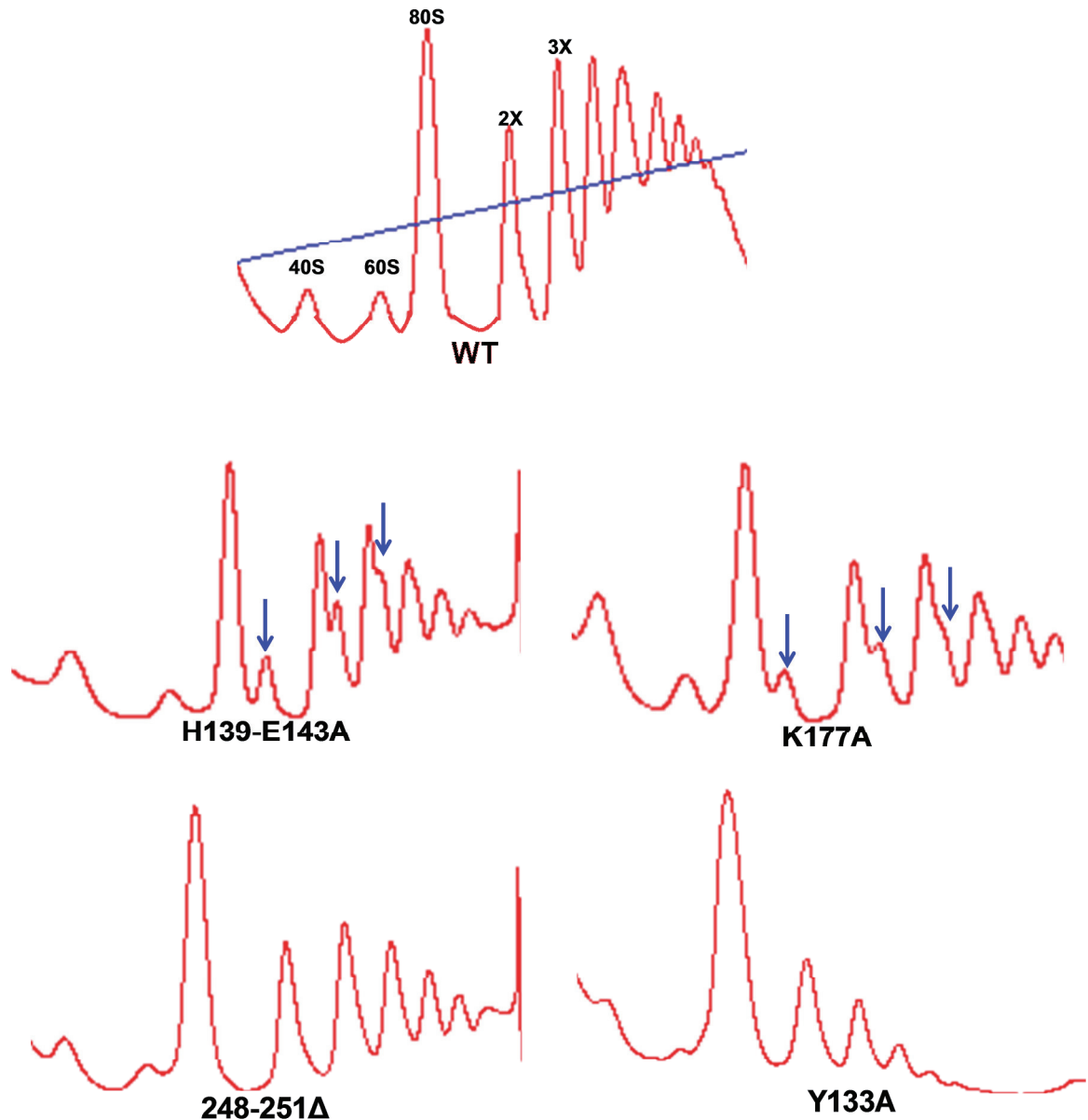


Figure 39 Polysome profiles of cells expressing WT and mutant uL2.

Polysome profiles were generated by Sucrose density gradient fractionation of cycloheximide arrested cell lysates of WT and mutant *rpL2A* expressing strains of yeast. The first two peaks stand for 40S and 60S subunits respectively, the third peak is 80S ribosome and the subsequent peaks represent two or more ribosomes present on the same mRNA. In WT cells, the ratio 40S:60S is about 1, while in mutants the 60S peak is significantly lowered due to ribosome biogenesis defects. Shoulders to regular peaks are called half-mers and they represent subunit joining defects in translation or lack of adequate subunits (in this case 60S) due to biogenesis defects.

In mutants uL2-248-254Δ and uL2-Y133A, these ratios are slightly raised, cells expressing uL2-H139-E143A or uL2-K177A display severe defects in 60S biogenesis. The ribosomes that survive the surveillance in ribosome biogenesis are exported to the cytoplasm and can participate in translation there. The presence of shoulders to the regular peaks (half-mers) in polysome profiles demonstrate mutants uL2-H139-E143A and uL2-K177A display subunit joining defects; where 60S subunit fails to join the initiation complex for translation to proceed either due to lack of adequate free 60S subunits or because of reduced intermolecular interactions resulting from the mutations.

Disruption of ribosome rotational equilibrium by uL2 mutants affects binding of translation elongation factors.

Structural analyses of the translation elongation cycle suggested that ribosome rotational status determines the affinity of the two elongation factors with the A-site ribosome; the TC that delivers aminoacylated tRNAs and the translocase²⁴⁴. In yeast ribosomes, this model was supported using mutants of uL16, i.e. unrotated ribosomes had higher affinity for TC (eEF1A•aminoacyl-tRNA•GTP) and rotated ribosomes had higher affinity for translocase (eEF2•GTP)²³². To test the universality of this model, steady-state filter binding assays were performed using the uL2 mutants identified in the current study. Ribosomes containing the two most rotated mutants, uL2-K177A and uL2-Y133A displayed more than two-fold increases in K_D for TC ($P<0.01$), and conversely, nearly 2-fold decreases in K_D for eEF2•GDPNP ($P<0.06$) (Fig. 40A, 40B, Fig. 41A – 41D). uL2-248-254Δ mutant ribosomes, which promoted a lesser extent of shift in equilibrium towards rotated state, also promoted significantly decreased affinity for TC, while uL2-

H139-E143A, having the least pronounced effect on rotational equilibrium, did not significantly affect TC binding. The uL2-K177A and C-terminal deletion mutants also conferred decreased affinity for N-acetyl-aminoacyl-tRNA (Ac-aa-tRNA) to the P-site, while the uL2-H139-E143A mutant promoted a small but significant increase in this parameter (Fig 40C, 41E, F).

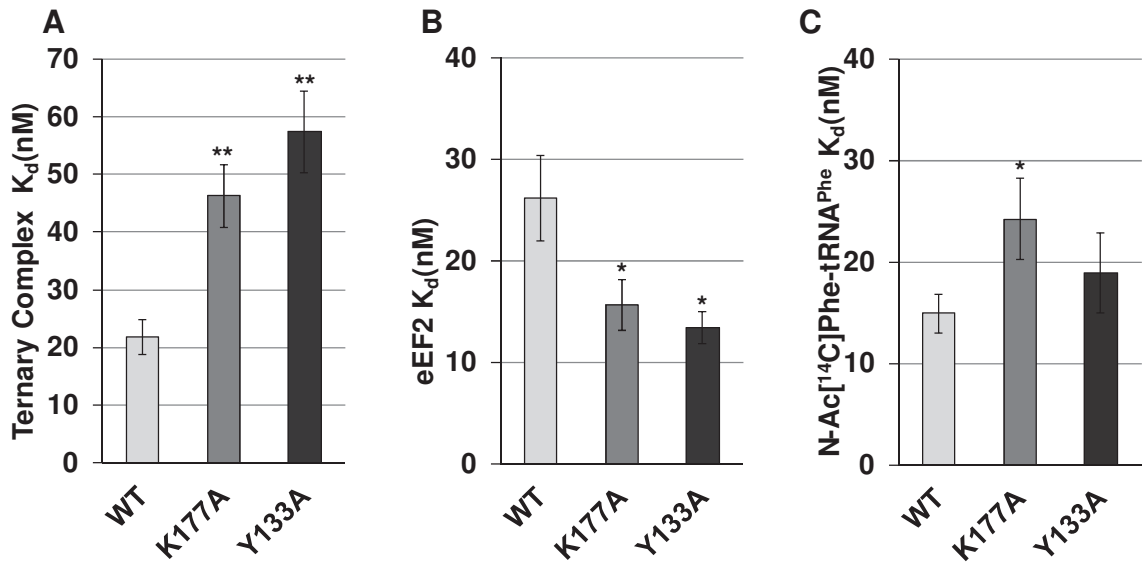


Figure 40 uL2 B7b bridge mutants of alter the binding of translation elongation factors.

Dissociation constants (K_d) were generated by analysis of single-site binding isotherms of [14 C]Phe-tRNA^{Phe}•eEF1A•GTP (ternary complex) (A), or of eEF2 to the ribosomal A-site (B), and Ac-[14 C]Phe-tRNA^{Phe} to the P-site (C). Binding assays are explained in chapter 3: Materials and Methods. Error bars indicate standard error (n=4, * $p < 0.05$, ** $p < 0.01$).

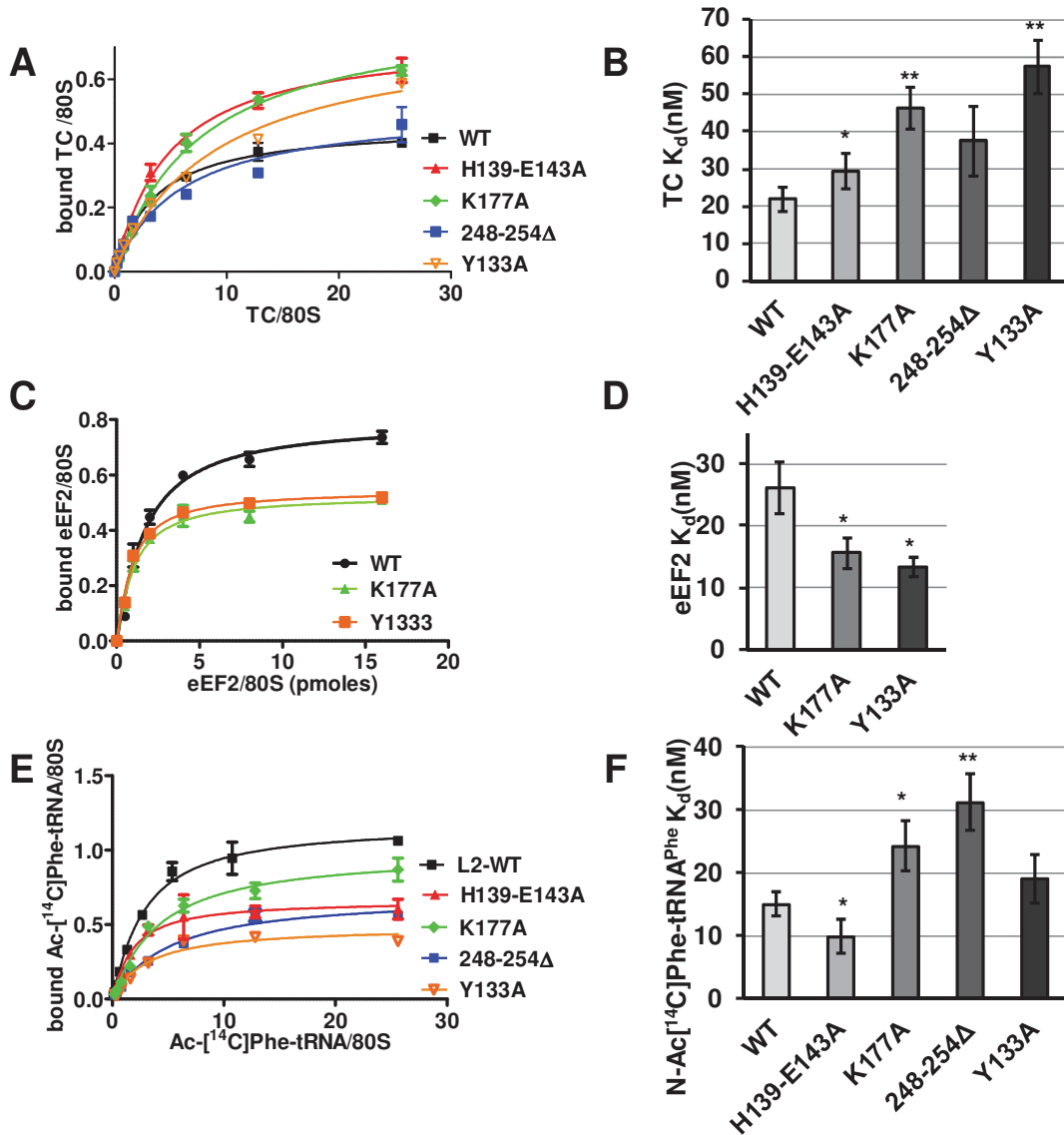


Figure 41 Biochemical analyses of *rpl2A* mutants.

Single site binding isotherms of ternary complex to the A-site of ribosomes isolated from wild-type, *rpl2-H139-E143A*, *rpl2-K177A*, *rpl2-G248-D254Δ* and *rpl2-Y133A* cells (panel a). B. Ternary complex binding dissociation constants (K_ds) calculated using ligand depletion model (Graphpad Prism). C. Single site binding isotherms of eEF2 to ribosomes isolated from wild-type, *rpl2-K177A*, and *rpl2-Y133A* cells. D. eEF2 binding K_ds calculated using ligand depletion model (Graphpad Prism). E. Single site binding isotherms N-Ac-Phe-tRNA^{Phe} to the P-site of ribosomes isolated from wild-type, *rpl2-H139-E143A*, *rpl2-K177A*, *rpl2-G248-D254Δ* and *rpl2-Y133A* cells. F. N-Ac-Phe-tRNA^{Phe} binding K_ds calculated using ligand depletion model (Graphpad Prism). Error bars indicate standard error. (n=4, * *P* < 0.06, ** *P* < .001)

Mutants of rpl2A encoding uL2-248-254Δ and uL2-K177A do not affect the rates of puromycyl-peptidyltransferase reaction, a proxy for peptidyltransfer reaction.

Ribosomes purified from WT uL2 and uL2-248-254Δ or uL2-K177A expressing cells were purified as previously described. Complex C were formed by incubating N-Ac-[¹⁴C]Phe-tRNA^{Phe}, followed by glycerol ultracentrifugation to remove access tRNA. Apparent rates of peptidyltransfer from single turnover peptidylpuromycin reactions revealed that the mutants do not vary largely in their peptidyltransferase activity from the wild type. There was a very mild decrease in uL-K177A activity while uL2-248-254Δ displayed no significant difference from the WT.

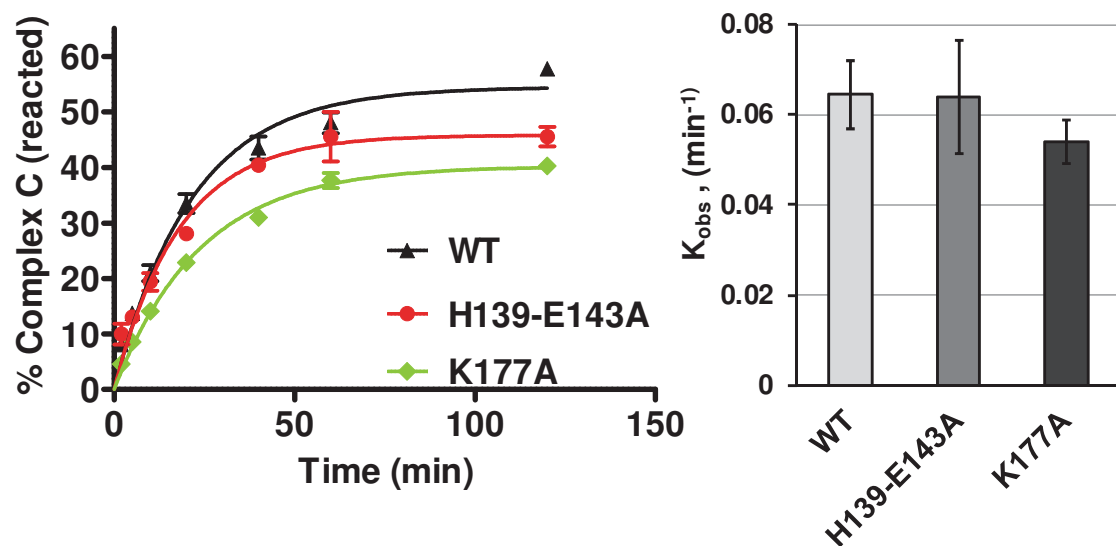


Figure 42 Single turnover peptidylpuromycin reactions.

Extent on complex C conversion to peptidyl Puromycin is measured radioactively.

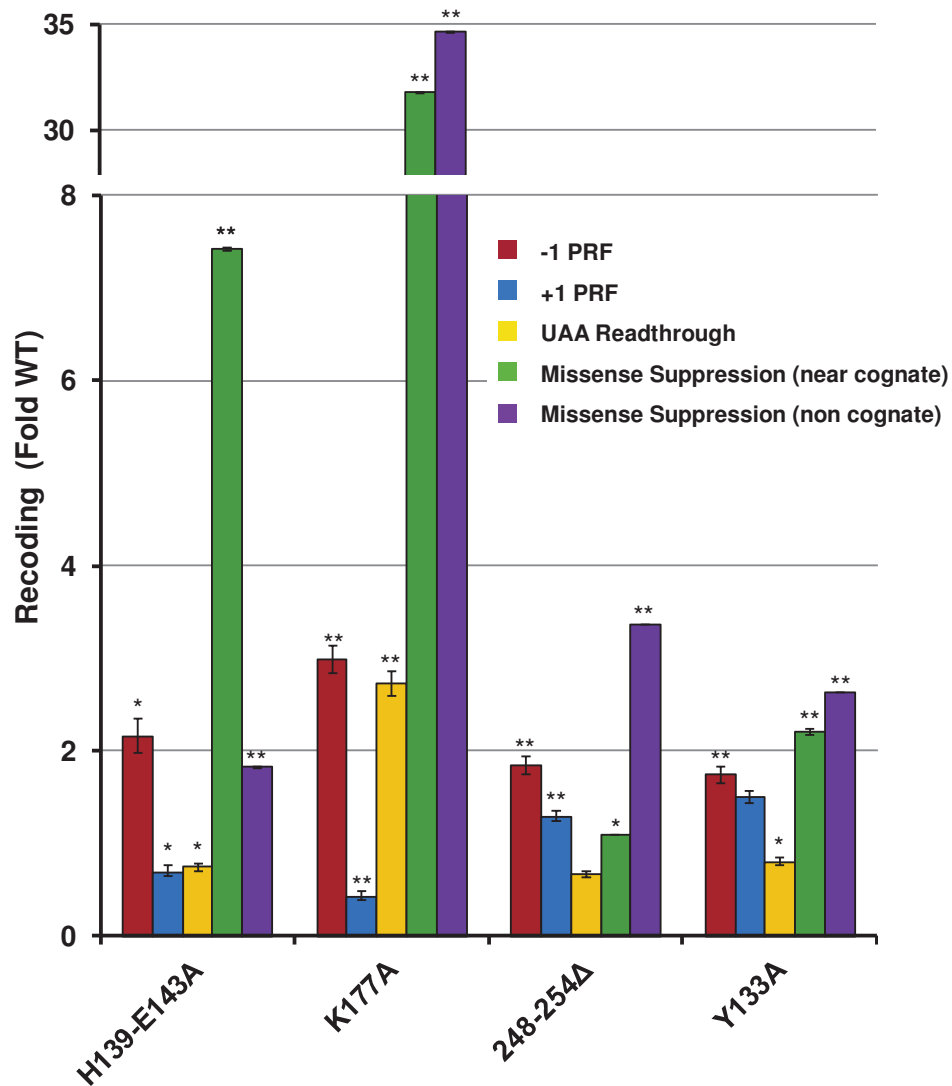


Figure 43 Translation fidelity assays for selected uL2 mutants.

Isogenic yeast cells expressing either wild-type or mutant forms of uL2 were transformed with dual luciferase reporters and control plasmids and rates of translational recoding were determined. All results are graphed as fold wild type. -1 PRF was measured using the yeast L-A virus frameshift signal. +1 PRF was directed by the frameshift signal derived from the *TyI* retrotransposable element. Rates of termination codon readthrough were measured using a reporter harboring an in-frame UAA termination codon positioned between the *Renilla* and firefly luciferase reporter genes. Rates of suppression of missense suppression near- and non-cognate codons were evaluated by incorporation of an arginine (AGA) instead of a cognate serine (AGC) or a non-cognate serine (TCT) at the firefly luciferase catalytic codon 218. Error bars denote standard error. *n*=4-10 biological replicates repeated in quadruplicate, **p*<0.05, ***p*<0.01.

The uL2-K177A and uL2-Y133A mutants promote significant changes in translational fidelity.

Dual luciferase based *in vivo* assays were used to monitor the effects of the two mutants on five different aspects of translational fidelity. In general, and consistent with the strongest effects on intersubunit rotation, the uL2-K177A mutant conferred the strongest changes in translational fidelity (Fig. 43). Both mutants conferred increased rates of -1 PRF, consistent with studies indicating that rotated ribosomes are substrates for this reaction^{172,245}. In contrast, uL2-K177A ribosomes promoted a >50% decrease in rates of +1 PRF, while uL2-Y133A mutants promoted a modest but statistically insignificant increase. uL2-K177A also led to a nearly 3-fold increase in readthrough of the UAA termination codon. However, the most pronounced effects were observed in conjunction with the effects of this mutant on the ability of ribosomes to discriminate between cognate and either near-or non-cognate tRNAs, where greater than 30-fold increases in suppression of these classes of codons were observed for both mutants.

The uL2-K177A mutant affects gene expression and telomere maintenance through changes in programmed ribosomal frameshifting.

In yeast, the mRNAs encoding at least four proteins (EST1, EST2, STN1, CDC13) involved in telomere maintenance contain -1 PRF signals that function as destabilizing elements by directing translating ribosomes to premature termination codons¹⁸². The EST3 mRNA encoding a fifth telomere maintenance protein harbors a +1 PRF signal that is identical to the *Ty1* recoding element that is required for synthesis of the full-length protein^{246,247}. Additionally, OAZ1, encoding ornithine decarboxylase

antizyme requires a +1 PRF event for its synthesis²⁴⁸. Dual luciferase reporters harboring these frameshift signals were assayed in isogenic wild-type and uL2-K177A cells (Fig. 44A). These assays revealed that -1 PRF directed by signals in the *EST1*, *EST2*, and *STN1* mRNAs was stimulated in the mutant cells. -1 PRF directed by the *CDC13* sequence only slightly stimulated by the uL2 mutation. +1 PRF directed by the *OAZ1* sequence was also strongly inhibited in mutant cells (<25% of wild-type). qRT-PCR assays revealed decreases in the steady state abundances of all of the PRF signal containing mRNAs.

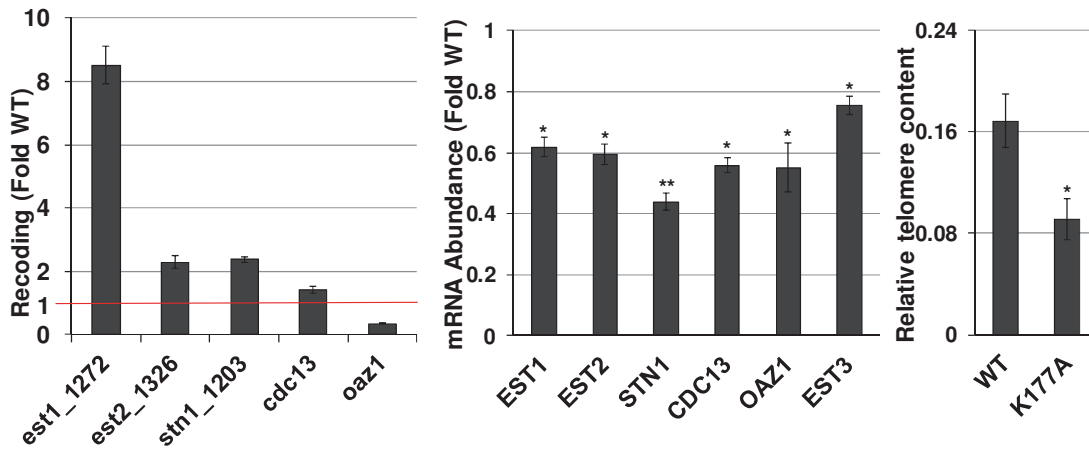


Figure 44 uL2-K177A mutant ribosomes promote defects in cellular gene expression and telomere maintenance through altered frameshifting.

A. Rates of -1 PRF were determined by sequences derived from yeast *EST1* (signal beginning at nucleotide 1,272), *EST2* (signal beginning at nucleotide 1,326), *STN1* (signal beginning at nucleotide 1,203), and *CDC13* (signal beginning at nucleotide 1,272), and of +1 PRF directed by sequence in the *OAZ1* mRNA. **B.** Steady-state abundance of endogenous *EST1*, *EST2*, *STN1*, *CDC13*, *OAZ1* and *EST3* mRNAs was monitored by quantitative RT-PCR. Bars indicate SEM. **C.** The abundance of telomere repeat sequences was quantified by PCR, with the single-copy reference gene *SGS1* as the loading control. T/S ratios of calculated from C_t values represent relative telomere content. Bars indicate SEM (n=9). * $p < 0.05$; ** $p < 0.01$.

Decreased abundance of the -1 PRF signal containing mRNAs is consistent with findings that they function as mRNA destabilizing elements by directing translating ribosomes to premature termination codons^{181,182}. Similarly, since +1 PRF events are required for synthesis of full-length Est3p and Oaz1p, decreased rates of +1 PRF is predicted to increase the fraction of ribosomes directed to premature termination codons on these mRNAs, also reducing their steady-state abundances. qRT-PCR assays revealed that the abundance of telomere DNA repeats (a proxy for telomere length) in uL2-K177A mutant cells was reduced approximately two-fold compared to isogenic wild-type cells (Fig. 44C). This is consistent with the idea that PRF plays an important role in yeast telomere maintenance.

Discussion

The ribosome transits through a large number of conformational states during the translation elongation cycle, the two extremes of which are called unrotated and rotated²⁴⁹. The structural and biochemical analyses with the uL2 mutants (Figs. 32-37) demonstrate a direct relationship between ribosome rotational status and affinity for the two elongation factors. These observations broaden the support for the general model in which unrotated ribosomes have higher affinity for TC and lower affinity for the translocase, and these properties are reversed upon intersubunit rotation (Fig. 45A).

The selection of appropriate ligands to the ribosomal A-site during translation elongation is governed by a delicate series of kinetically separated steps^{250,251}. Disruption of these parameters by the uL2 mutants examined here is manifested at the level of rRNA structure by the observed changes in rRNA chemical modification patterns. The

demonstration of changes in rRNA structure in all of the functional centers located in both subunits is consistent with allosteric information exchange pathways identified using other mutants of yeast proteins and rRNA bases^{232,252–259}. Increased reactivity of bases in the B7a intersubunit bridge is diagnostic of the intersubunit rotational equilibrium having shifted toward the rotated state. This is further supported by the observed closing of the tRNA accommodation corridor (decreased reactivity in H89 – H92), stabilization of A2971 (*E. coli* 2602) in the peptidyltransferase center, and stabilization of h27. These observations lend further support to the model linking ribosome rotational status to elongation factor binding affinity. Here, we present a model illustrating how these changes in structure and biochemistry account for the observed changes in translational fidelity (Fig. 45). The substrate for TyI and EST3 directed +1 PRF is a ribosome paused at the CUU AGG C heptameric slippery site with a peptidyl-tRNA base paired to the P-site CUU codon, and awaiting the rare cognate tRNA(CCUArg) at the A-site¹⁸⁶, i.e. an unrotated ribosome (Fig. 45A). In contrast, rotated ribosomes containing hybrid-state tRNAs have been demonstrated to be the substrates for -1 PRF^{164,172,173,245} (Fig. 45A). By shifting the rotational equilibrium towards the rotated state, these mutants increase the steady-state abundance of -1 PRF substrate, thus stimulating this process. In contrast, decreased abundance of the +1 PRF substrate results in decreased rates of +1 PRF. Similarly, since the release factors bind to unrotated ribosomes, decreasing this substrate inhibits this function, leading to increased rates of UAA termination codon readthrough, at least for the uL2-K177A mutant (i.e. the mutant that most disrupted rotational equilibrium). The most dramatic changes in translational fidelity were observed as defects in the ability of ribosomes to discriminate between cognate tRNAs and near-/non-

cognate tRNAs. As shown in Fig. 45B, the unrotated ribosomes are the substrate for TC binding. Elegant biochemical studies have detailed the kinetic parameters underlying the high fidelity selection of cognate tRNAs during the translation elongation process^{250,260}. Importantly, these analyses have shown that rapid dissociation of near-cognate tRNAs from ribosomes is the first step of discrimination. Specifically, near cognate tRNAs dissociate at rates of $\sim 80 \text{ sec}^{-1}$ as compared to $\sim 0.2 \text{ sec}^{-1}$ for cognate tRNAs, a 400-fold difference. However, shifting the population of ribosomes toward the rotated state increases the steady-state K_D of ribosomes for all TCs. We suggest that this disproportionately affects TCs harboring cognate tRNAs, reducing ability of ribosomes to discriminate between cognate and near-cognate TCs. Alternatively, increased rate of misincorporation of tRNAs could be resulting from a higher rate of tRNA accommodation in mutant uL2 ribosomes. Increased propensity of these ribosomes to rest in rotated state could speed up the transition from unrotated to rotated state thus driving the accommodation of tRNAs at higher rates.

Expression of up to 10% of cellular genes is predicted to be regulated by -1 PRF^{261,262}, and +1 PRF has been demonstrated in at least two additional yeast mRNAs^{263,264}. -1 PRF events in yeast mRNAs encoding proteins critical for telomere maintenance direct translating ribosomes to premature termination codons, resulting in mRNA degradation through the nonsense-mediated mRNA decay pathway (NMD)^{181,233}. Thus, increased rates of -1 PRF promoted by the uL2-K177A mutant promoted decreased abundances of the -1 PRF signal containing EST1, EST2, STN1 and CDC13 mRNAs. In contrast, +1 PRF is required to complete translation of the EST3 and OAZ1 mRNAs.

Here, decreased rates of +1 PRF results in a greater fraction of ribosomes encountering the 0-frame termination codons in these mRNAs, decreasing their abundances presumably also through NMD. At the biological level, the proteins encoded by *EST* family of genes, *STN1* and *CDC13* are all involved in yeast telomere maintenance²⁶⁵. The observed changes in -1 and +1 PRF resulted in decreased abundance of yeast telomere repeats, indicative of enhanced telomere shortening. While it is not known if mRNAs encoding proteins required for human telomere maintenance are regulated by PRF, should this be demonstrated in the future, the findings presented here may provide a link between PRF and the progeria-like presentations of some ribosomopathies²⁶⁶. *OAZ1* encodes ornithine decarboxylase antizyme, the critical control node in polyamine biosynthesis²⁶⁷. Disruption of this pathway has pleiotropic effects, including control of cellular proliferation and development^{183,268}. The recent demonstration of -1 PRF and termination codon readthrough regulated gene expression humans provide evidence for importance of translational recoding in fine-tuning the immune system and control of tumor progression^{162,163}. The effects of the uL2 mutants on translational fidelity described in this study may be helpful in deepening our understanding the complex nature of cancer progression.

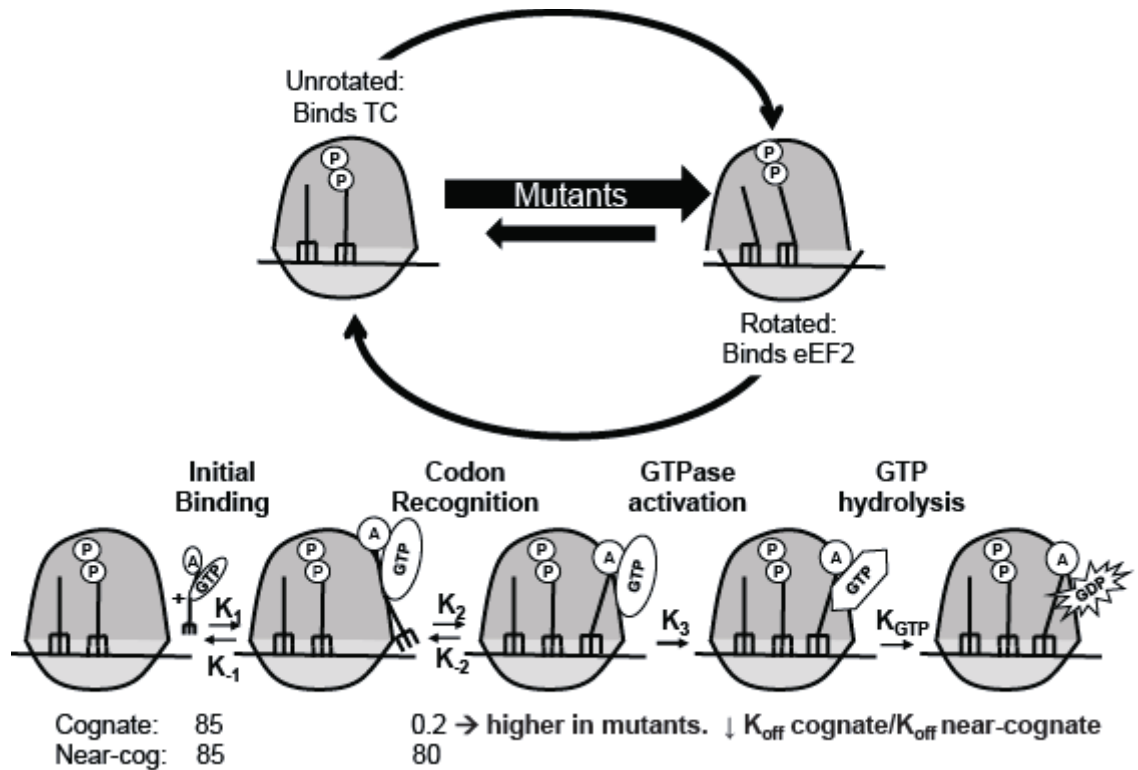


Figure 45 Model describing the effects of disturbed ribosomal rotational equilibrium on tRNA selection and translational fidelity.

(A) The uL2 B7b Bridge mutants perturb the dynamic rotational equilibrium of ribosomes by shifting it towards the rotated state. This increases the steady-state abundance of -1PRF substrate (rotated ribosomes) while creating a deficit of +1 PRF substrate (unrotated ribosomes). (B) Kinetics of initial selection and ternary complex binding is affected by uL2 mutants. In wild type ribosomes, lower k_{off} rates for cognate ternary complex than the near-cognate normally ensures high fidelity of tRNA selection (~400-fold)⁹⁴. Shifting rotational equilibrium toward the rotated state disproportionately increases the k_{off} for cognate ternary complex relative to near- or non-cognate (which are already fast). This results in decreased selectivity at the codon recognition step of translation elongation.

Chapter 3: Materials and Methods

Strains, Plasmids and media in generation of *rpl2A* mutants

S. cerevisiae strain JD1269 containing wild-type *RPL2A* on a centromeric URA3 vector (pRPL2A-URA3) was previously described²³⁹. In JD1315, the wild type vector was replaced by wild type *RPL2A* on a centromeric *LEU2* vector (pRPL2A-LEU2 or pJD957) through standard 5-FOA shuffling technique²⁶⁹. Mutations in the *rpl2A* ORF of pRPL2A-*LEU2* were generated by site-directed mutagenesis technique. Site-directed mutagenesis was carried out using the Quikchange XL site-directed mutagenesis kit following the directions of the manufacturer (Stratagene, Madison, WI, USA). Plasmids were amplified in *E. coli* strain DH5 α . Mutant RPL2A strains were generated by replacing pRPL2A-URA3 with pRPL2A_{mut}-LEU2 through standard 5-FOA plasmid shuffle technique. *Escherichia coli* were transformed using a calcium chloride method²⁷⁰ and yeast cells were transformed with an alkali cation protocol²⁷¹. YPAD, synthetic complete (SC), synthetic dropout medium (H-), and 4.7 MB plates for testing the killer phenotype were used as previously described^{272,273}. The *S. cerevisiae* strains, and oligonucleotides (IDT, Coralville, IA, USA) used in this study are shown in appendices.

Growth and Drug Sensitivity assays

Dilution spot assays were used to qualitatively monitor cell growth at various temperatures and drug concentrations. For all conditions, yeast cells were grown to logarithmic growth phase and then diluted to 1X10⁶ CFU/ml. Subsequently, 10-fold serial dilutions of each strain were spotted onto YPAD and incubated at 15°, 30° and 37°C, or

onto YPAD containing paromomycin (5mg/ml) or anisomycin (25 mg/ml). To test sensitivity to Sparsomycin, filter discs with water, 20µg and 30µg Sparsomycin respectively were placed on a lawn of WT and mutant cells. The size of killer zones for each disc was observed. Growth curves were generated in quadruplicate with a Synergy HT micro-plate reader utilizing the KC4 software package (Bio-Tek Instruments, Inc., Winooski, VT). Yeast growth at 30°C was measured in 96-well plates beginning with 0.1 ml cultures of cells in YPAD medium diluted to OD₅₉₅=0.05. Cultures were subjected to constant high-intensity shaking and automatic OD₅₉₅ readings were taken of each well at 20-min intervals for 40h. Duplicate cultures were independently assayed twice and the four readings were averaged for each time point.

Translation fidelity assays

The dual luciferase reporter plasmids pYDL-control, pYDL-LA, pYDL-TyI, pYDL-UAA, pYDL-AGC₂₁₈ and pYDL-TCT₂₁₈ were employed to monitor programmed -1 ribosomal frameshifting, programmed +1 ribosomal frameshifting, suppression of UAA, and suppression of an AGC near-cognate serine codon and a TCT non-cognate serine codon in place of the cognate AGA codon in the firefly luciferase catalytic site, respectively^{273–277}. The reporters were expressed from high-copy *URA3*-based plasmids (pJD375, pJD376, pJD376, pJD431, pJD642, pJD643). Assays were performed as previously described²⁷⁷. Sample readings were collected using a GloMax Multi-Microplate luminometer (Promega). All assays were repeated 4 times.

Polysome analyses

Sucrose density gradient fractionation experiments were performed by growing yeast cells in YPAD to mid-log growth phase (OD₅₉₅ of 0.6-1.0). To generate polysome profiles, cycloheximide was added to cultures to a final concentration of 0.1 mg/ml and cultures were placed on ice for 10 min. Cells were pelleted by centrifugation and washed with polysome lysis buffer (20 mM Tris-HCl pH 7.0 at room temperature, 50 mM KCl, 12 mM MgCl₂, 1 mM DTT, 200 µg/ml cycloheximide). Cells were resuspended in polysome lysis buffer and disrupted using glass beads (dia 0.5mm) in two 2-min pulses using a Min-beadbeater. Lysates were clarified by centrifugation, and aliquots of 7.0 absorption units at OD₂₆₀ were frozen at -80°C. Aliquots were layered on top of 10.5 ml 7–47% sucrose gradients (polysome lysis buffer with 15–55% weight/volume sucrose). Gradients were centrifuged at 17,000 rpm for 16 hours at 4°C using a Beckman Coulter SW41Ti rotor. After centrifugation, samples were continuously monitored at 254 nm using an ISCO gradient fractionator Model UA-5.

Ribosome purification

Chromatographic purification of yeast ribosomes was performed as described previously²⁵⁹. Lysates of mid-log phase yeast cells were clarified by low-speed centrifugation and supernatants were chromatographically purified (Binding buffer- 20 mM HEPES-KOH pH 7.6, 10 mM MgCl₂, 60 mM NH₄Cl, 2 mM DTT, 1 mM PMSF; Elution Buffer- 20 mM HEPES-KOH pH 7.6, 10 mM MgCl₂, 60 mM NH₄Cl, 2 mM DTT, 1 mM PMSF, 500 mM KCl, 0.5 mg/ml heparin). Remaining tRNAs were cleared from eluted ribosomes with pH-neutralized puromycin. Ribosomes were purified in high-

salt cushion buffer (20 mM HEPES-KOH pH 7.6, 60 mM NH₄Cl, 500 mM KCl, 10 mM Mg(OAc)₂, 2 mM DTT, 25% glycerol) by ultracentrifugation, and subsequently washed and re-suspended in low-salt storage buffer (50 mM HEPES-KOH pH 7.6, 50 mM NH₄Cl, 5 mM Mg(OAc)₂, 1 mM DTT, 25% glycerol). Residual salt was removed from the re-suspended ribosomes by dialyzing against low-salt storage buffer.

Aminoacylation of tRNA^{Phe}

Recombinant His-tagged Yeast Phenylalanyl-tRNA synthetase (yPheRS) was expressed in *E. coli* using an inducible system²⁷⁸. pQE32- expressing the alpha and beta subunits of yPheRS as a fusion protein yPheRS (a generous gift from Dr. David Tirrell, California Institute of Technology) was transformed into *E. coli* strain SG13009 [pREP4] (Qiagen). Transformed cells were grown in 2xYT media containing 100µg/ml Carbenicillin and 35µg/ml Kanamycin to 0.6 O.D.₅₉₅ and protein expression was induced with 1mM isopropyl-β-D-thiogalactopyranoside (IPTG). Cells were harvested after 4 hours and the His-tagged protein was purified over nickel-NTA agarose affinity purification resin under native condition according to manufacturer's protocol (Qiagen). Imidazole and high salt in the elution buffer were removed by dialyzing against storage buffer (50mM Tris-HCl, pH 7.5, and 1mM DTT) using Amicon ultra 50kDa columns. The 3'-terminal CCA ends of yeast tRNA^{Phe} (obtained from Sigma-Aldrich) were repaired in reactions containing 20mM Glycine-NaOH, pH 9.0, 10mM MgCl₂, 16µM tRNA, 160µM CTP, 160µM ATP using tRNA terminal nucleotidyl transferase purified from yeast by gel filtration and ion-exchange chromatography (300mM KCl fraction) of whole cell yeast lysates²⁷⁹. Repaired tRNA was purified by phenol extraction followed by

ethanol precipitation. Yeast tRNA^{Phe} was aminoacylated in a 4ml reaction mixture containing 16μM tRNA^{Phe}, 40μM [¹⁴C]Phe, 10mM ATP, 100mM HEPES-KOH (pH=7.6), 9mg yPheRS (1AU/250mg) 10mM KCl, 20mM MgCl₂ and 1mM DTT. Charged tRNAs were precipitated in 70% ethanol, pelleted and dissolved in 3mM CH₃COONa, pH 5.2 and purified by HPLC as previously described²⁸⁰. N-Ac[¹⁴C] Phe-tRNA^{Phe} was synthesized by adding 400μl acetic anhydride at the end of aminoacylation reactions and incubated for one hour twice. Modified tRNAs were precipitated and purified by HPLC as above.

Assays of Ribosome and tRNA interactions

Determination of steady-state binding constants for tRNAs were performed as previously described^{259,281} with modifications. To monitor [¹⁴C] Phe-tRNA^{Phe} binding to the A site, ribosomes were pre-activated in binding buffer containing polyU and deacylated tRNA^{Phe}. Ternary complex was preassembled using HPLC-purified [¹⁴C] Phe-tRNA^{Phe}, GTP, and soluble ammonium sulfate fraction containing yeast elongation factors²⁸². Binding reactions containing ribosomes (33.33 nM) and two-fold serial dilutions of ternary complexes (0–128 pmoles) were filtered through nitrocellulose filters. Similar assays to monitor binding of Ac-[¹⁴C] Phe-tRNA^{Phe} to the ribosomal P site were performed using preactivated ribosomes incubated with serial dilutions of HPLC-purified Ac-[¹⁴C] Phe-tRNA^{Phe} and processed as described above.

Peptidyltransferase assay

Peptidyltransferase activity assays were carried out as previously described²⁵⁹. Complex C [ribosome-poly(U)-AcPhe-tRNA] was formed in 400 μ l of binding buffer (80mM Tris-HCl, pH 7.4, 160mM ammonium chloride, 11mM magnesium acetate, 2mM spermidine and 6mM β -mercaptoethanol 500pmol ribosomes, 0.4mg/ml poly(U) and 700pmol Ac-[¹⁴C]Phe-tRNA^{Phe}). Mixtures were incubated for 20min at 30°C and then placed on ice. Complexes were purified from free Ac-[¹⁴C]Phe-tRNA^{Phe} by centrifugation through a glycerol cushion (0.5ml; 20% glycerol in binding buffer by centrifugation at 50,000rpm for 2h in MLS 50 rotor). Ribosome pellets were rinsed twice with 1ml of binding buffer and suspended in 1.15ml of binding buffer. For puromycin reactions, 1.15ml of complex C extract was pre-incubated at 30C for 5min, and reactions were initiated by adding pH neutralized puromycin to final concentrations of 10mM. Aliquots of 100 μ l were removed, and reactions were terminated at the indicated time intervals by addition of 100 μ l of 1.0N NaOH. Reaction products were extracted with 0.4ml of ethyl acetate, 0.2ml of organic phase was transferred to scintillation vials, and radioactivity was determined by scintillation counting. A 50 μ l aliquot of initial reaction mixture was also transferred to scintillation vials, and total radioactivity (N_0) was determined. Controls without puromycin were included in each experiment, and the values obtained were subtracted as background. The percent of the bound Ac-[¹⁴C]Phe-tRNA^{Phe} converted to Ac-[¹⁴C]Phe-puromycin was corrected with the extent factor α (determined if complex C were allowed to react for 1h; $C_0 = \alpha N_0$), as described earlier (ref,ref). The reaction plots were fit to a first-order exponential equation, and values of K_{obs} (the

apparent rate constant of entire course of reaction at a given concentration of puromycin) were calculated by using Graphpad Prism software.

Ribosome protein interactions

6xHis-tagged eEF2 was purified from TKY675 yeast cells (kindly provided by Dr T. Kinzy) as previously described²⁸³ with the following modifications. EDTA was added to 5mM to eluted eEF2 just before dialysis to bind leached Ni^{2+} ions and prevent precipitate formation during dialysis due to aggregation of His-tagged protein. eEF2 concentration was determined by [^{14}C]ADP-ribosylation with diphtheria toxin. For eEF2-binding experiments, reaction mixes (50 μl) containing 5pmol of salt washed 80S ribosomes and various concentrations of 6xHis-tagged eEF2 in binding buffer (50mM Tris-HCl, pH 7.5, 50mM ammonium acetate, 10mM magnesium acetate, 2mM DTT, 100mM GDPNP) were incubated for 20min at room temperature. Estimation of bound eEF2 was carried out as follows by assuming that ribosome bound eEF2 is not susceptible to ADP-ribosylation by diphtheria toxin^{284–286}. Free (unbound) eEF2 was estimated by ADP-ribosylation of eEF2: 100pmol [^{14}C] NAD⁺ and 0.2mg of diphtheria toxin were added to each reaction mix and incubated for 30min at 30°C. Total eEF2 in each reaction mix was determined by ADP-ribosylation reaction after bound eEF2 was released by adding EDTA to 10mM. Reaction mixes were precipitated with TCA, and amounts of [^{14}C]ADP-ribosylated eEF2 were determined by liquid scintillation counting. Control values (lacking diphtheria toxin) were subtracted. Ribosome bound eEF2 was calculated by subtracting free values from total amount. K_d values were determined assuming single binding sites using Graphpad Prism software.

rRNA Structure probing analysis

hSHAPE²⁸⁷ of rRNA with 1M7 was performed as described²⁴² using the following primers: 969 and 1780 in the SSU, and 25-2, 1466, 2632, 2836, 25-7, and 3225 in the LSU. Briefly, rRNA from chemically treated wild type and mutant ribosomes was extracted and extension reactions performed using fluorescently labeled primers, followed by fragment analysis using capillary electrophoresis. Data were analyzed using SHAPEFinder²⁸⁸. For kethoxal studies, 25 pmoles of purified ribosomes in a 50 μ l volume were treated with 1 μ l of a 4% kethoxal solution (in pure ethanol), or 1 μ l of ethanol as control, and incubated for 10 min at 30°C. Reactions were stopped by the addition of one half volume of stop solution (150mM sodium acetate, 250mM potassium borate), followed by ethanol extraction and extension reactions were performed as described above using primer 969. Scored data were mapped onto 3.0 Å resolution yeast ribosomes²³ using pymol.

mRNA Abundance and Telomere length assay.

Quantitative PCR experiments to assay mRNA abundance were carried out as described¹⁸². Similar methods were used to quantify telomere length in yeast cells. Genomic DNA was isolated from mid-logarithmic cell cultures as previously described²⁶⁹. Quantitative polymerase chain reactions to determine yeast telomere content (T) relative to the single-copy reference gene SGS1 (S) were performed on serially diluted DNA using the Bio-Rad iTaQ™ Universal SYBR Green system utilizing primer pairs complementary to telomere repeats (Table S2), and cycle threshold values were determined. The T/S ratios (relative telomere content) were calculated from three

experimental replicates at each of three DNA concentrations (100, 200, and 400 ng). The Student t-test for two-tailed P value calculations was used throughout.

Chapter 4: Conclusions and Future Direction

Summary

Protein synthesis is an extraordinarily complex and highly regulated process. There can be two possible layers of regulatory controls acting in protein synthesis: the synthesizing machinery and the template molecule. Here we have shown that ribosomes the protein synthesis machine for cells are very sensitive to small changes in their component “gears” and can very easily malfunction if not break down.

Here we demonstrated that the universal two subunit identity of ribosomes and their continuous intersubunit rotation is of prime importance for protein synthesis. It is through this rotational capacity that the ribosomes are able to use the same binding platform for a variety of ligands which include tRNAs, initiation factors, elongation factors, release and recycling factors, rescue factors like UPF1 etc. Interestingly, the same ribosomes that can so strongly differentiate between cognate, near-cognate and non-cognate tRNAs at the time of accommodation, allow the binding of proteins that are merely mimics of tRNA structures displaying some a “temporal specificity” towards their ligands. This capacity to temporally distinguish between its ligands comes from within the ribosomes, from its 4 rRNAs and its 80 proteins. The chemical properties of rRNAs and r-proteins do not just keep the machine working but also provide it with the selectivity. In solution, 80S ribosomes have an intrinsic capacity to have intersubunit rotation. Several small contact points between the subunits at the interface called intersubunit bridges are crucial for this motion. These contact elements can be imagined

as tiny tangled springs with magnetic forces (analogy for attractive and repulsive electrostatic forces on the subunit interphase) embedded on two interfacing surfaces. When these surfaces rotate from one state to another because of the magnetic forces, the springs (analogous to several r-protein c-terminals embedded into the opposite subunit) store the elastic potential energy in order to make the surface rotate back. When the surface rotates back to unrotated state, the magnetic force is still at work and possibly another set of springs that make the surfaces to rotate against each other again. If some of these springs break or lose their elasticity (analogous to mutations in ribosomal components), the rotational equilibrium will be hampered and the surfaces lose their dynamic rotational equilibrium or experience a shift in it. So does the ribosome.

The ribosome functionally depends upon its ability to rotate back and forth. It transits through several rotated states during elongation cycle. The two extremes of these states are called rotated and unrotated. Through mutants of uL2 we have demonstrated that there is a direct relationship between rotational status of the ribosome and ligand selection. Ribosomes stabilized in the rotated state have a higher affinity for the translocase eEF2, and lower than usual affinity for ternary complex. This finding explains the unidirectional nature of the elongation cycle.

Having reduced affinity towards cognate ternary complex, mutant ribosomes also lose their selectivity. The selection of correct ligand also heavily depends upon a delicate series of kinetic balances. Deleterious mutations in r-proteins can disrupt these parameter and cause structural changes that modify the allosteric information exchange pathways between the functional centers of the ribosome. As seen in uL2 mutants, equilibrium shift

towards the rotated state of ribosomes lead to variety of instances of increase in translational fidelity defects. We have proposed a kinetic model to explain the correlation between rotational equilibrium shift and abrogated translation fidelity (figure 43). This model is based on the findings of elegant biochemical studies that have detailed the parameters underlying the high fidelity selection of cognate tRNA. As discussed before, the initial selection of tRNA is based on the rapid dissociation of non-cognate tRNA after initial binding, demonstrated by their high dissociation rates (~400 times cognate tRNA). However a shift in equilibrium towards the rotated state leads to disproportionately increase the rate of dissociation of cognate tRNAs thus resulting in reduced ability to discriminate between the cognate and near-cognate ternary complexes.

Mutations in ribosomal proteins do not just affect the structural details and ligand affinities of the ribosomes. They can have severe and biologically relevant effects on gene expression. Non- canonical translation pathways are of great interest for studying the effect of ribosomal defects on specific mRNA templates expressed by special mechanisms like programmed ribosomal frameshift, Stop codon readthrough, or incorporation of missense codons. Rotated ribosomes with hybrid state tRNAs have also been shown to be substrates for -1PRF. We showed that mutations in the intersubunit bridge forming residues of uL2 display high rates of frameshifting in both L-A virus directed frameshifting signal as well as -1PRF signals in the yeast EST1, EST2 and STN1 mRNAs. In eukaryotic cells, -1 PRF signals can act as mRNA destabilizing agents which can affect cellular pathways involved in homeostasis. We demonstrated here that mutants of uL2, that showed increased -1PRF efficiency promoted decreased abundance of

mRNAs of involved genes. These genes are important for telomere maintenance and we observed decreased abundance of telomere repeats for the uL2-mutant. This is an important finding because we directly showed that mutations in ribosomes lead to altered gene expression and affected the telomere length in cells.

Medical relevance and Future Direction

Once we have established that ribosomal components are regulating gene expression through several molecular pathways, there are many avenues to consider the importance of ribosomal proteins in health and well-being.

A fairly newly characterized class of disorders called “ribosomopathies” has gained the attention of researchers studying translation. These are genetic disorders associated with mutations in ribosomal biogenesis factors or ribosomal proteins. Ribosomal proteins act as biogenesis factors also, as many of them bind to the pre-rRNA in its nascent unprocessed phase and assist in the proper assembly of ribosome from the very start. Mutations in any of these proteins can obviously be devastating for ribosome biogenesis and all the processes downstream, like ribosome export, protein synthesis and overall homeostasis. Since, ribosome biogenesis and translation are so fundamentally important for growth and viability, it would be expected that mutations in genes coding these proteins should be inviable. However, surprisingly ribosomopathies display tissue specific disease proclivities, bringing to notice the notion of “specialized ribosomes”. Specialized ribosomes form a task force of special translation machinery geared towards the translation of specific mRNAs expressed only in specific tissue types either by canonical or non-canonical pathways. One study showed that mutations in RPL38

specifically abrogated the translation of Homeobox mRNAs without affecting global protein synthesis²⁰⁶. A variegated pattern of ribosomal protein expression in the different parts of a mouse embryo was observed at different stages of development. Thus ribosomes vary tissue-specifically and thus deficiency in ribosomal proteins can affect one tissue type more than others. Possible cis-acting features of Homeobox mRNAs may indispensably require RPL38 for translation. Inability to translate the tissue specific mRNAs as a result of mutations in genes coding for ribosomal proteins can be the seed cause for tissue specific ribosomopathies.

Ribosomopathies are generally hypoproliferative disorders like anemia, because of too few ribosomes to fulfill cellular demands. However, patients with diseases like Diamond Blackfan anemia also have predisposition to occurrence of tumors and cancers. It is elusive how a hypoproliferative disorder turns into a hyperproliferative one. Here the study of uL2 mutants in yeast makes an attempt at explaining this transition. Ribosomes with mutant proteins showing high translation fidelity defects can explain the onset of cancer in ribosomopathies. Figure 46 suggests a flowchart of disease progression in ribosomopathies. Mutation in ribosomal proteins and biogenesis factors slow down a steady production of ribosomes in the cell leading to slow growth and more complex phenotypes like inefficient organ development in complex organisms. This phenotype marks the onset of ribosomopathies in individuals. However slowly, some ribosomes escape the strong cellular surveillance and participate in translation. If there are mutations in ribosomal proteins, these ribosomes are likely to be inefficient in performing protein synthesis and thus can display altered rates of translation fidelity defects. As explained

above, such alterations can be deleterious to the translation of tissue specific mRNAs and cause tissue specific diseases.

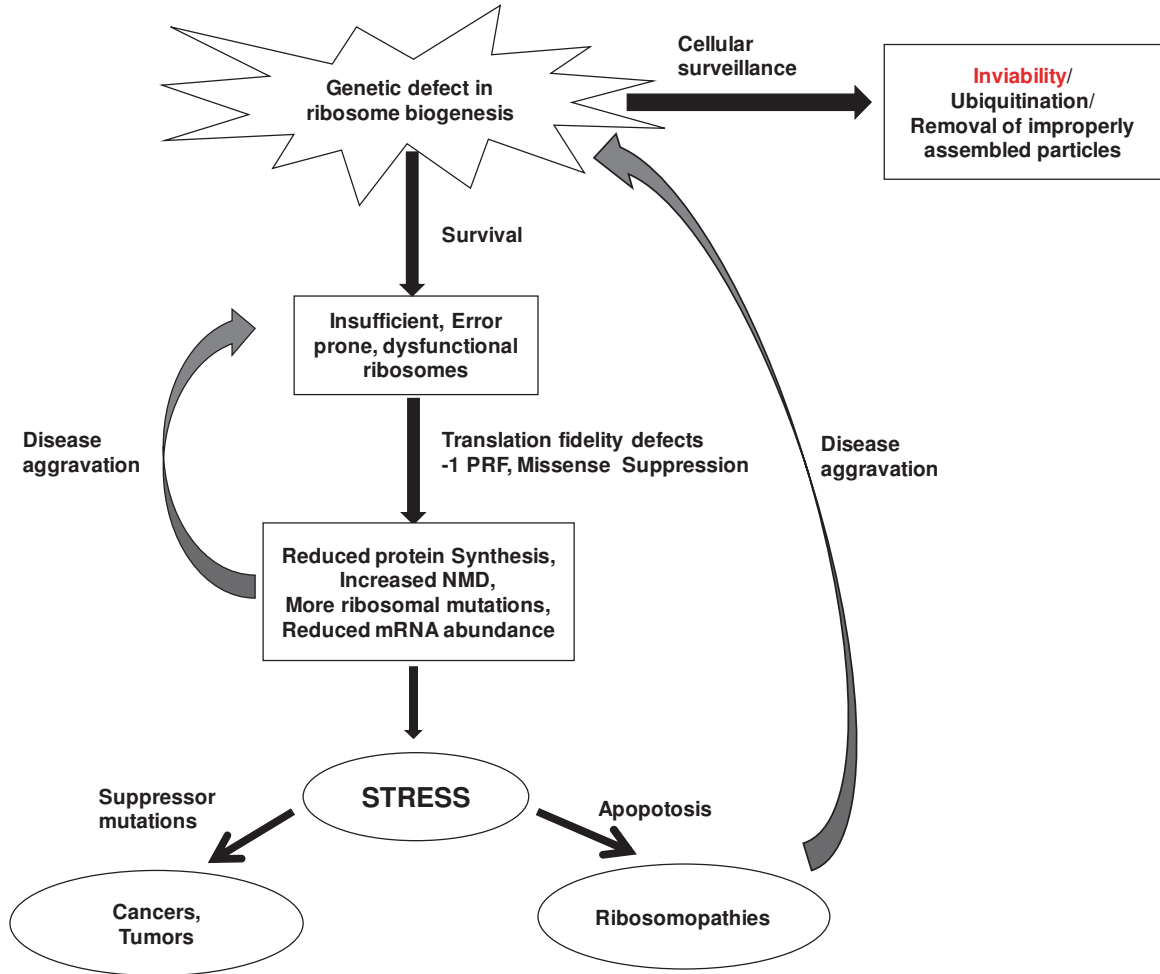


Figure 46 Model describing the disease progression and cancer onset in ribosomopathies

Altered gene expression further slows down cell growth and can lead to cellular stress. Stress causes appearance of new mutants which suppress the slow growth phenotype of the original mutation and accelerate cellular proliferation. Such suppressor mutations can have oncogenic properties^{236,289}. These new mutations allow the cells to

bypass cellular surveillance leading to hyperproliferative phenotype characteristic of cancers.

In a recent study published by our research group, it was demonstrated that cellular -1PRF leads to destabilization of the coding mRNA^{162,181} by recruiting the nonsense mediated mRNA decay pathway (NMD) or No-go decay pathway (NGD). Mutants of ribosomal proteins often show increased instances of -1PRF, and bring down protein synthesis. Another study has demonstrated a programmed translation readthrough event in human cells that leads to a synthesis of a longer variant of a protein called Vascular Endothelial Growth Factor (VEGF) with antiangiogenic properties¹⁶³. Both of these studies have reported possible target mRNAs which can be affected by mutant ribosomes. We demonstrated here that ribosomes carrying mutant L2 show increased rates of -1PRF and UAA readthrough. Such mutant ribosomes can affect gene expression by destabilize the mRNA abundance by triggering NMD or NGD in mRNAs containing -1 PRF signals. In case of the VEGF mRNA, ribosomes displaying higher rates of translational readthrough events produce higher amounts of the longer protein with antiangiogenic properties. The antiangiogenic property is useful in inhibiting the tumor progression as shown by Sandeepa et al.¹⁶³. However, the same property can be deleterious in the developmental stages of an organism and can be the underlying cause of certain ribosomopathies.

It can thus be useful to target the NMD machinery in order to slow the mRNA degradation in mutants with high -1PRF efficiencies. Small molecule inhibitors of -1PRF can slow down the aggravation of disease. To develop therapeutics against tissue specific

disorders of ribosomal proteins, high throughput studies of tissue specific elements involved in disease progression are required. Such studies may help finding specific targets of mutants ribosomes at the level of single cell, tissue or whole organism.

This study provides a kinetic model linking the rotational equilibrium of the ribosomes to their ability to discriminate between cognate and near-cognate tRNAs. uL2 is a core ribosomal protein and essential for peptidyltransferase function of the ribosome. Given the essential nature of uL2, for ribosome function, it is less likely to isolate disease causing mutants of L2 that survive to the symptomatic stage. This study nevertheless provides a general model for understanding ribosome related disorders.

Appendix 1: Yeast strain list

Strain	Genotype
5X47	<i>MATa/MATa his1/+ trp1/+ ura3/+ K⁻</i>
yJD1269	<i>MATa his3D1 leu2D0 met15D0 ura3D0 rpl2a::KAN^r rpl2b::KAN^r [L-A HN M_I] pRPL2A-URA3</i>
yJD1315	<i>MATa his3D1 leu2D0 met15D0 ura3D0 rpl2a::KAN^r rpl2b::KAN^r [L-A HN M_I] pRPL2A-LEU2</i>
yJD1676	<i>MATa his3D1 leu2D0 met15D0 ura3D0 rpl2a::KAN^r rpl2b::KAN^r [L-A HN M_I] pRPL2A(H139-E143A)-LEU2</i>
yJD1677	<i>MATa his3D1 leu2D0 met15D0 ura3D0 rpl2a::KAN^r rpl2b::KAN^r [L-A HN M_I] pRPL2A(D176A)-LEU2</i>
yJD1678	<i>MATa his3D1 leu2D0 met15D0 ura3D0 rpl2a::KAN^r rpl2b::KAN^r [L-A HN M_I] pRPL2A(K177A)-LEU2</i>
yJD1679	<i>MATa his3D1 leu2D0 met15D0 ura3D0 rpl2a::KAN^r rpl2b::KAN^r [L-A HN M_I] pRPL2A(V148A)-LEU2</i>
yJD1680	<i>MATa his3D1 leu2D0 met15D0 ura3D0 rpl2a::KAN^r rpl2b::KAN^r [L-A HN M_I] pRPL2A(G138A)-LEU2</i>
yJD1681	<i>MATa his3D1 leu2D0 met15D0 ura3D0 rpl2a::KAN^r rpl2b::KAN^r [L-A HN M_I] pRPL2A(L245-S249A)-LEU2</i>
yJD1682	<i>MATa his3D1 leu2D0 met15D0 ura3D0 rpl2a::KAN^r rpl2b::KAN^r [L-A HN M_I] pRPL2A(H139-P141A)-LEU2</i>
yJD1683	<i>MATa his3D1 leu2D0 met15D0 ura3D0 rpl2a::KAN^r rpl2b::KAN^r [L-A HN M_I] pRPL2A(D142-E143A)-LEU2</i>
yJD1684	<i>MATa his3D1 leu2D0 met15D0 ura3D0 rpl2a::KAN^r rpl2b::KAN^r [L-A HN M_I] pRPL2A(P108-E109A)-LEU2</i>
yJD1685	<i>MATa his3D1 leu2D0 met15D0 ura3D0 rpl2a::KAN^r rpl2b::KAN^r [L-A HN M_I] pRPL2A(G110-T111A)-LEU2</i>
yJD1686	<i>MATa his3D1 leu2D0 met15D0 ura3D0 rpl2a::KAN^r rpl2b::KAN^r [L-A HN M_I] pRPL2A(K155A)-LEU2</i>
yJD1687	<i>MATa his3D1 leu2D0 met15D0 ura3D0 rpl2a::KAN^r rpl2b::KAN^r [L-A HN M_I] pRPL2A(G248-K254A)-LEU2</i>
yJD1688	<i>MATa his3D1 leu2D0 met15D0 ura3D0 rpl2a::KAN^r rpl2b::KAN^r [L-A HN M_I] pRPL2A(248-254Δ)-LEU2</i>
yJD1689	<i>MATa his3D1 leu2D0 met15D0 ura3D0 rpl2a::KAN^r rpl2b::KAN^r [L-A HN M_I] pRPL2A(V145A)-LEU2</i>
yJD1690	<i>MATa his3D1 leu2D0 met15D0 ura3D0 rpl2a::KAN^r rpl2b::KAN^r [L-A HN M_I] pRPL2A(R147A)-LEU2</i>
yJD1691	<i>MATa his3D1 leu2D0 met15D0 ura3D0 rpl2a::KAN^r rpl2b::KAN^r [L-A HN M_I] pRPL2A(R147-V148A)-LEU2</i>
yJD1692	<i>MATa his3D1 leu2D0 met15D0 ura3D0 rpl2a::KAN^r rpl2b::KAN^r [L-A HN M_I] pRPL2A(Y133A)-LEU2</i>

Appendix 2: List of synthetic oligonucleotides

Oligo name	Sequence
L2A-5'UTR(FOR)	5'CCCTGCCCCCTCCCCTCCTTCAATATCATTACCTCG3'
L2A-3'UTR(REV)	5'GCCATTTTATTCAAGAAGTCAACCCCCTCCATGAAGCAATGCTT3'
L2A-P108-T111A(REV)	5'GGAGACAATagcagcagcagcGACAGAACCC3'
L2A-H139-E143A(REV)	5'GTCTTGTTtagcagcagcagcACCGATG3'
L2A-S152-K155A(FOR)	5'GATTACCAgctgctgctgctAAGGTTATC3'
L2A-D176-K177A(FOR)	5'GGTGGTAGAGTTgctgctCCATTGTTGAAGG3'
L2A-R241-G244A(FOR)	5'GCCGCCgctgctgctgctTTGTTACGTGG3'
L2A-D176A(FOR)	5'GCCGGTGGTGGTAGAGTTgctAAACCATTGTTGAAGGC3'
L2A-K177A(FOR)	5'GCCGGTGGTGGTAGAGTTGACgctCCATTGTTGAAGGC3'
L2A-V148A(FOR)	5'CGAAAACAAGACTAGAgctAGATTACCATCCGGTGCC3'
L2A-G138A(REV)	5'CGTCTGGGTTGTGagcGATGATAATAACGTAGTTACCGG3'
L2A-L245-S249A(REV)	5'ATAATACTAGTCTAagcagcagcagcAGAACACGTAACA3'
L2A-H139-P141A(REV)	5'CTCTAGTCTTGTTCGTCagcagcagcACCGATGATAATAACG3'
L2A-D142-E143A(REV)	5'CTGACTCTAGTCTTGTtagcagcTGGGTTGTGACCGATGATA3'
L2A-P108-E109A(REV)	5'GGAGACAATagcagcTTCTGGGACAGAACCC3'
L2A-G110-T111A(REV)	5'GGAGACAATGGTACCagcagcGACAGAACCC3'
L2A-S152-G153A(FOR)	5'GATTACCAgctgctGCCAAGAAGGTTATC3'
L2A-K155A(FOR)	5'GATTACCATCCGGTgctgctAAGGTTATC3'
L2A-G248-	5'CTAATCTTGGGTtagcagcagcagcACGTAACAAACC3'

K251A(REV)	
L2A-G248-D254Δ(REV)	5'GACTATTTTACTAGTACATAATctacaaaccagttcttctggc3'
L2A-V175A(FOR)	5'GCCGGTGGTGGTAGAgctGACAAACCATTGTTGAAGGC3'
L2A-R147A(FOR)	5'GACGAAAACAAGACTgctGTCAGATTACCATCCGG3'
L2A-R147-V148A(FOR)	5'GACGAAAACAAGACTgctgctAGATTACCATCCGG3'
L2A-Y133A(FOR)	5'GCCAGAGCTTCCGGTAACgctGTTATTATCATCGG3'
Tel_Fwd	5'CAGTGGTGTGGGTGTGCATGGTGGTGTGGGTGTGTGGAC3'
yTel_Rev	5'GCCCACAACCACACCCAACACATCCCACACCACCTA3'
SGS1_Fwd	5'GGCTCTCGTACACTGCCACATCGAATCAATATGCTGACGTA CCC3'
ySGS1_Rev	5'CATGTGGAGATGCGGGAATGCGGGAGAATGTGGAG3'

Appendix 3: Genetic analyses of uL2 basic extension loop mutants

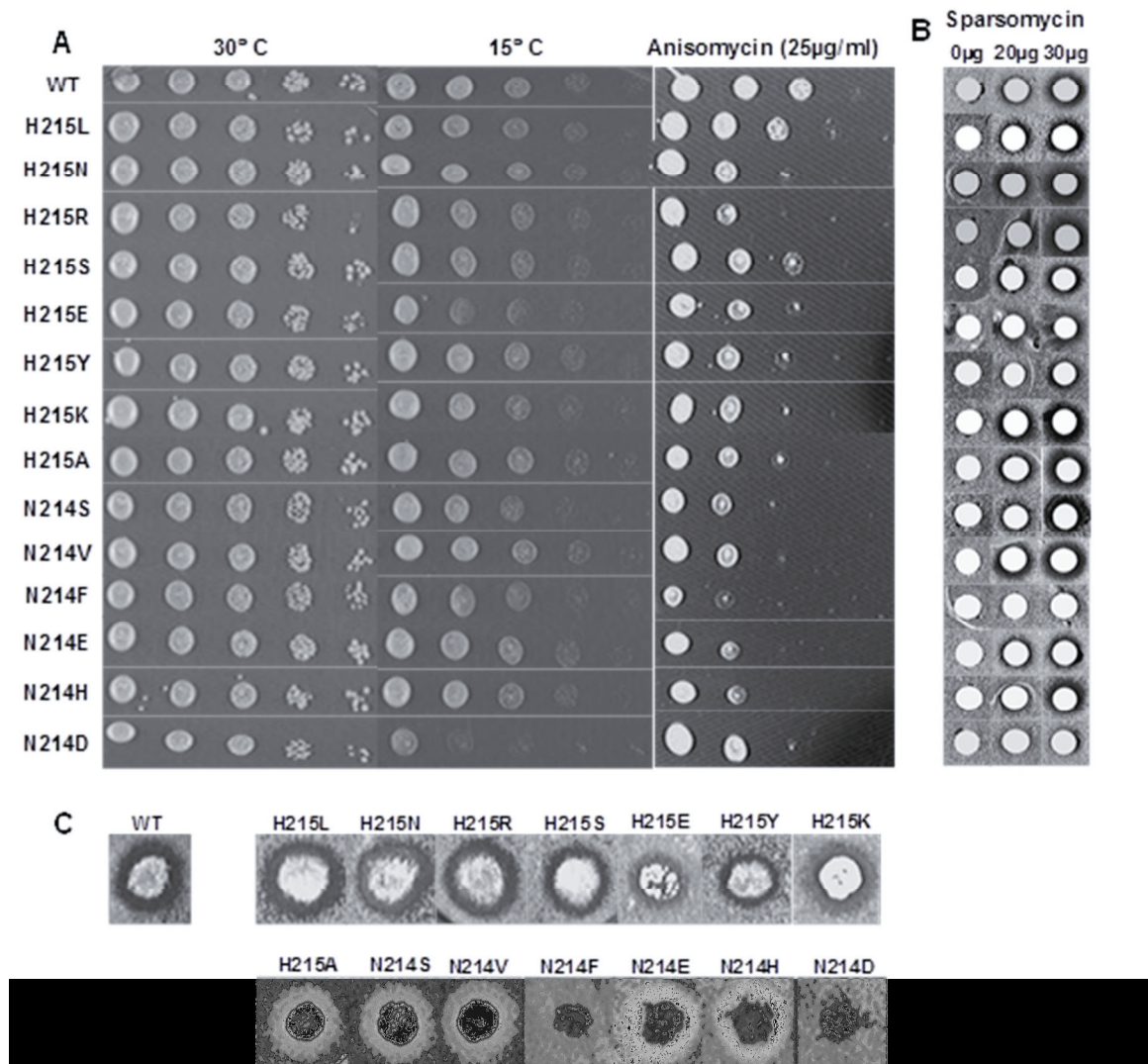


Figure 47 rpL2A basic extension loop mutants promote various phenotypic defects.

Residues in the basic extension domain of L2 were replaced by aminoacids covering the whole range of biochemical properties. **(A)** Ten-fold serial dilutions of cultures of indicated *S.cerevisiae* strains were spotted on rich medium and incubated for 48 hours at 30°C, 15°C, and 25µg/ml Anisomycin (30°C) to score for growth, cold and heat sensitivity respectively. **(B)** “Killer” virus phenotypes: The Killer+ phenotype is scored by the presence of a halo of growth inhibition around wild-type colony. Lack of the halo around colonies expressing the N214F and N214D L2 mutants indicates the Killer-phenotype. Mutant H215E displays a weak killer phenotype.

Appendix4: Biochemical and functional analyses of uL2-basic extension mutants

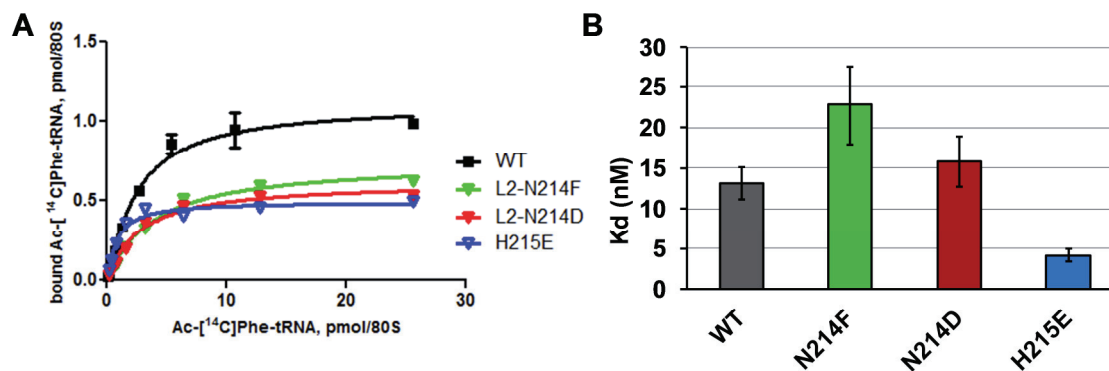


Figure 48 Mutations of uL2 basic extension domain affect peptidyl-tRNA binding in the P-site

A. Single site binding isotherms N-Ac-Phe-tRNA^{Phe} to the P-site of ribosomes isolated from wild-type, *rpl2-N214F*, *rpl2-N214D*, *rpl2-H215E* and *rpl2-Y133A* cells. **B.** N-Ac-Phe-tRNA^{Phe} binding K_ds calculated using ligand depletion model (Graphpad Prism). Error bars indicate standard error. (n=4, * *P* < 0.06, ** *P* < .001)

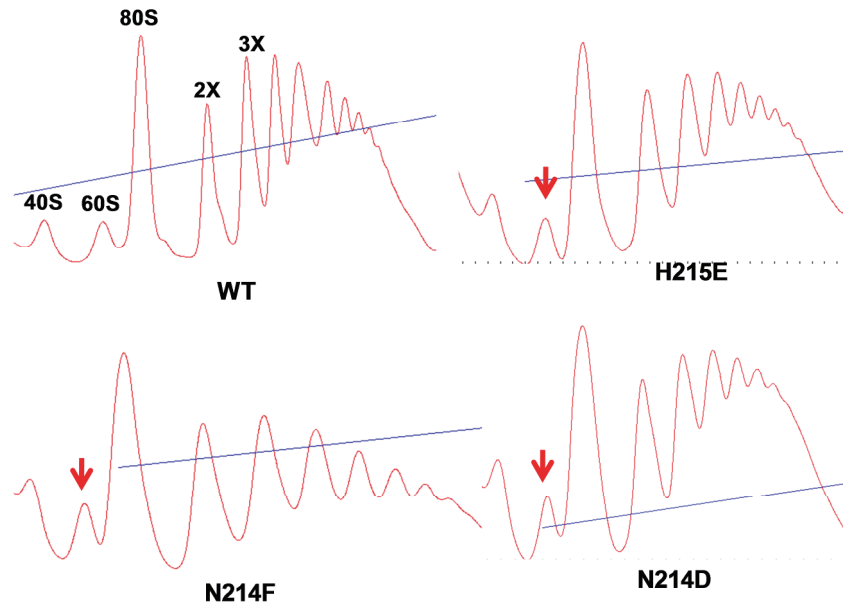
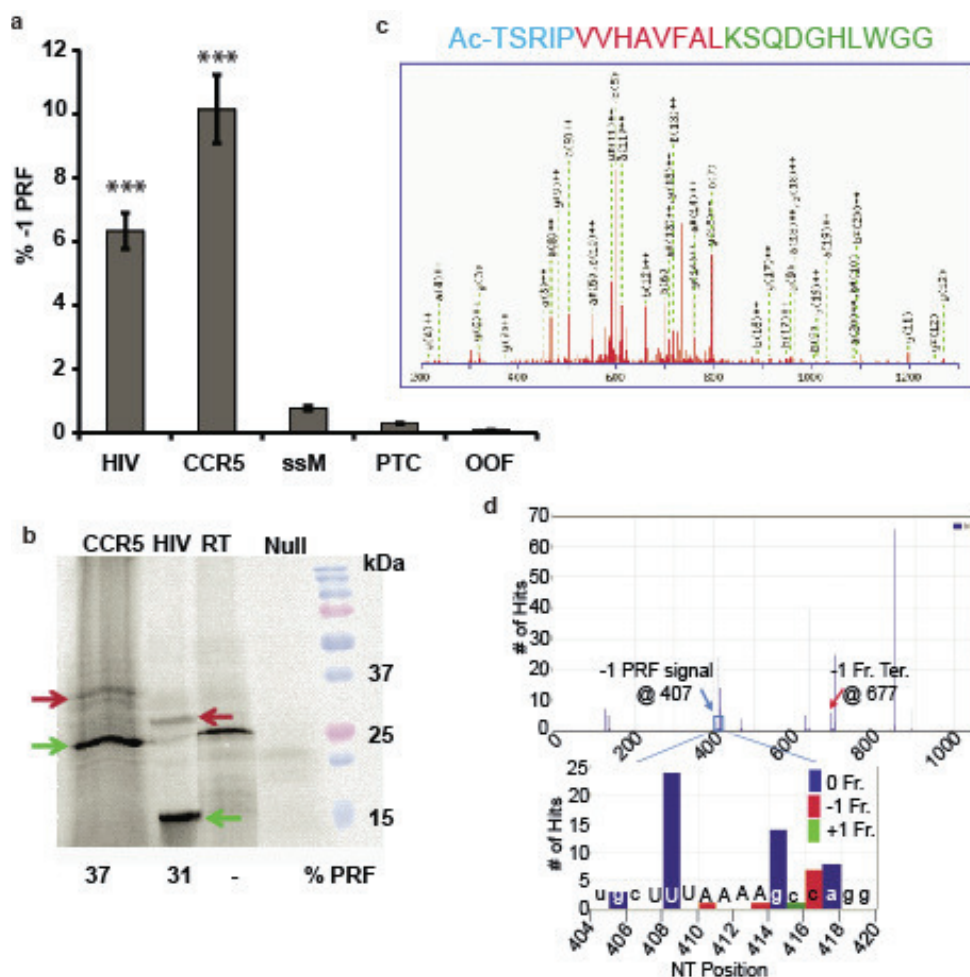


Figure 49 Polysome profiles of cells expressing WT and mutant uL2.

Polysome profiles were generated by Sucrose density gradient fractionation of cycloheximide arrested cell lysates of WT and mutant *rpL2A* expressing strains of yeast. The first two peaks stand for 40S and 60S subunits respectively, the third peak is 80S ribosome and the subsequent peaks represent two or more ribosomes present on the same mRNA. In WT cells, the ratio 40S:60S is about 1, while in mutants the 60S is peak is significantly lowered due to ribosome biogenesis defects. Shoulders to regular peaks are called half-mers and they represent subunit joining defects in translation or lack of adequate subunits (in this case 60S) due to biogenesis defects.

Appendix 5: Contributions to other Projects

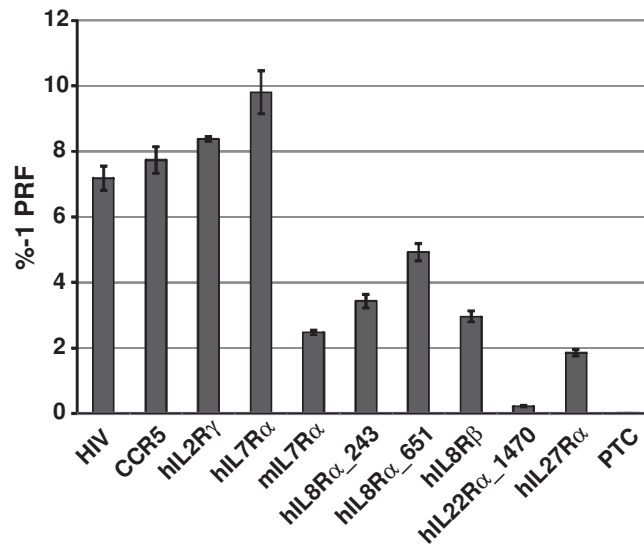
1. Ribosomal frameshifting in the *CCR5* mRNA is regulated by miRNAs and the NMD pathway. (*Nature*(2014) doi:10.1038/nature13429)



The *CCR5* sequence promotes efficient frameshifting.

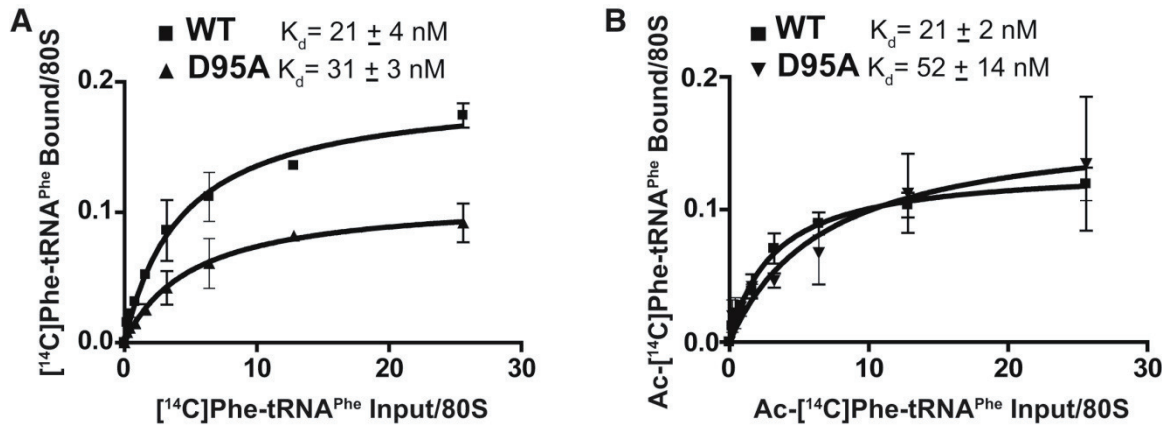
- Measurement of -1 PRF in HeLa cells.** -1 PRF efficiency using the dualuciferase reporters was monitored in HeLa cells. Error bars denote an approximation of standard errors. *** $P < 0.001$ compared to the out of frame control

- b. **Efficient -1 PRF promoted by the CCR5 sequence *in vitro*.** Autoradiogram of *in vitro* translation reaction using synthetic mRNAs harboring CCR5 or HIV-1 derived -1 PRF signals. Green arrows denote 0-frame encoded products. Red arrows denote -1 PRF encoded peptides. RT indicates the readthrough control. Percent -1 PRF promoted by CCR5 and HIV-1 frameshift signals is indicated below lanes.
- c. **MSMS spectrum of Ac-TSRIPVVHAVFALKSQDGHLWGG (2-24) AspN proteolytic fragment containing CCR5 fusion peptide.** N-terminally acetylated leader peptide sequence is colored blue, CCR5-derived 0-frame sequence beginning at V94 is red, and CCR5 -1 frame encoded sequence beginning after L101 is colored green.
- d. **Ribosome profile of the CCR5 mRNA mined from Hsieh et al.** Top panel: Locations of the -1 PRF signal and -1 frame termination codon are indicated. Bottom panel: profiling data at the slippery site (indicated in capital letters) at single nucleotide resolution. Ribosomes arrested in the three different reading frames are color coded.



Computationally identified putative -1 PRF signals cloned into dual-luciferase reporters were assayed in HeLa cells. Numbers in hIL8R α and hIL22R α denote the nucleotide positions of the beginning of the slippery sites in the native mRNAs. Error bars denote standard error. * $P < 0.05$, ** $P < 0.01$

2. rRNA Pseudouridylation defects affect ribosomal ligand binding and translational fidelity from yeast to human cells. (*Molecular Cell* (2011), DOI: 10.1016/j.molcel.2011.09.017)



A) Single-site isotherms of eEF1A stimulated binding of [^{14}C]Phe-tRNA^{Phe} (2-fold serial dilutions from 1 to 128 pmoles) to the A sites of 20 pmoles of poly(U) primed ribosomes preloaded with tRNA^{Phe} in their A sites.

(B) Single-site isotherms of Ac- ^{14}C]Phe-tRNA^{Phe} (2-fold serial dilutions from 1 to 128 pmoles) to P sites of 20 pmoles of poly(U) primed ribosomes. Steady-state K_d values and standard deviations for each sample are indicated. All tRNA binding assays were performed in triplicate.

References

1. Claude, A. The constitution of mitochondria and microsomes, and the distribution of nucleic acids in the cytoplasm of a leukemic cell. *J. Exp. Med.* **80**, 19–29 (1944).
2. Claude, A. The constitution of protoplasm. *Science* **97**, 451–6 (1943).
3. Palade, G. E. A small particulate component of the cytoplasm. *J. Biophys. Biochem. Cytol.* **1**, 59–68 (1955).
4. Palade, G. E. & Siekevitz, P. Liver microsomes; an integrated morphological and biochemical study. *J. Biophys. Biochem. Cytol.* **2**, 171–200 (1956).
5. Frank, J. Image analysis of single macromolecules. *Electron Microsc. Rev.* **2**, 53–74 (1989).
6. Stark, H. *et al.* The 70S Escherichia coli ribosome at 23 Å resolution: fitting the ribosomal RNA. *Structure* **3**, 815–21 (1995).
7. Schlueder, F. *et al.* Structure of Functionally Activated Small Ribosomal Subunit at 3.3 Å Resolution. *Structure* **102**, 615–623 (2000).
8. Wimberly, B. T. *et al.* Structure of the 30S ribosomal subunit. *Nature* **407**, 327–39 (2000).
9. Ban, N., Nissen, P., Hansen, J., Moore, P. B. & Steitz, T. A. The Complete Atomic Structure of the Large Ribosomal Subunit at 2.4 Å Resolution. *Science* **289**, 905–920 (2000).
10. Harms, J. *et al.* High resolution structure of the large ribosomal subunit from a mesophilic eubacterium. *Cell* **107**, 679–688 (2001).
11. Yusupov, M. M. *et al.* Crystal structure of the ribosome at 5.5 Å resolution. *Science* **292**, 883–96 (2001).
12. Schuwirth, B. S. *et al.* Structures of the Bacterial Ribosome at 3.5 Å Resolution. *Science* (80-.). **310**, 827–834 (2005).
13. Selmer, M. *et al.* Structure of the 70S ribosome complexed with mRNA and tRNA. *Science* **313**, 1935–1942 (2006).
14. Lake, J. A. Evolving Ribosome Structure: Domains in Archaeobacteria, Eubacteria, Eocytes and Eukaryotes. *Annu. Rev. Biochem.* **54**, 507–30 (1985).

15. Beckmann, R. *et al.* Architecture of the protein-conducting channel associated with the translating 80S ribosome. *Cell* **107**, 361–372 (2001).
16. Spahn, C. M. *et al.* Structure of the 80S ribosome from *Saccharomyces cerevisiae*-tRNA-ribosome and subunit-subunit interactions. *Cell* **107**, 373–86 (2001).
17. Sengupta, J. *et al.* Identification of the versatile scaffold protein RACK1 on the eukaryotic ribosome by cryo-EM. *Nat. Struct. Mol. Biol.* **11**, 957–962 (2004).
18. Taylor, D. J. *et al.* Comprehensive molecular structure of the eukaryotic ribosome. *Structure* **17**, 1591–1604 (2009).
19. Armache, J.-P. *et al.* Cryo-EM structure and rRNA model of a translating eukaryotic 80S ribosome at 5.5-Å resolution. *Proc. Natl. Acad. Sci. U. S. A.* **107**, 19748–19753 (2010).
20. Armache, J.-P. *et al.* Localization of eukaryote-specific ribosomal proteins in a 5.5-Å cryo-EM map of the 80S eukaryotic ribosome. *Proc. Natl. Acad. Sci. U. S. A.* **107**, 19754–19759 (2010).
21. Klinge, S., Voigts-Hoffmann, F., Leibundgut, M., Arpagaus, S. & Ban, N. Crystal structure of the eukaryotic 60S ribosomal subunit in complex with initiation factor 6. *Science* **334**, 941–8 (2011).
22. Rabl, J., Leibundgut, M., Ataide, S. F., Haag, A. & Ban, N. Crystal structure of the eukaryotic 40S ribosomal subunit in complex with initiation factor 1. *Science* **331**, 730–6 (2011).
23. Ben Shem, A. *et al.* The structure of the eukaryotic ribosome at 3.0 Å resolution. *Science* **334**, 1524–1529 (2011).
24. Klinge, S., Voigts-Hoffmann, F., Leibundgut, M., Arpagaus, S. & Ban, N. Crystal structure of the eukaryotic 60S ribosomal subunit in complex with initiation factor 6. *Science* **334**, 941–8 (2011).
25. Spahn, C. M. T. *et al.* Domain movements of elongation factor eEF2 and the eukaryotic 80S ribosome facilitate tRNA translocation. *EMBO J.* **23**, 1008–1019 (2004).
26. Budkevich TV, Giesebrecht J, Behrmann E, Loerke J, Ramrath DJ, Mielke T, Ismer J, Hildebrand PW, Tung CS, Nierhaus KH, Sanbonmatsu KY, S. C. Regulation of the mammalian elongation cycle by subunit rolling: a eukaryotic-specific ribosome rearrangement. *Cell* **158**, 121–131 (2014).

27. Budkevich, T. *et al.* Structure and dynamics of the mammalian ribosomal pretranslocation complex. *Mol. Cell* **44**, 214–24 (2011).
28. Ogle, J. M. & Ramakrishnan, V. Structural insights into translational fidelity. *Annu. Rev. Biochem.* **74**, 129–177 (2005).
29. Schmeing, T. M., Voorhees, R. M., Kelley, A. C. & Ramakrishnan, V. How mutations in tRNA distant from the anticodon affect the fidelity of decoding. *Nat. Struct. Mol. Biol.* **18**, 432–6 (2011).
30. Noller, H. F. *et al.* Structure of the ribosome at 5.5 Å resolution and its interactions with functional ligands. in *Cold Spring Harb. Symp. Quant. Biol.* **66**, 57–66 (Cold Spring Harbor Laboratory Press, 2001).
31. Gao, Y.-G. *et al.* The structure of the ribosome with elongation factor G trapped in the posttranslocational state. *Science* **326**, 694–9 (2009).
32. Nissen, P., Hansen, J., Ban, N., Moore, P. B. & Steitz, T. A. The structural basis of ribosome activity in peptide bond synthesis. *Science* **289**, 920–930 (2000).
33. Frank, J. *et al.* A model of the translational apparatus based on a three-dimensional reconstruction of the Escherichia coli ribosome. *Biochem. Cell Biol.* **73**, 757–65 (1995).
34. Beckmann, R. *et al.* Alignment of conduits for the nascent polypeptide chain in the ribosome-Sec61 complex. *Science* **278**, 2123–6 (1997).
35. Wilson, D. N. & Beckmann, R. The ribosomal tunnel as a functional environment for nascent polypeptide folding and translational stalling. *Curr. Opin. Struct. Biol.* **21**, 274–82 (2011).
36. Warner, J. R. The economics of ribosome biosynthesis in yeast. *Trends Biochem. Sci.* **24**, 437–440 (1999).
37. Woolford, J. L. & Baserga, S. J. Ribosome biogenesis in the yeast *Saccharomyces cerevisiae*. *Genetics* **195**, 643–81 (2013).
38. Miller, O. L. & Beatty, B. R. Visualization of nucleolar genes. *Science* **164**, 955–957 (1969).
39. Thiry, M. & Lafontaine, D. L. J. Birth of a nucleolus: The evolution of nucleolar compartments. *Trends Cell Biol.* **15**, 194–199 (2005).
40. French, S. L., Osheim, Y. N., Cioci, F., Nomura, M. & Beyer, A. L. In exponentially growing *Saccharomyces cerevisiae* cells, rRNA synthesis is

determined by the summed RNA polymerase I loading rate rather than by the number of active genes. *Mol. Cell. Biol.* **23**, 1558–1568 (2003).

41. Zhang, Y., Smith, A. D., Renfrow, M. B. & Schneider, D. A. The RNA polymerase-associated factor 1 complex (Paf1C) directly increases the elongation rate of RNA polymerase I and is required for efficient regulation of rRNA synthesis. *J. Biol. Chem.* **285**, 14152–14159 (2010).
42. Sandmeier, J. J. *et al.* RPD3 is required for the inactivation of yeast ribosomal DNA genes in stationary phase. *EMBO J.* **21**, 4959–4968 (2002).
43. Moy, T. I. & Silver, P. A. Nuclear export of the small ribosomal subunit requires the ran-GTPase cycle and certain nucleoporins. *Genes Dev.* **13**, 2118–33 (1999).
44. Stage-Zimmermann, T., Schmidt, U. & Silver, P. A. Factors affecting nuclear export of the 60S ribosomal subunit in vivo. *Mol. Biol. Cell* **11**, 3777–89 (2000).
45. Hurt, E. *et al.* A novel in vivo assay reveals inhibition of ribosomal nuclear export in ran-cycle and nucleoporin mutants. *J. Cell Biol.* **144**, 389–401 (1999).
46. Valenzuela, D. M., Chaudhuri, A. & Maitra, U. Eukaryotic ribosomal subunit anti-association activity of calf liver is contained in a single polypeptide chain protein of Mr = 25,500 (eukaryotic initiation factor 6). *J. Biol. Chem.* **257**, 7712–7719 (1982).
47. Menne, T. F. *et al.* The Shwachman-Bodian-Diamond syndrome protein mediates translational activation of ribosomes in yeast. *Nat. Genet.* **39**, 486–495 (2007).
48. West, M., Hedges, J. B., Chen, A. & Johnson, A. W. Defining the order in which Nmd3p and Rpl10p load onto nascent 60S ribosomal subunits. *Mol. Cell. Biol.* **25**, 3802–3813 (2005).
49. Hedges, J., West, M. & Johnson, A. W. Release of the export adapter, Nmd3p, from the 60S ribosomal subunit requires Rpl10p and the cytoplasmic GTPase Lsg1p. *EMBO J.* **24**, 567–579 (2005).
50. Senger, B. *et al.* The nucle(ol)ar Tif6p and Efl1p are required for a late cytoplasmic step of ribosome synthesis. *Mol. Cell* **8**, 1363–1373 (2001).
51. Dez, C., Houseley, J. & Tollervey, D. Surveillance of nuclear-restricted pre-ribosomes within a subnucleolar region of *Saccharomyces cerevisiae*. *EMBO J.* **25**, 1534–1546 (2006).
52. Allmang, C., Mitchell, P., Petfalski, E. & Tollervey, D. Degradation of ribosomal RNA precursors by the exosome. *Nucleic Acids Res.* **28**, 1684–1691 (2000).

53. Zaher, H. S. & Green, R. Fidelity at the Molecular Level: Lessons from Protein Synthesis. *Cell* **136**, 746–762 (2009).
54. Asano, K. *et al.* A multifactor complex of eIF1, eIF2, eIF3, eIF5, and tRNA(i)Met promotes initiation complex assembly and couples GTP hydrolysis to AUG recognition. *Cold Spring Harb. Symp. Quant. Biol.* **66**, 403–415 (2001).
55. Lorsch, J. R. & Dever, T. E. Molecular view of 43 S complex formation and start site selection in eukaryotic translation initiation. *J. Biol. Chem.* **285**, 21203–7 (2010).
56. Hinnebusch, A. G. Molecular mechanism of scanning and start codon selection in eukaryotes. *Microbiol. Mol. Biol. Rev.* **75**, 434–67 (2011).
57. Hinnebusch, A. G. & Lorsch, J. R. The mechanism of eukaryotic translation initiation: new insights and challenges. *Cold Spring Harb. Perspect. Biol.* **4**, a011544– (2012).
58. Lomakin, I. B., Shirokikh, N. E., Yusupov, M. M., Hellen, C. U. T. & Pestova, T. V. The fidelity of translation initiation: reciprocal activities of eIF1, IF3 and YciH. *EMBO J.* **25**, 196–210 (2006).
59. Pestova, T. V. *et al.* The joining of ribosomal subunits in eukaryotes requires eIF5B. *Nature* **403**, 332–5 (2000).
60. Yatime, L., Mechulam, Y., Blanquet, S. & Schmitt, E. Structure of an archaeal heterotrimeric initiation factor 2 reveals a nucleotide state between the GTP and the GDP states. *Proc. Natl. Acad. Sci. U. S. A.* **104**, 18445–50 (2007).
61. Shin, B.-S. *et al.* Initiation factor eIF2 γ promotes eIF2-GTP-Met-tRNAⁱ(Met) ternary complex binding to the 40S ribosome. *Nat. Struct. Mol. Biol.* **18**, 1227–34 (2011).
62. Asano, K. *et al.* Multiple roles for the C-terminal domain of eIF5 in translation initiation complex assembly and GTPase activation. *EMBO J.* **20**, 2326–37 (2001).
63. Mitchell, S. F. *et al.* The 5'-7-methylguanosine cap on eukaryotic mRNAs serves both to stimulate canonical translation initiation and to block an alternative pathway. *Mol. Cell* **39**, 950–62 (2010).
64. Korneeva, N. L., Lamphear, B. J., Hennigan, F. L. & Rhoads, R. E. Mutually cooperative binding of eukaryotic translation initiation factor (eIF) 3 and eIF4A to human eIF4G-1. *J. Biol. Chem.* **275**, 41369–76 (2000).

65. LeFebvre, A. K. *et al.* Translation initiation factor eIF4G-1 binds to eIF3 through the eIF3e subunit. *J. Biol. Chem.* **281**, 22917–32 (2006).
66. Etchison, D., Milburn, S. C., Edery, I., Sonenberg, N. & Hershey, J. W. Inhibition of HeLa cell protein synthesis following poliovirus infection correlates with the proteolysis of a 220,000-dalton polypeptide associated with eucaryotic initiation factor 3 and a cap binding protein complex. *J. Biol. Chem.* **257**, 14806–10 (1982).
67. Alvarez, E., Menéndez-Arias, L. & Carrasco, L. The eukaryotic translation initiation factor 4GI is cleaved by different retroviral proteases. *J. Virol.* **77**, 12392–400 (2003).
68. Ventoso, I., Blanco, R., Perales, C. & Carrasco, L. HIV-1 protease cleaves eukaryotic initiation factor 4G and inhibits cap-dependent translation. *Proc. Natl. Acad. Sci. U. S. A.* **98**, 12966–71 (2001).
69. Connor, J. H. & Lyles, D. S. Vesicular stomatitis virus infection alters the eIF4F translation initiation complex and causes dephosphorylation of the eIF4E binding protein 4E-BP1. *J. Virol.* **76**, 10177–87 (2002).
70. Gingras, A. C., Svitkin, Y., Belsham, G. J., Pause, A. & Sonenberg, N. Activation of the translational suppressor 4E-BP1 following infection with encephalomyocarditis virus and poliovirus. *Proc. Natl. Acad. Sci. U. S. A.* **93**, 5578–83 (1996).
71. Plotch, S. J., Bouloy, M., Ulmanen, I. & Krug, R. M. A unique cap(m7GpppXm)-dependent influenza virion endonuclease cleaves capped RNAs to generate the primers that initiate viral RNA transcription. *Cell* **23**, 847–58 (1981).
72. Reguera, J., Weber, F. & Cusack, S. Bunyaviridae RNA polymerases (L-protein) have an N-terminal, influenza-like endonuclease domain, essential for viral cap-dependent transcription. *PLoS Pathog.* **6**, (2010).
73. Fujimura, T. & Esteban, R. Cap-snatching mechanism in yeast L-A double-stranded RNA virus. *Proc. Natl. Acad. Sci. U. S. A.* **108**, 17667–71 (2011).
74. Walsh, D., Mathews, M. B. & Mohr, I. Tinkering with translation: protein synthesis in virus-infected cells. *Cold Spring Harb. Perspect. Biol.* **5**, (2013).
75. Jackson, R. J. The current status of vertebrate cellular mRNA IRESs. *Cold Spring Harb. Perspect. Biol.* **5**, (2013).
76. Dever, T. E. & Green, R. The elongation, termination, and recycling phases of translation in eukaryotes. *Cold Spring Harb. Perspect. Biol.* **4**, 1–16 (2012).

77. Rodnina, M. V & Wintermeyer, W. Recent mechanistic insights into eukaryotic ribosomes. *Curr. Opin. Cell Biol.* **21**, 435–43 (2009).
78. Francklyn, C. & Schimmel, P. Aminoacylation of RNA minihelices with alanine. *Nature* **337**, 478–481 (1989).
79. Frugier, M., Florentz, C. & Giegé, R. Efficient aminoacylation of resected RNA helices by class II aspartyl-tRNA synthetase dependent on a single nucleotide. *EMBO J.* **3**, 2218–2226 (1994).
80. Park S, J. & Schimmel, P. Evidence for interaction of an aminoacyl transfer RNA synthetase with a region important for the identity of its cognate transfer RNA. *J. Biol. Chem.* **263**, 16527–16530 (1988).
81. Schimmel, P. & Schmidt, E. Making connections: RNA-dependent amino acid recognition. *Trends Biochem. Sci.* **20**, 1–2 (1995).
82. Lin, L. & Schimmel, S. P. H. P. Aminoacylation error correction. *Nature* **384**, 33–34 (1996).
83. Nureki, O. *et al.* Enzyme structure with two catalytic sites for double-sieve selection of substrate. *Science* **280**, 578–582 (1998).
84. Godinic-Mikulcic, V. *et al.* Archaeal aminoacyl-tRNA synthetases interact with the ribosome to recycle tRNAs. *Nucleic Acids Res.* **42**, 5191–5201 (2014).
85. Hirschmann, W. D. *et al.* Scp160p is required for translational efficiency of codon-optimized mRNAs in yeast. *Nucleic Acids Res.* **42**, 4043–4055 (2014).
86. Schimmel, P., Tao, J. & Hill, J. Aminoacyl tRNA synthetases as targets for new anti-infectives. *FASEB J.* **12**, 1599–1609 (1998).
87. Palencia, A. *et al.* Structural dynamics of the aminoacylation and proofreading functional cycle of bacterial leucyl-tRNA synthetase. *Nat. Struct. Mol. Biol.* **19**, 677–684 (2012).
88. Sivan, G., Aviner, R. & Elroy-Stein, O. Mitotic Modulation of Translation Elongation Factor 1 Leads to Hindered tRNA Delivery to Ribosomes. *J. Biol. Chem.* **286**, 27927–27935 (2011).
89. Moazed, D. & Noller, H. F. Transfer RNA shields specific nucleotides in 16S ribosomal RNA from attack by chemical probes. *Cell* **47**, 985–94 (1986).
90. Schmeing, T. M. & Ramakrishnan, V. What recent ribosome structures have revealed about the mechanism of translation. *Nature* **461**, 1234–42 (2009).

91. Geggier, P. *et al.* Conformational sampling of aminoacyl-tRNA during selection on the bacterial ribosome. *J. Mol. Biol.* **399**, 576–595 (2010).
92. Blanchard, S. C., Gonzalez, R. L., Kim, H. D., Chu, S. & Puglisi, J. D. tRNA selection and kinetic proofreading in translation. *Nat. Struct. Mol. Biol.* **11**, 1008–1014 (2004).
93. Wohlgemuth, I., Pohl, C., Mittelstaet, J., Konevega, A. L. & Rodnina, M. V. Evolutionary optimization of speed and accuracy of decoding on the ribosome. *Philos. Trans. R. Soc. Lond. B. Biol. Sci.* **366**, 2979–86 (2011).
94. Gromadski, K. B. & Rodnina, M. V. Kinetic Determinants of High-Fidelity tRNA Discrimination on the Ribosome. *Mol. Cell* **13**, 191–200 (2004).
95. Pape, T., Wintermeyer, W. & Rodnina, M. Induced fit in initial selection and proofreading of aminoacyl-tRNA on the ribosome. *EMBO J.* **18**, 3800–3807 (1999).
96. Pape, T., Wintermeyer, W. & Rodnina, M. V. Complete kinetic mechanism of elongation factor Tu-dependent binding of aminoacyl-tRNA to the A site of the E. coli ribosome. *EMBO J.* **17**, 7490–7497 (1998).
97. Kruger, K. *et al.* Self-splicing RNA: autoexcision and autocyclization of the ribosomal RNA intervening sequence of Tetrahymena. *Cell* **31**, 147–57 (1982).
98. Zaug, A. J., Grabowski, P. J. & Cech, T. R. Autocatalytic cyclization of an excised intervening sequence RNA is a cleavage–ligation reaction. *Science (80-.).* **301**, 578 – 583 (1983).
99. Green, R. & Noller, H. F. Ribosomes and translation. *Annu.Rev.Biochem.* **66:679-716**, 679–716 (1997).
100. Noller, H., Hoffarth, V. & Zimniak, L. Unusual resistance of peptidyl transferase to protein extraction procedures. *Science (80-.).* **256**, 1416–1419 (1992).
101. Beringer, M. & Rodnina, M. V. The Ribosomal Peptidyl Transferase. *Mol. Cell* **26**, 311–321 (2007).
102. Dorner, S., Panuschka, C., Schmid, W. & Barta, A. Mononucleotide derivatives as ribosomal P-site substrates reveal an important contribution of the 2'-OH to activity. *Nucleic Acids Res.* **31**, 6536–6542 (2003).
103. Weinger, J. S., Parnell, K. M., Dorner, S., Green, R. & Strobel, S. A. Substrate-assisted catalysis of peptide bond formation by the ribosome. *Nat. Struct. Mol. Biol.* **11**, 1101–1106 (2004).

104. Zaher, H. S., Shaw, J. J., Strobel, S. a & Green, R. The 2'-OH group of the peptidyl-tRNA stabilizes an active conformation of the ribosomal PTC. *EMBO J.* **1**–9 (2011). doi:10.1038/emboj.2011.142
105. Sievers, A., Beringer, M., Rodnina, M. V & Wolfenden, R. The ribosome as an entropy trap. *Proc. Natl. Acad. Sci.* **101**, 7897–7901 (2004).
106. Valle, M. *et al.* Locking and unlocking of ribosomal motions. *Cell* **114**, 123–134 (2003).
107. Fischer, N., Konevega, A. L., Wintermeyer, W., Rodnina, M. V & Stark, H. Ribosome dynamics and tRNA movement by time-resolved electron cryomicroscopy. *Nature* **466**, 329–333 (2010).
108. Agirrezabala, X. *et al.* Visualization of the hybrid state of tRNA binding promoted by spontaneous ratcheting of the ribosome. *Mol. Cell* **32**, 190–197 (2008).
109. Julián, P. *et al.* Structure of ratcheted ribosomes with tRNAs in hybrid states. *Proc. Natl. Acad. Sci. U. S. A.* **105**, 16924–7 (2008).
110. Cornish, P. V, Ermolenko, D. N., Noller, H. F. & Ha, T. Spontaneous intersubunit rotation in single ribosomes. *Mol. Cell* **30**, 578–588 (2008).
111. Horan, L. H. & Noller, H. F. Intersubunit movement is required for ribosomal translocation. *Proc. Natl. Acad. Sci.* **104**, 4881 (2007).
112. Lill, R., Robertson, J. M. & Wintermeyer, W. Binding of the 3' terminus of tRNA to 23S rRNA in the ribosomal exit site actively promotes translocation. *EMBO J.* **8**, 3933–8 (1989).
113. Taylor, D. J. *et al.* Structures of modified eEF2 80S ribosome complexes reveal the role of GTP hydrolysis in translocation. *EMBO J* **26**, 2421–2431 (2007).
114. Stark, H., Rodnina, M. V, Wieden, H. J., van Heel, M. & Wintermeyer, W. Large-scale movement of elongation factor G and extensive conformational change of the ribosome during translocation. *Cell* **100**, 301–9 (2000).
115. Liu, S. *et al.* Identification of the Proteins Required for Biosynthesis of Diphthamide , the Target of Bacterial ADP-Ribosylating Toxins on Translation Elongation Factor 2 Identification of the Proteins Required for Biosynthesis of Diphthamide , the Target of Bacterial . (2004). doi:10.1128/MCB.24.21.9487
116. Chen, C.-M. & Behringer, R. R. *Ovca1* regulates cell proliferation, embryonic development, and tumorigenesis. *Genes Dev.* **18**, 320–32 (2004).

117. Liu, S. *et al.* Dph3 , a small protein required for diphthamide biosynthesis , is essential in mouse development. *Mol. Cell. Biol.* **26**, 1–8 (2006).
118. Webb, T. R. *et al.* Diphthamide modification of eEF2 requires a J-domain protein and is essential for normal development. *J. Cell Sci.* **121**, 3140–5 (2008).
119. Andersen, G. R., Valente, L., Pedersen, L., Kinzy, T. G. & Nyborg, J. Crystal structures of nucleotide exchange intermediates in the eEF1A- eEF1B α complex. *Nat.Struct.Biol.* **8**, 531–534 (2001).
120. Triana-Alonso, F. J., Chakraborty, K. & Nierhaus, K. H. The elongation factor 3 unique in higher fungi and essential for protein biosynthesis is an E site factor. *J. Biol. Chem.* **270**, 20473–78 (1995).
121. Song, H. *et al.* The crystal structure of human eukaryotic release factor eRF1-- mechanism of stop codon recognition and peptidyl-tRNA hydrolysis. *Cell* **100**, 311–321 (2000).
122. Weixlbaumer, A. *et al.* Insights into translational termination from the structure of RF2 bound to the ribosome. *Science* **322**, 953–956 (2008).
123. Trobro, S. & Aqvist, J. A Model for How Ribosomal Release Factors Induce Peptidyl-tRNA Cleavage in Termination of Protein Synthesis. *Mol. Cell* **27**, 758–766 (2007).
124. Laurberg, M. *et al.* Structural basis for translation termination on the 70S ribosome. *Nature* **454**, 852–857 (2008).
125. Merkulova, T. I., Frolova, L. Y., Lazar, M., Camonis, J. & Kisselev, L. L. C-terminal domains of human translation termination factors eRF1 and eRF3 mediate their in vivo interaction. *FEBS Lett.* **443**, 41–47 (1999).
126. Cheng, Z. *et al.* Structural insights into eRF3 and stop codon recognition by eRF1. *Genes Dev.* **23**, 1106–1118 (2009).
127. Kononenko, A. V. *et al.* Role of the individual domains of translation termination factor eRF1 in GTP binding to eRF3. *Proteins Struct. Funct. Genet.* **70**, 388–393 (2008).
128. Pisareva, V. P., Pisarev, A. V., Hellen, C. U. T., Rodnina, M. V & Pestova, T. V. Kinetic analysis of interaction of eukaryotic release factor 3 with guanine nucleotides. *J. Biol. Chem.* **281**, 40224–40235 (2006).
129. Gao, N. *et al.* Mechanism for the disassembly of the posttermination complex inferred from Cryo-EM studies. *Mol. Cell* **18**, 663–674 (2005).

130. Dunkle, J. A. *et al.* Structures of the bacterial ribosome in classical and hybrid states of tRNA binding. *Science* **332**, 981–984 (2011).
131. Hirokawa, G. *et al.* The role of ribosome recycling factor in dissociation of 70S ribosomes into subunits. *RNA* **11**, 1317–1328 (2005).
132. Peske, F., Rodnina, M. V. & Wintermeyer, W. Sequence of steps in ribosome recycling as defined by kinetic analysis. *Mol. Cell* **18**, 403–412 (2005).
133. Zavialov, A. V., Hauryliuk, V. V. & Ehrenberg, M. Splitting of the posttermination ribosome into subunits by the concerted action of RRF and EF-G. *Mol. Cell* **18**, 675–686 (2005).
134. Pisarev, A. V., Hellen, C. U. T. & Pestova, T. V. Recycling of Eukaryotic Posttermination Ribosomal Complexes. *Cell* **131**, 286–299 (2007).
135. Doma, M. K. & Parker, R. Endonucleolytic cleavage of eukaryotic mRNAs with stalls in translation elongation. *Nature* **440**, 561–564 (2006).
136. Becker, T. *et al.* Structure of the no-go mRNA decay complex Dom34-Hbs1 bound to a stalled 80S ribosome. *Nat. Struct. Mol. Biol.* **18**, 715–720 (2011).
137. Shoemaker, C. J., Eyler, D. E. & Green, R. Dom34:Hbs1 promotes subunit dissociation and peptidyl-tRNA drop-off to initiate no-go decay. *Science* **330**, 369–72 (2010).
138. Lee, H. H. *et al.* Structural and Functional Insights into Dom34, a Key Component of No-Go mRNA Decay. *Mol. Cell* **27**, 938–950 (2007).
139. Graille, M., Chaillet, M. & van Tilbeurgh, H. Structure of yeast Dom34: a protein related to translation termination factor Erf1 and involved in No-Go decay. *J. Biol. Chem.* **283**, 7145–7154 (2008).
140. Shoemaker, C. J. & Green, R. Kinetic analysis reveals the ordered coupling of translation termination and ribosome recycling in yeast. *Proc. Natl. Acad. Sci.* **108**, E1392–E1398 (2011).
141. Khoshnevis, S. *et al.* The iron-sulphur protein RNase L inhibitor functions in translation termination. *EMBO Rep.* **11**, 214–219 (2010).
142. Wilson, D. N. The A-Z of bacterial translation inhibitors. *Crit. Rev. Biochem. Mol. Biol.* **44**, 393–433 (2009).
143. Wilson, D. N. Ribosome-targeting antibiotics and mechanisms of bacterial resistance. *Nat. Rev. Microbiol.* **12**, 35–48 (2014).

144. Brodersen, D. E. *et al.* The structural basis for the action of the antibiotics tetracycline, pactamycin, and hygromycin B, on the 30S ribosomal subunit. *Cell* **103**, 1143–1154 (2000).
145. Carter, A. P. *et al.* Functional insights from the structure of the 30S ribosomal subunit and its interactions with antibiotics. *Nature* **407**, 340–348 (2000).
146. Auerbach, T., Bashan, A. & Yonath, A. Ribosomal antibiotics: structural basis for resistance, synergism and selectivity. *Trends Biotechnol.* **22**, 570–6 (2004).
147. Bulkley, D., Innis, C. A., Blaha, G. & Steitz, T. a. Revisiting the structures of several antibiotics bound to the bacterial ribosome. *Proc. Natl. Acad. Sci. U. S. A.* **107**, 17158–63 (2010).
148. Hansen, J. Structures of Five Antibiotics Bound at the Peptidyl Transferase Center of the Large Ribosomal Subunit. *J. Mol. Biol.* **330**, 1061–1075 (2003).
149. Schlünzen, F., Pyetan, E., Fucini, P., Yonath, A. & Harms, J. M. Inhibition of peptide bond formation by pleuromutilins: the structure of the 50S ribosomal subunit from *Deinococcus radiodurans* in complex with tiamulin. *Mol. Microbiol.* **54**, 1287–94 (2004).
150. Schlünzen, F. *et al.* Structural basis for the interaction of antibiotics with the peptidyl transferase centre in eubacteria. *Nature* **413**, 814–21 (2001).
151. Gürel, G., Blaha, G., Moore, P. B. & Steitz, T. a. U2504 determines the species specificity of the A-site cleft antibiotics: the structures of tiamulin, homoharringtonine, and bruceantin bound to the ribosome. *J. Mol. Biol.* **389**, 146–56 (2009).
152. Davis, B. D. Mechanism of bactericidal action of aminoglycosides. *Microbiol. Rev.* **51**, 341–350 (1987).
153. Kohanski, M. A., Dwyer, D. J., Wierzbowski, J., Cottarel, G. & Collins, J. J. Mistranslation of Membrane Proteins and Two-Component System Activation Trigger Antibiotic-Mediated Cell Death. *Cell* **135**, 679–690 (2008).
154. Kohanski, M. A., Dwyer, D. J., Hayete, B., Lawrence, C. A. & Collins, J. J. A Common Mechanism of Cellular Death Induced by Bactericidal Antibiotics. *Cell* **130**, 797–810 (2007).
155. Schlunzen, F. *et al.* The antibiotic kasugamycin mimics mRNA nucleotides to destabilize tRNA binding and inhibit canonical translation initiation. *Nat. Struct. Mol. Biol.* **13**, 871–878 (2006).

156. Woodcock, J., Moazed, D., Cannon, M., Davies, J. & Noller, H. F. Interaction of antibiotics with A- and P-site-specific bases in 16S ribosomal RNA. *EMBO J.* **10**, 3099–3103 (1991).
157. Belova, L., Tenson, T., Xiong, L., McNicholas, P. M. & Mankin, A. S. A novel site of antibiotic action in the ribosome: interaction of evernimicin with the large ribosomal subunit. *Proc. Natl. Acad. Sci. U. S. A.* **98**, 3726–3731 (2001).
158. Brandi, L. *et al.* Specific, efficient, and selective inhibition of prokaryotic translation initiation by a novel peptide antibiotic. *Proc. Natl. Acad. Sci. U. S. A.* **103**, 39–44 (2006).
159. Stark, H. Three-dimensional electron cryomicroscopy of ribosomes. *Curr. Protein Pept. Sci.* **3**, 79–91 (2002).
160. Ermolenko, D. N. *et al.* The antibiotic viomycin traps the ribosome in an intermediate state of translocation. *Nat. Struct. Mol. Biol.* **14**, 493–7 (2007).
161. Eyler, D. E. & Green, R. Distinct response of yeast ribosomes to a miscoding event during translation. *RNA* **17**, 925–32 (2011).
162. Belew, A. T. *et al.* Ribosomal frameshifting in the CCR5 mRNA is regulated by miRNAs and the NMD pathway. *Nature* **512**, 265–269 (2014).
163. Sandeepa M. Eswarappa, Alka A. Potdar, William J. Koch, Yi Fan, Kommireddy Vasu, Daniel Lindner, Belinda Willard, Linda M. Graham, Paul E. DiCorleto, P. L. F. Programmed Translational Readthrough Generates Antiangiogenic VEGF-Ax. *Cell* **157**, 1605–1618 (2014).
164. Namy, O., Moran, S. J., Stuart, D. I., Gilbert, R. J. & Brierley, I. A mechanical explanation of RNA pseudoknot function in programmed ribosomal frameshifting. *Nature* **441**, 244–247 (2006).
165. Dinman, J. D. Mechanisms and implications of programmed translational frameshifting. *Wiley Interdiscip. Rev. RNA* **3**, 661–673 (2012).
166. Harger, J. W., Meskauskas, A. & Dinman, J. D. An “integrated model” of programmed ribosomal frameshifting and post-transcriptional surveillance. *TIBS* **27**, 448–454 (2002).
167. Kollmus, H., Hentze, M. W. & Hauser, H. Regulated ribosomal frameshifting by an RNA-protein interaction. *RNA* **2**, 316 (1996).

168. Baril, M., Dulude, D., Steinberg, S. V & Brakier-Gingras, L. The frameshift stimulatory signal of human immunodeficiency virus type 1 group O is a pseudoknot. *J. Mol. Biol.* **331**, 571–583 (2003).
169. Yu, C. H., Noteborn, M. H., Pleij, C. W. A. & Olsthoorn, R. C. L. Stem-loop structures can effectively substitute for an RNA pseudoknot in -1 ribosomal frameshifting. *Nucleic Acids Res.* **39**, 8952–8959 (2011).
170. Rheinberger, H. J., Sternbach, H. & Nierhaus, K. H. Three tRNA binding sites on Escherichia coli ribosomes. *Proc. Natl. Acad. Sci.* **78**, 5310 (1981).
171. Weiss, R. B., Dunn, D. M., Shuh, M., Atkins, J. F. & Gesteland, R. F. E. coli ribosomes re-phase on retroviral frameshift signals at rates ranging from 2 to 50 percent. *New Biol.* **1**, 159 (1989).
172. Caliskan, N., Katunin, V. I., Belardinelli, R., Peske, F. & Rodnina, M. V. Programmed -1 Frameshifting by Kinetic Partitioning during Impeded Translocation. *Cell* **157**, 1619–31 (2014).
173. Chen, J. *et al.* Dynamic pathways of -1 translational frameshifting. *Nature* **512**, 328–332 (2014).
174. Dinman, J. D. & Wickner, R. B. Ribosomal frameshifting efficiency and gag/gag-pol ratio are critical for yeast M1 double-stranded RNA virus propagation. *J. Virol.* **66**, 3669–3676 (1992).
175. Biswas, P., Jiang, X., Pacchia, A. L., Dougherty, J. P. & Peltz, S. W. The human immunodeficiency virus type 1 ribosomal frameshifting site is an invariant sequence determinant and an important target for antiviral therapy. *J. Virol.* **78**, 2082 (2004).
176. Park, J. & Morrow, C. D. Overexpression of the gag-pol precursor from human immunodeficiency virus type 1 proviral genomes results in efficient proteolytic processing in the absence of virion production. *J. Virol.* **65**, 5111 (1991).
177. Hung, M., Patel, P., Davis, S. & Green, S. R. Importance of ribosomal frameshifting for human immunodeficiency virus type 1 assembly and replication. *J. Virol.* **72**, 4819–4824 (1998).
178. Karacostas, V., Wolffe, E. J., Nagashima, K., Gonda, M. A. & Moss, B. Overexpression of the HIV-1 gag-pol polyprotein results in intracellular activation of HIV-1 protease and inhibition of assembly and budding of virus-like particles. *Virology* **193**, 661–671 (1993).

179. Masters, P. S. The Molecular Biology of Coronaviruses. *Adv. Virus Res.* **65**, 193–292 (2006).
180. Plant, E. P., Wang, P., Jacobs, J. L. & Dinman, J. D. A programmed -1 ribosomal frameshift signal can function as a cis-acting mRNA destabilizing element. *Nucleic Acids Res.* **32**, 784–90 (2004).
181. Belew, A. T., Advani, V. M. & Dinman, J. D. Endogenous ribosomal frameshift signals operate as mRNA destabilizing elements through at least two molecular pathways in yeast. *Nucleic Acids Res.* **39**, 2799–808 (2011).
182. Advani, V. M., Belew, A. T. & Dinman, J. D. Yeast telomere maintenance is globally controlled by programmed ribosomal frameshifting and the nonsense-mediated mRNA decay pathway. *Translation* **1**, 38–47 (2013).
183. Kurian, E., Palanimurugan, R., Gödderz, D. & Dohmen, & R. J. Polyamine sensing by nascent ornithine decarboxylase antizyme stimulates decoding of its mRNA. *Nature* **7365**, 490–494 (2011).
184. Craigen, W. J. & Caskey, C. T. Expression of peptide chain release factor 2 requires high-efficiency frameshift. *Nature* **322**, 273–275 (1986).
185. Farabaugh, P. J., Zhao, H. & Vimaladithan, A. A Novel Programmed Frameshift Expresses the Pol3 Gene of Retrotransposon-Ty3 of Yeast - Frameshifting Without Transfer-Rna Slippage. *Cell* **74**, 93–103 (1993).
186. Belcourt, M. F. & Farabaugh, P. J. Ribosomal frameshifting in the yeast retrotransposon Ty: tRNAs induce slippage on a 7 nucleotide minimal site. *Cell* **62**, 339–352 (1990).
187. Ivanov, I. P., Anderson, C. B., Gesteland, R. F. & Atkins, J. F. Identification of a new antizyme mRNA+ 1 frameshifting stimulatory pseudoknot in a subset of diverse invertebrates and its apparent absence in intermediate species. *J. Mol. Biol.* **339**, 495–504 (2004).
188. Wills, N. M., Gesteland, R. F. & Atkins, J. F. Evidence that a downstream pseudoknot is required for translational read-through of the Moloney murine leukemia virus gag stop codon. *Proc. Natl. Acad. Sci. U. S. A.* **88**, 6991–6995 (1991).
189. Yoshinaka, Y., Katoh, I., Copeland, T. D. & Oroszlan, S. Murine leukemia virus protease is encoded by the gag-pol gene and is synthesized through suppression of an amber termination codon. *Proc. Natl. Acad. Sci. U. S. A.* **82**, 1618–22 (1985).

190. Leibundgut, M., Frick, C., Thanbichler, M., Böck, A. & Ban, N. Selenocysteine tRNA-specific elongation factor SelB is a structural chimaera of elongation and initiation factors. *EMBO J.* **24**, 11–22 (2005).
191. Schomburg, L., Schweizer, U. & Köhrle, J. Selenium and selenoproteins in mammals: extraordinary, essential, enigmatic. *Cell. Mol. Life Sci.* **61**, 1988–1995 (2004).
192. Hao, B. *et al.* A new UAG-encoded residue in the structure of a methanogen methyltransferase. *Science* **296**, 1462–1466 (2002).
193. Gonzales, B. *et al.* The Treacher Collins syndrome (TCOF1) gene product is involved in pre-rRNA methylation. *Hum. Mol. Genet.* **14**, 2035–2043 (2005).
194. Valdez, B. C., Henning, D., So, R. B., Dixon, J. & Dixon, M. J. The Treacher Collins syndrome (TCOF1) gene product is involved in ribosomal DNA gene transcription by interacting with upstream binding factor. *Proc. Natl. Acad. Sci. U. S. A.* **101**, 10709–10714 (2004).
195. Rohozinski, J., Lamb, D. J. & Bishop, C. E. UTP14c is a recently acquired retrogene associated with spermatogenesis and fertility in man. *Biol. Reprod.* **74**, 644–651 (2006).
196. Chagnon, P. *et al.* A missense mutation (R565W) in cirhin (FLJ14728) in North American Indian childhood cirrhosis. *Am. J. Hum. Genet.* **71**, 1443–1449 (2002).
197. Eschrich, D., Buchhaupt, M., Kötter, P. & Entian, K. D. Nep1p (Emg1p), a novel protein conserved in eukaryotes and archaea, is involved in ribosome biogenesis. *Curr. Genet.* **40**, 326–338 (2002).
198. Ganapathi, K. A. *et al.* The human Shwachman-Diamond syndrome protein, SBDS, associates with ribosomal RNA. *Blood* **110**, 1458–1465 (2007).
199. Reichow, S. L., Hamma, T., Ferré-D'Amaré, A. R. & Varani, G. The structure and function of small nucleolar ribonucleoproteins. *Nucleic Acids Res.* **35**, 1452–1464 (2007).
200. Cmejla, R., Cmejlova, J., Handrkova, H., Petrak, J. & Pospisilova, D. Ribosomal protein S17 gene (RPS17) is mutated in Diamond-Blackfan anemia. *Hum. Mutat.* **28**, 1178–1182 (2007).
201. Ellis, S. R. & Gleizes, P. E. Diamond Blackfan anemia: Ribosomal proteins going rogue. *Semin. Hematol.* **48**, 89–96 (2011).

202. Ebert, B. L. *et al.* Identification of RPS14 as a 5q- syndrome gene by RNA interference screen. *Nature* **451**, 335–339 (2008).
203. Oskarsson, T. & Trump, A. The Myc trilogy: lord of RNA polymerases. *Nat. Cell Biol.* **7**, 215–7 (2005).
204. White, R. J. RNA polymerases I and III, growth control and cancer. *Nat. Rev. Mol. Cell Biol.* **6**, 69–78 (2005).
205. Ruggero, D. Translational control in cancer etiology. *Cold Spring Harb. Perspect. Biol.* **5**, 1–27 (2013).
206. Kondrashov, N. *et al.* Ribosome-mediated specificity in Hox mRNA translation and vertebrate tissue patterning. *Cell* **145**, 383–397 (2011).
207. Monro, R. E. Catalysis of peptide bond formation by 50 s ribosomal subunits from *Escherichia coli*. *J. Mol. Biol.* **26**, 147–151 (1967).
208. Wower, J. *et al.* Transit of tRNA through the *Escherichia coli* ribosome. Cross-linking of the 3' end of tRNA to specific nucleotides of the 23 S ribosomal RNA at the A, P, and E sites. *J. Biol. Chem.* **275**, 37887–94 (2000).
209. Cooperman BS, W. C. and F. C. in *Ribosome Struct. Funct. Evol. Am. Soc. Microbiol. Washington, DC* 491–501 (1990).
210. Vladimirov, S. N., Druzina, Z., Wang, R. & Cooperman, B. S. Identification of 50S components neighboring 23S rRNA nucleotides A2448 and U2604 within the peptidyl transferase center of *Escherichia coli* ribosomes. *Biochemistry* **39**, 183–193 (2000).
211. Schulze, H. & Nierhaus, K. H. Minimal set of ribosomal components for reconstitution of the peptidyltransferase activity. *EMBO J.* **1**, 609–613 (1982).
212. Franceschi, F. J. & Nierhaus, K. H. Ribosomal proteins L15 and L16 are mere late assembly proteins of the large ribosomal subunit. Analysis of an *Escherichia coli* mutant lacking L15. *J. Biol. Chem.* **265**, 16676–16682 (1990).
213. Khaitovich P and Mankin A S. in *Ribosome Struct. Funct. Antibiot. Cell. Interact.* 229–243 (ASM Press,, 2000).
214. Noller, H. F., Hoffarth, V. & Zimniak, L. Unusual resistance of peptidyl transferase to protein extraction procedures. *Science* **256**, 1416–1419 (1992).
215. Müller, E. C. & Wittmann-Liebold, B. Phylogenetic relationship of organisms obtained by ribosomal protein comparison. *Cell. Mol. Life Sci.* **53**, 34–50 (1997).

216. Cooperman, B. S., Wooten, T., Romero, D. P. & Traut, R. R. Histidine 229 in protein L2 is apparently essential for 50S peptidyl transferase activity. *Biochem. Cell Biol.* **73**, 1087–94
217. Uhlein, M., Weglöhner, W., Urlaub, H. & Wittmann-Liebold, B. Functional implications of ribosomal protein L2 in protein biosynthesis as shown by in vivo replacement studies. *Biochem. J.* **331** (Pt 2, 423–430 (1998).
218. Nitta, I., Ueda, T. & Watanabe, K. Possible involvement of Escherichia coli 23S ribosomal RNA in peptide bond formation. *RNA* **4**, 257–267 (1998).
219. Nitta, I. Reconstitution of Peptide Bond Formation with Escherichia coli 23S Ribosomal RNA Domains. *Science* (80-.). **281**, 666–669 (1998).
220. Khaitovich, P., Tenson, T., Mankin, A. S. & Green, R. Peptidyl transferase activity catalyzed by protein-free 23S ribosomal RNA remains elusive. *RNA* **5**, 605–8 (1999).
221. Kruiswijk, T., Planta, R. J. & Mager, W. H. Quantitative Analysis of the Protein Composition of Yeast Ribosomes. *Eur. J. Biochem.* **83**, 245–252 (1977).
222. Kruiswijk, T. & Planta, R. J. Analysis of the protein composition of yeast ribosomal subunits by two-dimensional polyacrylamide gel electrophoresis. *Mol. Biol. Rep.* **1**, 409–415 (1974).
223. Rodnina, M. V, Savelsbergh, A., Katunin, V. I. & Wintermeyer, W. Hydrolysis of GTP by elongation factor G drives tRNA movement on the ribosome. *Nature* **385**, 37–41 (1997).
224. Rodnina, M. V & Wintermeyer, W. GTP consumption of elongation factor Tu during translation of heteropolymeric mRNAs. *Proc. Natl. Acad. Sci. U. S. A.* **92**, 1945–1949 (1995).
225. Alkalaeva, E. Z., Pisarev, A. V., Frolova, L. Y., Kisselev, L. L. & Pestova, T. V. In Vitro Reconstitution of Eukaryotic Translation Reveals Cooperativity between Release Factors eRF1 and eRF3. *Cell* **125**, 1125–1136 (2006).
226. Katunin, V. I., Savelsbergh, A., Rodnina, M. V. & Wintermeyer, W. Coupling of GTP hydrolysis by elongation factor G to translocation and factor recycling on the ribosome. *Biochemistry* **41**, 12806–12812 (2002).
227. Svidritskiy, E., Brilot, A. F., Koh, C. S., Grigorieff, N. & Korostelev, A. A. Structures of Yeast 80S ribosome-tRNA complexes in the rotated and nonrotated conformations. *Structure* **22**, 1210–1218 (2014).

228. Frank, J. Intermediate states during mRNA-tRNA translocation. *Curr. Opin. Struct. Biol.* **22**, 778–785 (2012).
229. Fu, J., Munro, J. B., Blanchard, S. C. & Frank, J. Cryoelectron microscopy structures of the ribosome complex in intermediate states during tRNA translocation. *Proc. Natl. Acad. Sci. U. S. A.* **108**, 4817–4821 (2011).
230. Zhang, W., Dunkle, J. A. & Cate, J. H. Structures of the ribosome in intermediate states of ratcheting. *Science (80-.)*. **325**, 1014–1017 (2009).
231. Konevega, A. L. *et al.* Spontaneous reverse movement of mRNA-bound tRNA through the ribosome. *Nat.Struct.Mol.Biol* **14**, 318–324 (2007).
232. Sulima, S. O. *et al.* Eukaryotic rpL10 drives ribosomal rotation. *Nucleic Acids Res.* **42**, 2049–2063 (2014).
233. Advani, V. M., Belew, A. T. & Dinman, J. D. Yeast telomere maintenance is globally controlled by programmed ribosomal frameshifting and the nonsense-mediated mRNA decay pathway. *Translation* **1**, 38–47 (2013).
234. Hekman, K. E. *et al.* A conserved eEF2 coding variant in SCA26 leads to loss of translational fidelity and increased susceptibility to proteostatic insult. *Hum.Mol.Genet.* **21**, 5472–5483 (2012).
235. Jack, K. *et al.* rRNA pseudouridylation defects affect ribosomal ligand binding and translational fidelity from yeast to human cells. *Mol.Cell* **44**, 660–666 (2011).
236. Sulima, S. O. *et al.* Bypass of the pre-60S ribosomal quality control as a pathway to oncogenesis. *Proc. Natl. Acad. Sci.* **111**, 5640–5 (2014).
237. Ban, N. *et al.* A new system for naming ribosomal proteins. *Curr. Opin. Struct. Biol.* **24**, 165–169 (2014).
238. Noller, H. F. & Green, R. Ribosomes and translation. *Annu.Rev.Biochem.* **66**, 679–716 (1997).
239. Meskauskas, A., Russ, J. R. & Dinman, J. D. Structure/function analysis of yeast ribosomal protein L2. *Nucleic Acids Res.* **36**, 1826–1835 (2008).
240. Diedrich, G. *et al.* Ribosomal protein L2 is involved in the association of the ribosomal subunits, tRNA binding to A and P sites and peptidyl transfer. *EMBO J.* **19**, 5241–5250 (2000).
241. Taylor, D. J. *et al.* Comprehensive molecular structure of the eukaryotic ribosome. *Structure* **17**, 1591–1604 (2009).

242. Leshin, J. A., Heselpoth, R., Belew, A. T. & Dinman, J. D. High throughput structural analysis of yeast ribosomes using hSHAPE. *RNA Biol.* **8**, 478–487 (2011).
243. Leshin, J. A., Heselpoth, R., Belew, A. T. & Dinman, J. D. High throughput structural analysis of yeast ribosomes using hSHAPE. *RNA Biol.* **8**, 478–487 (2011).
244. Taylor, D. J. *et al.* in 59–85 (Cold Spring Harbor Laboratory Press, 2006).
245. Liao, P.-Y. Y., Choi, Y. S., Dinman, J. D. & Lee, K. H. The many paths to frameshifting: kinetic modelling and analysis of the effects of different elongation steps on programmed -1 ribosomal frameshifting. *Nucleic Acids Res.* **39**, 300–312 (2010).
246. Lundblad, V. & Morris, D. K. Programmed translational frameshifting in a gene required for yeast telomere replication. *Curr. Biol.* **7**, 969–976 (1997).
247. Taliaferro, D. & Farabaugh, P. J. An mRNA sequence derived from the yeast EST3 gene stimulates programmed +1 translational frameshifting. *RNA* **13**, 606–613 (2007).
248. Ivanov, I. P. & Atkins, J. F. Ribosomal frameshifting in decoding antizyme mRNAs from yeast and protists to humans: close to 300 cases reveal remarkable diversity despite underlying conservation. *Nucleic Acids Res.* **35**, 1842–1858 (2007).
249. Frank, J. & Gonzalez Jr., R. L. Structure and dynamics of a processive Brownian motor: the translating ribosome. *Annu.Rev.Biochem.* **79**, 381–412 (2010).
250. Rodnina, M. V. Quality control of mRNA decoding on the bacterial ribosome. *Adv. Protein Chem. Struct. Biol.* **86**, 95–128 (2012).
251. Aitken, C. E., Petrov, A. & Puglisi, J. D. Single Ribosome Dynamics and the Mechanism of Translation. *Annu.Rev.Biophys.* **39**, 491–513 (2010).
252. Rakauskaitė, R. & Dinman, J. D. Mutations of highly conserved bases in the peptidyltransferase center induce compensatory rearrangements in yeast ribosomes. *RNA* **17**, 855–864 (2011).
253. Rhodin, M. H. J. & Dinman, J. D. A flexible loop in yeast ribosomal protein L11 coordinates P-site tRNA binding. *Nucleic Acids Res.* **38**, 8377–89 (2010).
254. Baxter-Roshek, J. L., Petrov, A. N. & Dinman, J. D. Optimization of ribosome structure and function by rRNA base modification. *PLoS One* **2**, e174 (2007).

255. Meskauskas, A. & Dinman, J. D. Ribosomal protein L3: gatekeeper to the A site. *Mol. Cell* **25**, 877–88 (2007).
256. Meskauskas, A. & Dinman, J. D. Ribosomal protein L3 functions as a “rocker switch” to aid in coordinating of large subunit-associated functions in eukaryotes and Archaea. *Nucleic Acids Res.* **36**, 6175 (2008).
257. Rakauskaite, R. & Dinman, J. D. An arc of unpaired “hinge bases” facilitates information exchange among functional centers of the ribosome. *Mol. Cell. Biol.* **26**, 8992 (2006).
258. Rhodin, M. H. J. & Dinman, J. D. An Extensive Network of Information Flow through the B1b/c Intersubunit Bridge of the Yeast Ribosome. *PLoS One* **6**, e20048 (2011).
259. Meskauskas, A. & Dinman, J. D. A molecular clamp ensures allosteric coordination of peptidyltransfer and ligand binding to the ribosomal A-site. *Nucleic Acids Res.* (2010).
260. Daviter, T., Gromadski, K. B. & Rodnina, M. V. The ribosome’s response to codon-anticodon mismatches. *Biochimie* **88**, 1001–1011 (2006).
261. Jacobs, J. L., Belew, A. T., Rakauskaite, R. & Dinman, J. D. Identification of functional, endogenous programmed -1 ribosomal frameshift signals in the genome of *Saccharomyces cerevisiae*. *Nucleic Acids Res.* **35**, 165–174 (2007).
262. Belew, A. T., Hepler, N. L., Jacobs, J. L. & Dinman, J. D. PRFdb: a database of computationally predicted eukaryotic programmed -1 ribosomal frameshift signals. *BMC Genomics* **9**, 339 (2008).
263. Palanimurugan, R., Scheel, H., Hofmann, K. & Dohmen, R. J. Polyamines regulate their synthesis by inducing expression and blocking degradation of ODC antizyme. *EMBO J.* **23**, 4857–4867 (2004).
264. Lingner, J., Cech, T. R., Hughes, T. R. & Lundblad, V. Three Ever Shorter Telomere (EST) genes are dispensable for in vitro yeast telomerase activity. *Proc. Natl. Acad. Sci. U.S.A* **94**, 11190–11195 (1997).
265. Zakian, V. A. Telomeres: the beginnings and ends of eukaryotic chromosomes. *Exp. Cell Res.* **318**, 1456–1460 (2012).
266. McCann, K. L. & Baserga, S. J. Genetics. Mysterious ribosomopathies. *Science* **341**, 849–50 (2013).
267. Tabor, C. W. & Tabor, H. Polyamines. *Annu. Rev. Biochem.* **53**, 749–790 (1984).

268. Tosaka, Y. *et al.* Identification and characterization of testis specific ornithine decarboxylase antizyme (OAZ-t) gene: expression in haploid germ cells and polyamine-induced frameshifting. *Genes to Cells* **DOI: 10.10**, (2001).
269. Rose, M. D., Winston, F. & Hieter, P. *Methods in Yeast Genetics*. (Cold Spring Harbor Press, 1990).
270. Sambrook, J., Fritsch, E. F. & Maniatis, T. *Molecular Cloning: A Laboratory Manual*. Cold Spring Harbor laboratory press. New York 931–957 (1989).
271. Ito, H., Fukuda, Y., Murata, K. & Kimura, A. Transformation of intact yeast cells treated with alkali cations. *J. Bacteriol.* **153**, 163–168 (1983).
272. Dinman, J. D. & Wickner, R. B. Translational maintenance of frame: mutants of *Saccharomyces cerevisiae* with altered -1 ribosomal frameshifting efficiencies. *Genetics* **136**, 75–86 (1994).
273. Wickner, R. B. & Leibowitz, M. J. Mak mutants of yeast: mapping and characterization. *J. Bacteriol.* **140**, 154 (1979).
274. Harger, J. W. An in vivo dual-luciferase assay system for studying translational recoding in the yeast *Saccharomyces cerevisiae*. *Rna* **9**, 1019–1024 (2003).
275. Harger, J. W., Meskauskas, A., Nielsen, N., Justice, M. C. & Dinman, J. D. Ty1 retrotransposition and programmed +1 ribosomal frameshifting require the integrity of the protein synthetic translocation step. *Virology* **286**, 216–224 (2001).
276. Plant, E. P. *et al.* Differentiating between near- and non-cognate codons in *Saccharomyces cerevisiae*. *PLoS One* **2**, e517 (2007).
277. Jacobs, J. L. & Dinman, J. D. Systematic analysis of bicistronic reporter assay data. *Nucleic Acids Res.* **32**, e160 (2004).
278. Kwon, I., Wang, P. & Tirrell, D. A. Design of a bacterial host for site-specific incorporation of p-bromophenylalanine into recombinant proteins. *J. Am. Chem. Soc.* **128**, 11778–11783 (2006).
279. Von der, H. F. Affinity elution: principles and applications to purification of aminoacyl-tRNA synthetases. *Methods Enzym.* **34**, 163–171 (1974).
280. Meskauskas, A., Petrov, A. N. & Dinman, J. D. Identification of functionally important amino acids of ribosomal protein L3 by saturation mutagenesis. *Mol. Cell. Biol.* **25**, 10863 (2005).

281. Landry, D. M., Hertz, M. I. & Thompson, S. R. RPS25 is essential for translation initiation by the Dicistroviridae and hepatitis C viral IRESs. *Genes Dev.* **23**, 2753–2764 (2009).
282. Synetos, D., Frantziou, C. P. & Alksne, L. E. Mutations in yeast ribosomal proteins S28 and S4 affect the accuracy of translation and alter the sensitivity of the ribosomes to paromomycin. *Biochim.Biophys.Acta* **1309**, 156–166 (1996).
283. Ortiz, P. A., Ulloque, R., Kihara, G. K., Zheng, H. & Kinzy, T. G. Translation elongation factor 2 anticodon mimicry domain mutants affect fidelity and diphtheria toxin resistance. *J. Biol. Chem.* **281**, 32639–32648 (2006).
284. Pappenheimer, A. M. Diphtheria toxin. *Annu. Rev. Biochem.* **46**, 69–94 (1977).
285. Gill, D. M. & Dinius, L. L. The elongation factor 2 content of mammalian cells: assay method and relation to ribosome number. *J. Biol. Chem.* **248**, 654–658 (1973).
286. Gill, D. M., Pappenheimer, A. M. & Baseman, J. B. Studies on Transferase II Using Diphtheria Toxin. *Cold Spring Harb. Symp. Quant. Biol.* **34**, 595–602 (1969).
287. Wilkinson, K. A., Merino, E. J. & Weeks, K. M. Selective 2'-hydroxyl acylation analyzed by primer extension (SHAPE): quantitative RNA structure analysis at single nucleotide resolution. *Nat.Protoc.* **1**, 1610–1616 (2006).
288. Vasa, S. M., Guex, N., Wilkinson, K. A., Weeks, K. M. & Giddings, M. C. ShapeFinder: a software system for high-throughput quantitative analysis of nucleic acid reactivity information resolved by capillary electrophoresis. *RNA* **14**, 1979–1990 (2008).
289. De Keersmaecker, K. *et al.* Exome sequencing identifies mutation in CNOT3 and ribosomal genes RPL5 and RPL10 in T-cell acute lymphoblastic leukemia. *Nat. Genet.* **45**, 186–90 (2013).